

**Inorganic Polymers
(Geopolymers) as Potential
Bioactive Materials**

by

Nils Rahner

A thesis
submitted to the Victoria University of Wellington
in fulfilment of the
requirements for the degree of
Master of Science
in Chemistry.

Victoria University of Wellington

2009

Abstract

The primary aim of this project was to synthesise potassium activated geopolymer composites with bioactivity, and this was realised by adding 10wt% of calcium hydroxide, nano-structured calcium silicate or calcium phosphate to the geopolymer matrix. The synthesised samples were cured at 40°C then heated to 550°C and 600°C to reduce their alkalinity. Tensile strength was measured by diametral compression. The effect of exposure to simulated body fluid (SBF) was determined by x-ray diffractometry (XRD), ^{27}Al , ^{29}Si and ^{43}Ca nuclear magnetic resonance spectroscopy with magic angle spinning (MAS NMR), pH measurements, inductively coupled plasma (ICP), scanning electron microscopy (SEM) and energy dispersive x-ray analysis (EDS).

XRD, ^{27}Al and ^{29}Si MAS NMR confirmed that all the samples retained their structural characteristics of a true aluminosilicate geopolymer, even after heating and exposure to SBF. EDS examination of the calcium-containing geopolymer composites showed that the calcium distribution was generally homogeneous. Exposure of the geopolymer composites to SBF at body temperature, was used to simulate the behaviour of the geopolymer composites in blood plasma. XRD and SEM/ EDS analysis showed that the geopolymers containing calcium hydroxide and calcium silicate formed hydroxyl apatite (HA) and carbonate hydroxyl apatite (HCA) after their exposure to SBF, indicating a degree of bioactivity. The absorp-

tion of calcium and phosphorus from the SBF and the observation of nano crystals rich in these elements provide some evidence of bioactive phases in the composite containing calcium phosphate and the reference geopolymer. The reference and the calcium phosphate geopolymer (both heated to 600°C) produced the lowest pH (≈ 8) in the SBF.

ICP analysis of the SBF after exposure shows that most of the aluminium remains in the geopolymer structure. The greatest release of aluminium (< 2.7 ppm after 168 hours) was found for the calcium hydroxide geopolymer (heated to 600°C). Diametral compression testing showed that the strength of the calcium phosphate-containing geopolymer heated to 550°C (4.17 MPa) is comparable with that of Bioglass® (5.56 MPa), currently used as a bio-material.

Although none of the composites are ideal in all respects, they show sufficient promise to suggest that with further refinement, geopolymer materials may well be become candidates as bioactive ceramics.

This Thesis is dedicated to my parents

Brigitte

and

Ewald Rahner

for their outstanding support and

encouragement

Acknowledgments

I would like to acknowledge and gratefully thank everybody who added their own individual and important part to a successful completion of this work.

Special thanks go to Prof. Kenneth MacKenzie for his outstanding supervision, time consuming support, advice, understanding, sharing his knowledge and also for his personal contact and off-topic conversations. Further thanks go to Aileen MacKenzie, his better half; they were both responsible for my great time during my stay in New Zealand, and also for an easy going start just after my arrival in its capital Wellington.

First contact with Kenneth MacKenzie was initiated by Dr. Martin Schmuecker (DLR - German Aerospace Center); he also supported and advised during this project from overseas. Without him, I would have never made my way to the Victoria University to carry out this project.

Further thanks go to Industrial Research Ltd. (IRL) for providing funding and facilities for this research project through a sub-contract from the Foundation for Research, Science and Technology.

Much appreciated was the input of Ross Fletcher (IRL), his support, advice, encouragement, ideas and the carrying out of the strength measurements, but also that he was always available for a laugh and a chat.

Thanks also for solving language difficulties and for voluntarily proof-reading of this work.

Without the great and warmhearted support of Teresa Gen (VUW) it would have almost been impossible to synthesise the SBF. Thanks are due to her for good times in her lab.

SEM and EDS imaging was carried out with the first-class guidance of David Flynn.

I also like to grateful acknowledge Prof. Mark Smith and Dr. Alan Wong from the University of Warwick (UK) who kindly carried out the natural abundance ^{43}Ca MAS NMR spectroscopy.

I shall not forget the staff of the IRL ceramics group, especially Martin Ryan, and all the other staff-members and students of the Victoria University of Wellington too numerous to name individually, who were also involved in making this work a success.

Last but not least, I wish to give special thanks to my parents. Without their encouragement and extraordinary support from Germany, I would have never started and finished this degree.

Contents

Contents	vii
List of Figures	xiii
List of Tables	xvii
1 Introduction	1
2 Literature review	3
2.1 What are geopolymers?	4
2.1.1 Characteristics of geopolymers	7
2.1.2 Benefits of geopolymers	10
2.2 History and Applications	10
2.2.1 History of geopolymers	10
2.2.2 Geopolymer applications and research	10
2.3 Bio-Materials	12
2.3.1 Bioinert materials	13
2.3.2 Resorbable biomaterials	13
2.3.3 Porous Biomaterials	14
2.3.4 Bioactive Materials	14

CONTENTS

2.4	Geopolymers as biomaterials	15
2.4.1	Current State of Art	15
2.5	Project Aims	19
3	Experimental	23
3.1	Introduction	24
3.1.1	Reagents	24
3.2	Preparation of raw materials	24
3.3	Sample Preparation	25
3.3.1	Sample formulation	25
3.4	Synthesis of the geopolymer specimens	27
3.4.1	Preparation of the moulds	27
3.4.2	Mixing and curing of the geopolymers	28
3.5	Heat-treatment of geopolymers	29
3.6	In-Vitro Studies	31
3.6.1	Synthesis of simulated body fluid (SBF)	31
3.6.2	In vitro experiments	33
4	Characterisation Methods	35
4.1	X-ray Diffractometry	36
4.1.1	Introduction	36
4.1.2	Theoretical background	36
4.1.3	XRD apparatus	38
4.1.4	Sample preparation	39
4.1.4.1	Monolithic sample preparation	39
4.1.4.2	Powder sample preparation	40
4.2	Nuclear Magnetic Resonance Spectroscopy	41

CONTENTS

4.2.1	Introduction	41
4.2.2	Sample preparation	43
4.2.3	NMR spectrometer	43
4.3	Scanning Electron Microscopy	45
4.3.1	Secondary electron imaging	47
4.3.2	Backscattered electron imaging	47
4.3.3	SEM/ EDS apparatus	48
4.3.4	Sample preparation	49
4.4	Compression Testing (Brazil Test)	50
4.4.1	Introduction	50
4.5	Inductively Coupled Plasma	53
4.6	pH studies	55
5	Results and Discussion	57
5.1	Strength measurement results	58
5.2	XRD results	63
5.2.1	XRD patterns of the raw materials	63
5.2.2	Reference geopolymer	67
5.2.3	Calcium hydroxide geopolymers	68
5.2.4	Calcium silicate geopolymers	73
5.2.5	Calcium phosphate geopolymers	75
5.3	MAS NMR results	79
5.3.1	²⁷ Al and ²⁹ Si MAS NMR results	79
5.3.1.1	Reference geopolymer	79
5.3.1.2	Calcium hydroxide geopolymers	82
5.3.1.3	Calcium silicate geopolymers	86

CONTENTS

5.3.1.4	Calcium phosphate geopolymers	90
5.3.2	³⁴ Ca MAS NMR of calcium phosphate geopolymers	96
5.4	Alteration of the pH of the SBF	98
5.4.1	Behaviour of the reference and calcium phosphate geopolymers in SBF	99
5.4.2	Behaviour of the calcium hydroxide geopolymers in SBF	101
5.4.3	Behaviour of the calcium silicate geopolymers in SBF	102
5.5	ICP analysis of the SBF after exposure of the geopolymers . .	105
5.5.1	Phosphorus analysis	106
5.5.2	Aluminium analysis	108
5.5.3	Calcium analysis	110
5.5.4	Silicon analysis	112
5.5.5	Potassium analysis	114
5.6	SEM results	116
5.6.1	Reference geopolymer	117
5.6.1.1	Before SBF exposure	117
5.6.1.2	After SBF exposure	121
5.6.2	Calcium hydroxide geopolymer	125
5.6.2.1	Before SBF exposure	125
5.6.2.2	After SBF exposure	128
5.6.3	Calcium silicate geopolymer	132
5.6.3.1	Before SBF exposure	132
5.6.3.2	After SBF exposure	137
5.6.4	Calcium phosphate geopolymer	142

CONTENTS

5.6.4.1	Before SBF exposure	142
5.6.4.2	After SBF exposure	147
6	Conclusions	153
6.1	Future work	157
	Bibliography	159

List of Figures

2.1	(Poly-)sialate structural units	5
2.2	(Poly-)sialate network structures	6
2.3	Typical XRD spectrum of a geopolymer	7
2.4	Geopolymer applications	9
2.5	Geopolymer implants	18
3.1	Geopolymer sample	29
4.1	X-Ray diffraction by lattice planes	37
4.2	NMR: Fourier transformation of FID to frequency domain . .	42
4.3	Chemical shifts of ^{29}Si and ^{27}Al NMR	44
4.4	Test setup for diametral compression testing	51
4.5	DCT-tesing, requirements on the sample	52
4.6	Emission of electromagnetic radiation	53
4.7	ICP-AES process steps	54
5.1	XRD pattern of calcium phosphate	63
5.2	XRD pattern of calcium silicate	64
5.3	XRD pattern of calcium hydroxide	65
5.4	XRD of halloysite before and after dehydroxylation	66

LIST OF FIGURES

5.5	XRD: reference geopolymer before and after heating	67
5.6	XRD: Ca-hydroxide geopolymer before and after heating . .	68
5.7	XRD: Ca-hydroxide geopolymer, unheated, before and after SBF exposure	70
5.8	XRD: Ca-hydroxide geopolymer, 550°C, before and after SBF exposure	71
5.9	XRD: Ca-hydroxide geopolymer, 600°C, before and after SBF exposure	72
5.10	XRD: Ca-silicate geopolymer before and after heating	73
5.11	XRD: Ca-silicate geopolymer, 600°C, before and after SBF exposure	74
5.12	XRD: Ca-phosphate geopolymer before and after heating . .	75
5.13	²⁷ Al MAS NMR, reference geopolymer	79
5.14	²⁹ Si MAS NMR, reference geopolymers, unheated	80
5.15	²⁹ Si MAS NMR, reference geopolymer, 550°C	81
5.16	²⁷ Al MAS NMR, Ca-hydroxide geopolymer	82
5.17	²⁷ Al MAS NMR, Ca-hydroxide geopolymer, 550°C	83
5.18	²⁹ Si MAS NMR, Ca-hydroxide geopolymer	84
5.19	²⁹ Si MAS NMR, Ca-hydroxide geopolymer, 550°C	85
5.20	²⁷ Al MAS NMR, Ca-silicate geopolymer	86
5.21	²⁷ Al MAS NMR, Ca-silicate geopolymer, 550°C	87
5.22	²⁹ Si MAS NMR, Ca-silicate geopolymer, 550°C	88
5.23	²⁹ Si MAS NMR, Ca-silicate geopolymer, 600°C	89
5.24	²⁷ Al MAS NMR, Ca-phosphate geopolymer	90
5.25	²⁷ Al MAS NMR, Ca-phosphate geopolymer, 550°C	91
5.26	²⁹ Si MAS NMR, Ca-phosphate geopolymer	92

LIST OF FIGURES

5.27	²⁹ Si MAS NMR, Ca-phosphate geopolymer, 550°C	93
5.28	²⁹ Si MAS NMR, Ca-phosphate geopolymer, 600°C	94
5.29	⁴³ Ca MAS NMR, Ca-phosphate geopolymers before and af- ter SBF exposure	97
5.30	pH results, exposure of reference geopolymers	99
5.31	pH results, exposure of Ca-phosphate geopolymers	100
5.32	pH results, exposure of Ca-hydroxide geopolymers	101
5.33	pH results, exposure of Ca-silicate geopolymers	102
5.34	ICP: P content in SBF	106
5.35	ICP: Al concentration in SBF	108
5.36	ICP: Ca concentration in SBF	110
5.37	ICP: Si concentration in SBF	112
5.38	ICP: K concentration in SBF	114
5.39	SEM: reference geopolymer, x1000, before SBF exposure . . .	117
5.40	SEM: reference geopolymer, x10k, before SBF exposure	118
5.41	SEM: reference geopolymer, x30k, before SBF exposure	119
5.42	EDS: reference geopolymer, 600°C, before SBF exposure . . .	120
5.43	SEM: reference geopolymer, x550, after SBF exposure	121
5.44	SEM: reference geopolymer, x5k, after SBF exposure	122
5.45	SEM: reference geopolymer, x20k, after SBF exposure	123
5.46	EDS: reference geopolymer, 600°C, after SBF exposure	124
5.47	SEM: Ca-phosphate geopolymer, x550, before SBF exposure .	125
5.48	SEM: Ca-phosphate geopolymer, x15k, before SBF exposure .	126
5.49	EDS: Ca-hydroxide geopolymer, 600°C, before SBF exposure	127
5.50	SEM: Ca-hydroxide geopolymer, x4k, after SBF exposure . .	128
5.51	SEM: Ca-hydroxide geopolymer, x20k, after SBF exposure . .	129

LIST OF FIGURES

5.52	EDS: Ca-hydroxid geopolymer, 600°C, after SBF exposure . . .	130
5.53	SEM: Ca-silicate geopolymer, x2k, before SBF exposure	132
5.54	SEM: Ca-silicate geopolymer, x9.5k, before SBF exposure . . .	133
5.55	SEM: Ca-silicate geopolymer, x20k, before SBF exposure	134
5.56	EDS: Ca-silicate geopolymer, 600°C, before SBF exposure . . .	135
5.57	SEM: Ca-silicate geopolymer, x4k, after SBF exposure	137
5.58	SEM: Ca-silicate geopolymer, x11k, after SBF exposure	138
5.59	SEM: Ca-silicate geopolymer, x20k, after SBF exposure	139
5.60	EDS: Ca-silicate geopolymer, 600°C, after SBF exposure	140
5.61	SEM: Ca-phosphate geopolymer, x1000, before SBF exposure	142
5.62	SEM: Ca-phosphate geopolymer, x10k, before SBF exposure .	143
5.63	SEM: Ca-phosphate geopolymer, x30k, before SBF exposure .	144
5.64	EDS: Ca-phosphate geopolymer, 600°C, before SBF exposure	145
5.65	SEM: Ca-phosphate geopolymer, x1000, after SBF exposure .	147
5.66	SEM: Ca-phosphate geopolymer, x10k, after SBF exposure . .	148
5.67	SEM: Ca-phosphate geopolymer, x15k, after SBF exposure . .	149
5.68	EDS: Ca-phosphate geopolymer, 600°C, after SBF exposure .	150

List of Tables

3.1	Geopolymer mixtures	26
3.2	Element ratios of the geopolymer mixtures	27
3.3	Molar ratios of the geopolymer mixtures	27
3.4	Heat-treatment schedules	30
3.5	Ingredients of the SBF	32
4.1	ICP-AES detection limits	55
5.1	Tensile strength measurement results	58
5.2	Tensile strength comparison with biomaterials	61
5.3	Bioactive phases in geopolymers after SBF exposure	78
5.4	⁴³ Ca MAS NMR results of Ca-phosphate geopolymers	96
6.1	Summary of the geopolymer properties	155

Chapter 1

Introduction

Geopolymers are materials based on a pure aluminosilicate system activated with strong alkali. These materials consist of tetrahedral aluminate and silicate units based on (poly-)sialates (shorthand for silicon-oxo-aluminates). A comprehensive overview of these group of materials was recently given by MacKenzie [1]. The expression “geopolymer” was proposed by Davidovits in the 1980’s due to their setting mechanism, a polycondensation process under alkaline conditions, similar to organic polymers. Geopolymers have ceramic-like properties but attain their strength and durability at ambient temperatures [2].

Geopolymers are presently used for a variety of applications including heat resistant materials and fire protection. Specialist geopolymers have been developed as biomaterials to replace/ repair damaged animal bones [3] [4].

The term bioactivity applies to biomaterials capable of forming the bone-like phase hydroxyl apatite by interaction with blood plasma. This can be simulated by exposing such materials to simulated body fluid (SBF) under laboratory conditions [5].

This project seeks to explore the concept of the bioactive geopolymer by introducing calcium-based compounds into a geopolymer matrix in order to promote bioactivity.

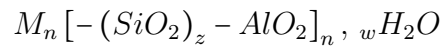
Chapter 2

Literature review

2.1 What are geopolymers?

According to Davidovits [2], the formation of geopolymers is a polymerisation process similar to the polycondensation of an organic polymer, and therefore he named the process “geopolymerisation”. Since geopolymerisation is exothermic and generally takes place at ambient temperatures, the synthesis of inorganic polymers does not require additional energy to achieve good mechanical properties. However, special conditions such as a controlled water content and high alkalinity are required to attain strength and durability.

During the setting process, (poly-)sialates are formed having a random 3-D network made of tetrahedral Si-O and Al-O units with Al³⁺-ions in IV-fold coordination. This produces a negative charge, balanced by alkali-ions (potassium or sodium) located in the network cavities [1], [2]. The empirical formula of a (poly-)sialate is:



in which “M” stands for a monovalent cation (e.g. potassium, sodium), “n” indicates the degree of polycondensation and “z” can take values of 1, 2 or 3.

Some (poly-)sialate structures are shown schematically in Figures 2.1 and 2.2 ([1], [6]).

Depending on the setting conditions, geopolymers can be crystalline or amorphous when cured under hydrothermal conditions or at ambient temperatures respectively [2].

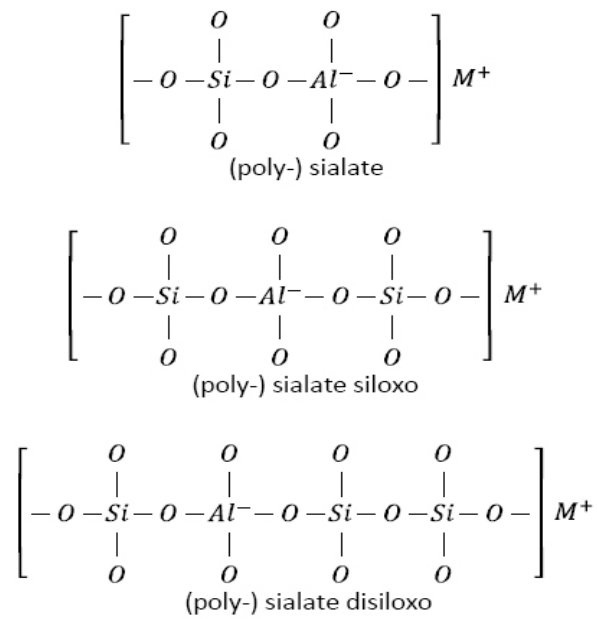


Figure 2.1: (Poly-)sialate structural units [1]

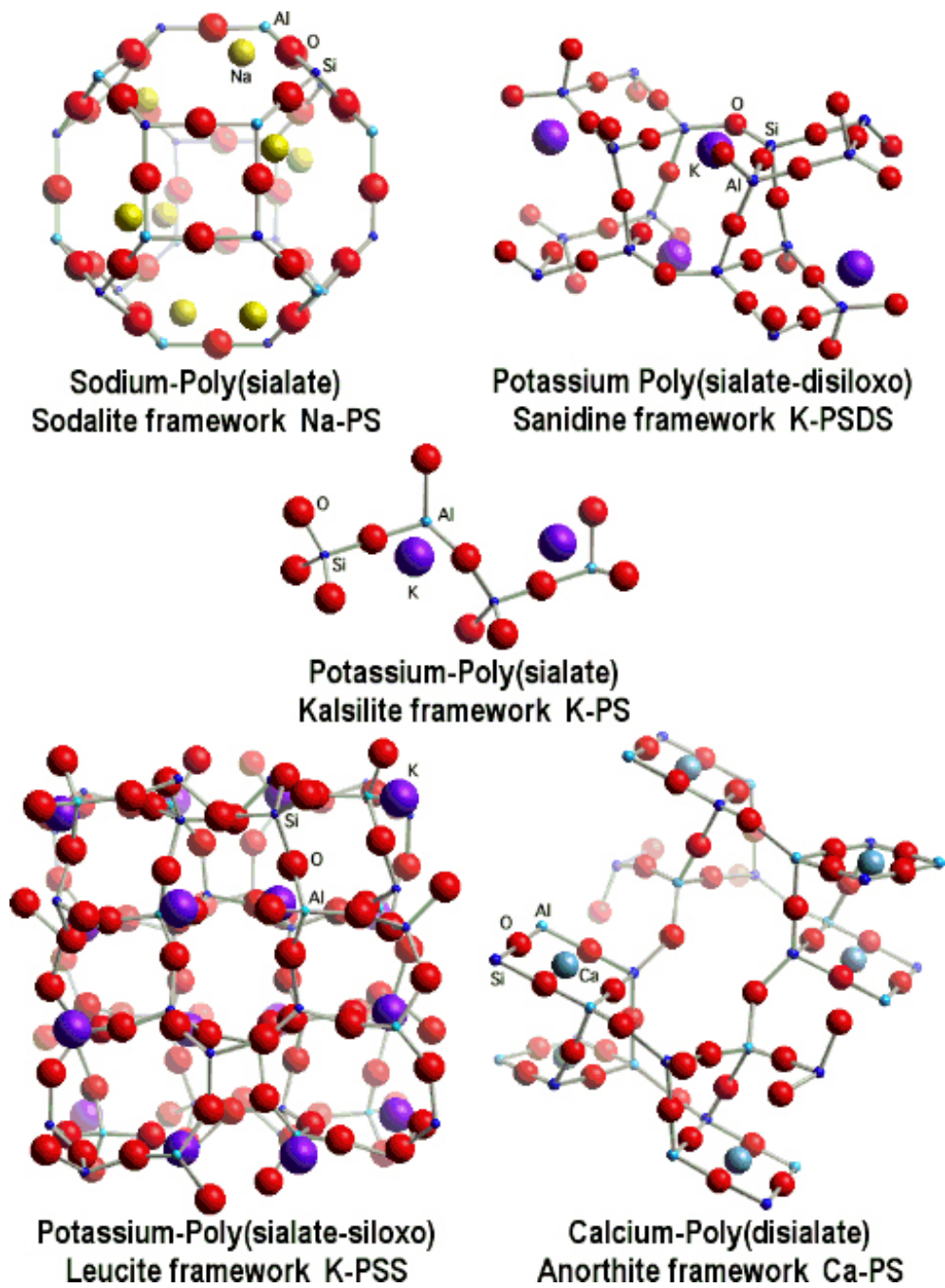


Figure 2.2: (Poly-)sialate network structures [6]

2.1.1 Characteristics of geopolymers

A typical characteristic of geopolymers cured at ambient temperatures is that they are x-ray amorphous. The x-ray diffraction patterns of well-cured geopolymers do not normally show sharp peaks but present a large hump at around 30 degrees $/2\theta$. A typical pattern is shown in Figure 2.3. The peak labelled "Q" is a quartz peak, from an impurity in a reactant.

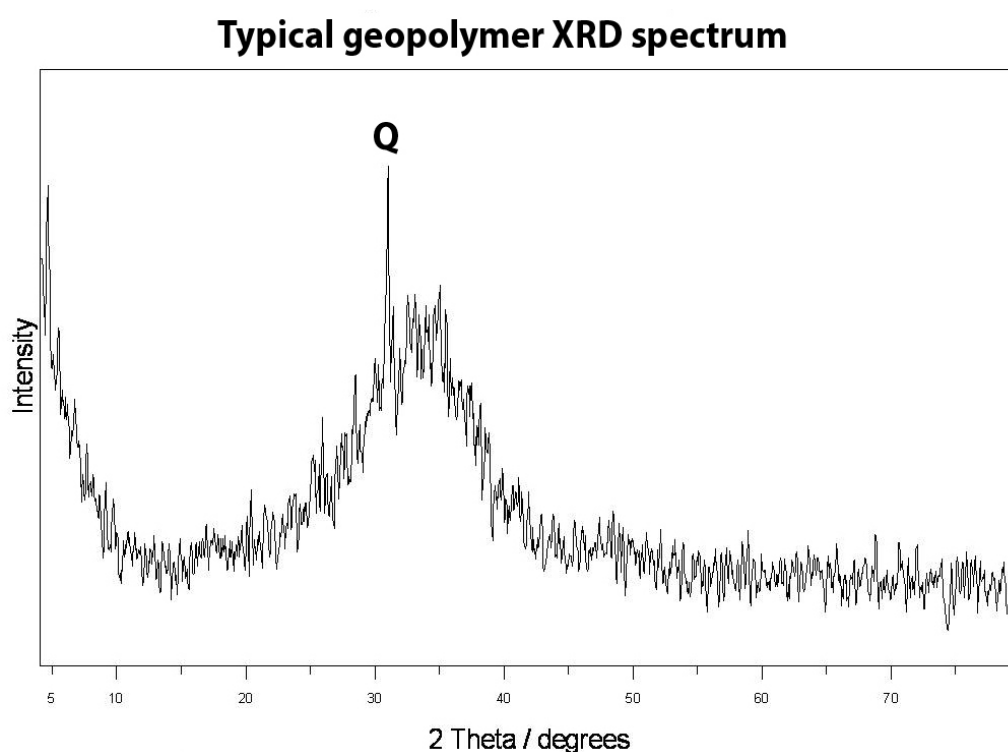


Figure 2.3: *Typical XRD spectrum of a geopolymer, Q = quartz impurity*

Further, silicon and aluminium in a well cured inorganic polymer must be in 4-fold coordination. Since XRD cannot determine the coordination state of atoms in amorphous materials, solid state nuclear magnetic resonance spectroscopy with magic angle spinning (MAS NMR) must be used

to provide this information [7].

Geopolymers can be produced with various microstructures in relation to the Al:Si ratio; high aluminium contents lead to three-dimensional structures and high silicon contents lead to two dimensional cross-linked structures. Because of the various microstructures, different mechanical and physical properties can be achieved. Hence, geopolymers are useful for a wide range of applications (Fig. 2.4), e.g. as heat resistant materials (up to 1400°C) [6, 8, 9] and sealants or encapsulation materials. Moreover, because of their properties, geopolymers could also provide a good alternative to conventional plastics or cements [2, 10]. A more recent approach is the application of geopolymers in the field of biomaterials which were successfully implanted in animals [3, 4, 11].

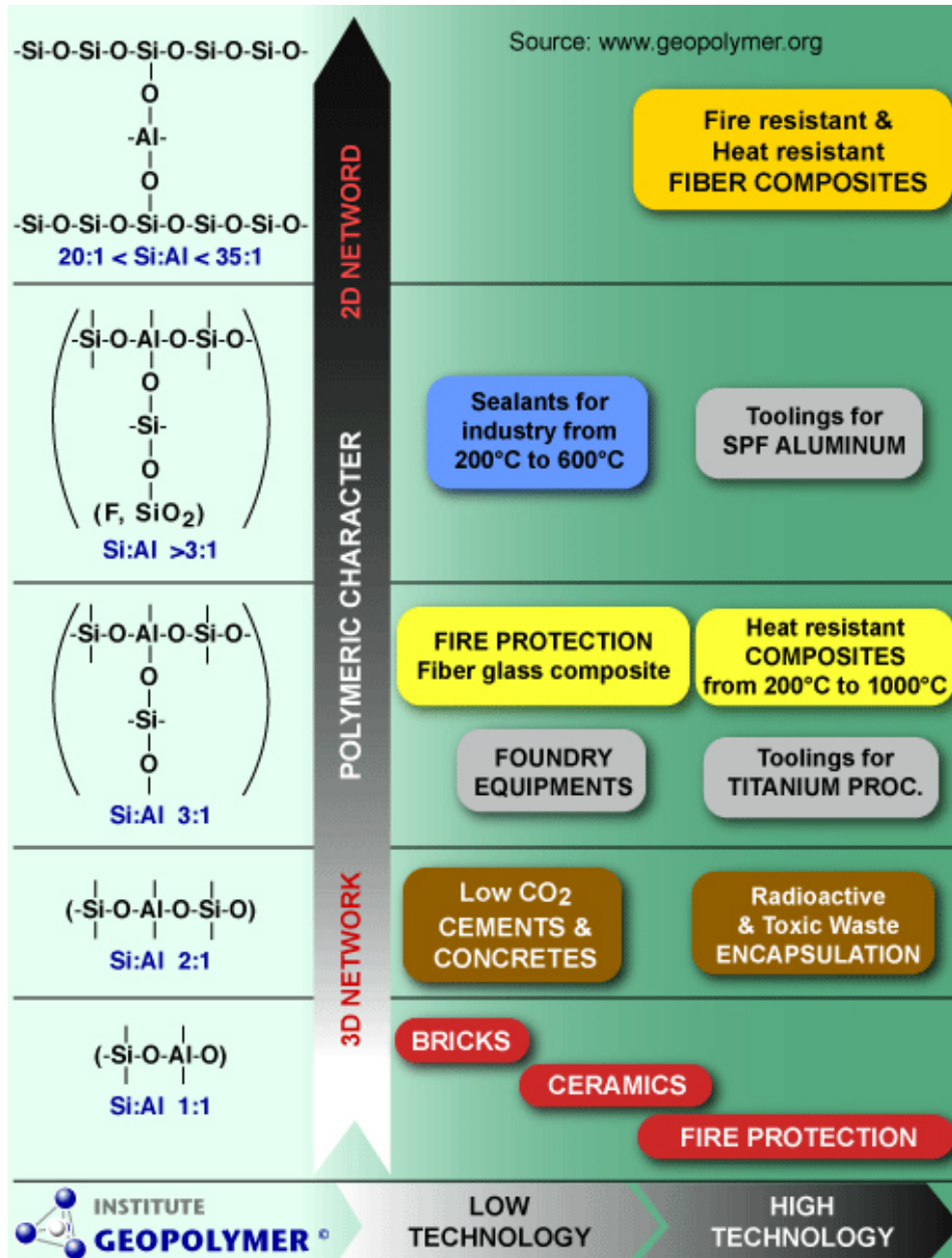


Figure 2.4: Applications of geopolymers related to their network structure [6]

2.1.2 Benefits of geopolymers

The synthesis of geopolymers does not create greenhouse gases and because of this energy efficiency, inorganic polymers have become increasingly attractive. This increasing attraction is not just because of the above-mentioned aspects but also because it is generally possible to produce these products using recycled materials. This is another benefit in the context of the current problems of global warming and environmental protection.

2.2 History and Applications

2.2.1 History of geopolymers

The usage of geopolymers may go back to the Romans and Egyptians, and probably further back to the Babylonians, as they used inorganic compounds mixed with organic matter to produce strong building materials. While there are still disagreements whether or not the Egyptian pyramids were made of geopolymers, it has been confirmed that the network structure of the building blocks matches the definition of inorganic polymers [12].

2.2.2 Geopolymer applications and research

A major application, and probably one of the most important ones for geopolymers is fire protection.

Davidovits and Latapie started extensive research in non-flammable materials after some disastrous fires in France between 1970 and 1973 [10]. They rediscovered the possibility of making ceramic-like materials without firing at temperatures below 100°C which had already been observed in the 1930's and reinvented in 1970 by Olsen and Berg et. al, [10] (although without any industrial success).

Due to the intensive research of Davidovits and Legrand, the first fire resistant building materials, containing chipboard panels with a geopolymer coating, were produced in the mid 1970's, thus initiating the geopolymer industry [10]. Ongoing research led to improvements in the materials and broadened their applications within the field of heat protection.

A wider range of applications and improvements were made due to continuous research in the geopolymers field. The properties of geopolymers were exploited, drawing on the fact that they are not only heat resistant but are also highly porous and therefore light weight. Using this knowledge and applying it to the ceramics field, composite geopolymeric materials were developed with improved specific properties, resulting in more technical or advanced applications, for example aeronautical applications, wall insulation for cabins and storage bins, wire insulation and automotive parts [10].

Beside these "high-tech" applications, special geopolymer concretes have been used for repairing runways or motorways because they set and harden quickly and develop a high compressive strength within four hours [10].

Likewise, geopolymers are used for structural and building applications. Flexible inorganic polymer fibre composites can be used to repair

structures made of stone, bricks or concrete. Such fibre composites are already used in Japan and America to reinforce existing bridges and other buildings but are also used in new constructions in hazardous areas [10]. Another important application is waste encapsulation. It has been reported that it is possible to synthesise geopolymers which trap heavy metals and radioactive materials in their network structures (see also Figure 2.4 [6] [13] [14]).

2.3 Bio-Materials

A general definition of biomaterials is: *“Any substance (other than a drug) or combination of substances, synthetic or natural in origin, which can be used for any period of time, as a whole or as a part of a system which treats, augments or replaces any tissue, organ or function of the body.”* And: *“A non-viable material used in a medical device intended to interact with biological systems.”* [15].

The development of materials suitable for imbedding in humans or animals is one of the recent human discoveries. Since such materials were introduced, life has become more comfortable for e.g. bone fracture patients or patient requiring joint replacements (e.g. hip or shoulder) [16]. Beside metals and metal-composites, ceramics and ceramic-composite materials play an important role for such applications and are called “bio-ceramics”. Larry Hench from the University of Florida is one of the best-known scientists involved in inventing bio-ceramics. He discovered numerous ceramics and glasses usable as implants in living tissue. Today, a wide range of his developments are used in operating theatres including the materials Bioglass® and Ceravital® [17]. During the last decade, attempts have been

made to create bio-compatible geopolymers to provide inorganic materials other than ceramics, for use as implants. All bio-ceramics have to form a stable interface with the living host tissue [16] [17]. Presently, there are four types of known bio-ceramics.

2.3.1 Bioinert materials

Bioinert materials have the characteristic that they are not biologically or chemically bonded, but physically attached to the living tissue. For this reason there may be movement between the implant and the surrounding tissue which leads to the development of unattached fibrous capsules in both soft and hard tissues. Movement of the implant-tissue interface may lead to malfunction of the implant or the interface-tissue, or both. Due to this relative movement, and depending on the material, the thickness of the non-adherent tissue layer alters significantly. Hence, it is essential that the implants are implanted with the correct load rates and possess suitable properties (e.g. elastic modulus) otherwise clinical failures are likely to occur, e.g. weakening of the implant, stress shielding etc. [16][17].

2.3.2 Resorbable biomaterials

The purpose of resorbable implants is to dissolve and be replaced by natural host tissue over time. One advantage is that the body is able to repair itself and reconstruct cell populations, and no artificial substances remain in the body. The use of resorbable materials as implants leads to a very thin or non-existent interface between implant and tissue. While these materi-

als are relatively weak and therefore limited in their application, they are excellent when only short term performance and low strength is required. Calcium phosphate materials are especially successful for such purposes, e.g. as implants in the jaw or forehead. Resorbable materials act as a support and help to regenerate the damaged body in natural way [16][17].

2.3.3 Porous Biomaterials

The use of porous materials provides the possibility for the host tissue to grow into the implant surface or even throughout the whole sample. In effect, this causes a larger interfacial connection area which results in a stronger movement resistance, and therefore reduction of the relative motion between implant and tissue. The interface is established by the growth of living tissue into the pores of the implant and is often called “biological fixation”. This type of interfacial connection can manage more complex stress patterns in contrast to implants attaining “morphological fixation”. However, there are limitations and certain requirements for these materials, such as the specific pore size necessary for the ingrowth of the living host tissue. Further, interfacial movement cannot be accommodated as it may cut off the blood supply and cause tissue death and inflammation and destruction of the interfacial connection [16] [17].

2.3.4 Bioactive Materials

The tissue response of this group of biomaterials when exposed to simulated body fluid (SBF) or implanted in living tissue ranges between that of

resorbable and bioinert materials. The general definition of bioactive materials is as follows: *“A bioactive material is one that elicits a specific biological response at the interface of the material, which results in the formation of a bond between the tissue and the material.”*[16]

Known bioactive materials form a biologically active hydroxyl-carbonate apatite layer (HCA) $[(Ca, Mg, Na)_{10}(PO_4, CO_3)_6(OH)_2]$ that bonds to hard and soft tissue. Substances with bioactive behaviour include calcium silicate, calcium hydroxide $(Ca(OH)_2)$ or tri-calcium phosphate $(Ca_3(PO_4)_2)$. This particular bond can also be achieved using bioactive glasses, bioactive glass-ceramics or dense hydroxyl apatite. The important point is that the HCA phase thus formed is equivalent to bone, both chemically and morphologically. The adherent interface formed between implant and surrounding tissue is very strong and can withstand significant mechanical forces. Often the adhesive strength of the interface has an equal or higher cohesive strength than the implant or the tissue. For that reason, failures are likely to occur either in the tissue or the implant material rather than in the interface [16] [17].

2.4 Geopolymers as biomaterials

2.4.1 Current State of Art

Calcium phosphate cements have been used for bone filling purposes for more than 50 years. Such cements are similar to geopolymers in terms of the setting process, which does not involve heat-treatment. In addition, these cements may be bioactive as well as biodegradable, which means

that they may be replaced by natural bone. However, calcium phosphate cements do not have good mechanical properties and can only be used under low load conditions, such as the forehead or jaw [18].

Relatively new products in the field of biomaterials applications are materials based on amorphous silicate network structures. These network structures are similar to those of inorganic polymers, suggesting that they may well be classified as such. Compared to calcium phosphate cements, geopolymers have better mechanical properties and may be used where load resistance is required. However, as yet, they have only restricted uses in biomedical applications because of their aluminium content and the possibility of leaching out “free” aluminium. However, Yap et al. [19] reported that the release of aluminium ions is controversial and that low concentrations of aluminium can actually be beneficial and stimulate the proliferation of osteoblasts and new bone formation, and for determining the in-vivo bio-compatibility. However, Yap [19], Geyer [20] and Hantson [21] reported that high concentrations of aluminium (< 2ppm) led to brain diseases. For safety, the release of aluminium-ions should be minimized or suppressed. In addition, geopolymers are very alkaline (pH 10 - 14) by contrast to the pH of the body (7 - 7.5) and therefore difficult to use as biomaterials.

Nevertheless, current research shows that it is possible to use geopolymers as biomaterials and these have been successfully implanted in living tissue [3] [4] [11] .

In 2005, Oudadesse et al. [11] investigated a standard geopolymer such as used for applications such as fireproof interior panels or marine structural composites. This had a high Si:Al ratio to minimise the aluminium

content. No additives were used to make the inorganic polymers bioactive or biocompatible in any way. Additionally, heat processing at temperatures between 250°C and 625°C was used to reduce the geopolymer alkalinity and increase its porosity. “In-vitro” and “in-vivo” studies were carried out using a geopolymer heated to 500°C, since this showed the best results in terms of pH and the most strongly bonded aluminium in the network structure. The studies were successful with regard to the stability of the material both after exposure to SBF and also after implantation in living tissue. However, the geopolymers chosen may not be bioactive, as no growth of HCA or other bioactive phases was reported [11].

Martin et al. [4] used geopolymer compositions which provided good mechanical properties but contained additional substances which are well known for their bio-compatibility, namely hydroxyl apatite (HA) and tricalcium phosphate (TCP). The aim was to create porous geopolymers compatible with living tissue. Pure HA and TCP as well as a mixture of both were used as additives in the aluminium silicates for the experiments. To increase the porosity and to lower the sample pH to about 7, the samples were heat treated to 500°C. They were later implanted in rabbits and left for various times to analyse the behaviour of the materials when exposed to living tissue. All of the synthesised geopolymers were accepted by the organism without causing inflammation or encapsulation effects. Bonding to bone was inferred from the penetration of bone into the implants. Figure 2.5 shows an example of in vivo studies; the top image presents the implant immediately after implantation, the bottom image 30 days after implantation [4].

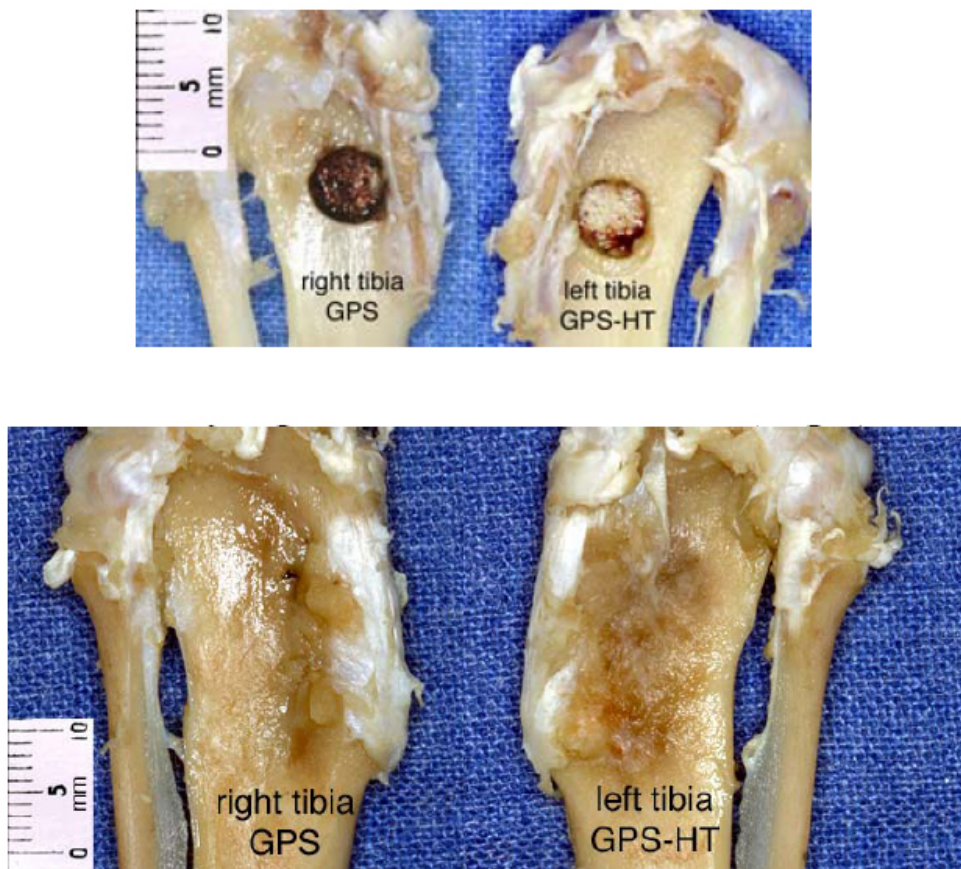


Figure 2.5: Geopolymer implants: 0 (top) and 30 days (bottom) after implantation [4]

More recent studies carried out by Oudadesse et al. [3] examined the behaviour of bioactive geopolymers. These focussed on geopolymer compositions with a zeolite-like structure and used hydroxyl apatite (HA) and tri-calcium phosphate (TCP) or a mixture of both as additives to make them bio-compatible. Aluminosilicates were mixed and synthesised in three steps:

1. Potassium silicate solution was depolymerised by adding potassium hydroxide

2. Dehydrated kaolinite was mixed with this solution, distilled water was added to optimise homogenisation. This mixture was left at -10°C for 24 hours in a sealed mould to produce a polycondensed aluminosilicate.
3. Hydroxyl apatite, tri-calcium phosphate or biphasic HA-TCP was added to the geopolymer mix, homogenised and re-sealed for curing.

The highly alkaline specimens were heat treated to 250°C and 500°C to reduce their pH values and to create a certain degree of porosity. "In-vitro" studies were carried out to determine the material behaviour when exposed to liquids, and "in vivo" experiments were executed to check whether or not the materials are suitable as biomaterials in terms of leaching out of aluminium and acceptance by the host tissue. Oudadesse et al. reported that they successfully made materials which were accepted by host bone and provided good mechanical properties. Further, neither inflammation or encapsulation of the surrounding tissue occurred nor leaching out of harmful elements from the sample was recorded [3].

In conclusion, current research suggests that it is possible to synthesise materials with biocompatible behaviour suitable as implants in living tissue.

2.5 Project Aims

This project is focussed on synthesising bio-geopolymer(s) as potential bioactive materials based on previous studies and suggestions by Prof.

Kenneth MacKenzie (supervisor of this work) [22]. By combining the good mechanical properties of inorganic polymers with the bioactive behaviour of substances such as calcium hydroxide, nano structured calcium silicate and calcium phosphate, we can develop a durable implant.

In contrast to previous experiments carried out by Oudadesse [3, 11] and Martin [4], this work aims to create an *in-situ* geopolymer containing calcium and possibly phosphorus, synthesised in a one-step process rather than in two or more steps. It has been reported that calcium and phosphorus can be successfully incorporated in inorganic polymers without disturbing the typical properties of a true geopolymer (producing an amorphous network structure as well as aluminium and silicon in tetrahedral sites) [22] [23].

Of the two geopolymerisation activators, potassium and sodium, potassium provides the lowest alkalinity (approximately pH 12), although this is still too high for a biological system. But it is possible to lower the alkalinity using the least possible potassium hydroxide necessary for the geopolymerisation process to occur. Further, heat-treatment of geopolymers above 250°C has been reported to lower the pH significantly. This thermal treatment causes a dehydroxylation of the material. Subsequently, a diminution of the quantities of protons occurs that reduces the alkalinity. As a side effect the aluminium can be stabilised in the network structure [11], and may therefore also be used.

The Al:Si ratios in a geopolymer can vary widely (Figure 2.4), thus a geopolymer composition with low aluminium content will be chosen to minimise the risk of releasing aluminium.

To verify that the typical geopolymer characteristics and properties are

present, several analysis methods will be used, including x-ray diffractometry (XRD), tensile strength measurements (Brazil test method), solid state ^{27}Al , ^{29}Si and ^{43}Ca nuclear magnetic resonance spectroscopy with magic angle spinning (MAS NMR) and scanning electron microscopy (SEM) with energy dispersive spectroscopy (EDS).

To determine whether or not the synthesised samples are bioactive and if the alkalinity meets the requirements, "in vitro" experiments in simulated body fluid will be performed viz. pH measurements, SEM, EDS, XRD and inductively coupled plasma (ICP), analysis of the soaking solution.

The present study will attempt to synthesise bioactive geopolymers that contain 10 wt% of bioactive substances in the bulk material. The added components will be calcium hydroxide ($\text{Ca}(\text{OH})_2$), nano structured calcium silicate ($\text{CaSi}_{1.67}\text{O}_{3.75}$) or calcium phosphate ($\text{Ca}_3(\text{PO}_4)_2$), giving geopolymers that harden and cure.

Studies have shown that it is possible to make aluminosilicate geopolymers containing tetrahedral phosphate [24]. Further, it is possible to put calcium into aluminosilicate geopolymers, either as the hydroxide, phosphate or as an amorphous silicate. ^{43}Ca MAS NMR studies have been carried out on these compounds [24]. The calcium phosphate geopolymer develops HCA precursors after 1 and 7 days exposure to SBF [22].

Studies of aluminosilicate materials as potential implants are only in their early stages but the initial results are sufficiently promising to encourage further research with the expectation that materials with good bioactivity might be produced [4].

Chapter 3

Experimental

3.1 Introduction

Synthesis of geopolymers involves material preparation and begins with the determination of suitable geopolymer formulations. This chapter describes the different preparation steps in detail.

3.1.1 Reagents

Reactants for the preparation of the inorganic polymers are listed below.

- aluminosilicate raw material (halloysite) (IMERYS, PREMIUM)
- calcium phosphate (BDH reagent grade)
- calcium hydroxide (BDH reagent grade)
- nano structured calcium silicate ($\text{CaSi}_{1.67}\text{O}_{3.75} \cdot 3\text{H}_2\text{O}$) (VUW, Patent-No: WO/2006/078176)
- potassium hydroxide (KOH) (BDH reagent grade)
- potassium silicate solution (K66, INEOS Silicas, Ltd. UK)

3.2 Preparation of raw materials

Thermal pre-treatment of halloysite is necessary to secure proper curing behaviour and the formation of true geopolymers. This method was used because it gives the best results compared with other treatments reported elsewhere [25]. Calcination of the halloysite was carried out in heat resistant containers in an electric furnace (Arum Products NZ). The containers

were not completely filled and were also loosely covered to minimise the effects of explosive loss of water.

Dehydroxylation was carried out at 600°C for 12 hours at a heating rate of 5 °C/min followed by unforced cooling to room temperature.

To ensure that only the fine fraction of the powder was used in the geopolymer synthesis for good homogeneity, the bigger grains were separated using an automatic sieve shaker (Retsch, Germany) and two sieves (500 and 180 microns).

3.3 Sample Preparation

3.3.1 Sample formulation

To prepare geopolymers that set and harden, attention must be paid to the ratios of Al : Si, K : Si and H₂O : K₂O. A geopolymer formulation which had been successfully used for previous in-vitro studies was used as a basis [22]. This material was reproduced, then the amount of alkaline compounds was progressively reduced to a minimum to produce a material with low alkalinity. Attempts were made to use less water and the least potassium hydroxide necessary to produce a geopolymer with good strength.

The actual synthesis of the inorganic polymer samples is described in detail in section 3.4.

The hardness of the sample was initially tested by scratching the surface with a fingernail. The formulations soft enough to be scratched were rejected. Once a usable mix was created, it was modified further by adding

the calcium compounds (calcium hydroxide, calcium silicate and calcium phosphate). The addition of these compounds made it necessary to introduce further slight adjustments to the original formulation to produce workable compositions which set and harden. Various trial and error experiments resulted in the best working geopolymer compositions which were used for all experiments and are listed in Table 3.1.

Samples containing 10 wt% added calcium hydroxide, calcium silicate and calcium phosphate are designated N1, N6 and N13 respectively, whereas the control samples without calcium additives are labelled N11.

Table 3.1: *Geopolymer mixtures, values are wt%*

Ingredients	N1	N6	N11	N13
Halloysite	40.6	30.6	43.0	42.2
Water	20.3	33.7	19.2	17.5
Potassium hydroxide	9.1	13.1	5.9	9.0
Potassium silicate (K66)	30.0	22.6	31.9	31.3
Calcium hydroxide	10.0			
Calcium silicate		10.0		
Calcium phosphate				10.0

The corresponding element and molar ratios, can be found in Table 3.2 and Table 3.3 respectively.

Table 3.2: *Element ratios of the geopolymer mixtures*

Ratios	N1	N6	N11	N13
Si : Al	2.9	2.9	2.9	2.9
K : Si	0.6	0.9	0.4	0.5
K : Al	1.6	2.6	1.1	1.5
H ₂ O : Al	29.6	47.7	28.0	27.0

Table 3.3: *Molar ratios of the geopolymer mixtures*

Ratios	N1	N6	N11	N13
SiO ₂ : Al ₂ O ₃	3.24	3.24	3.24	3.24
K ₂ O : SiO ₂	0.26	0.42	0.19	0.25
H ₂ O : K ₂ O	18.79	18.56	24.39	17.77

3.4 Synthesis of the geopolymer specimens

3.4.1 Preparation of the moulds

The 30 mm diameter and 25 mm high cylindrical plastic moulds were thoroughly cleaned and a light coat of petroleum jelly applied to the internal surfaces. The moulds have removable bases to facilitate sample removal.

3.4.2 Mixing and curing of the geopolymers

The reagents were weighed separately using a two-place top loading laboratory balance.

Powder chemicals such as dehydroxylated halloysite and the additives were weighed first, followed by the water and potassium hydroxide (KOH). The calculated amount of distilled water was measured into a plastic beaker. The KOH was then weighed and dissolved in the water, using eye protection and latex gloves. The reaction of KOH with water produces heat which may cause boiling. After the KOH was completely dissolved, potassium silicate solution (K66) was added using a plastic pipette and the solution was stirred well. Finally, the dehydroxylated halloysite was added and stirred well to achieve a well homogenised mixture which is pourable. At this stage, the calcium-containing substances were added. Thorough mixing and homogenising was essential to distribute the additive well throughout the mixture.

The resulting liquid geopolymer mixture was poured into the greased moulds, compacted and de-aired using a sieve shaker. For large sample numbers a vibrating table was found to be useful for this task. As soon as no more bubbles appeared on the surface of the liquid mixture the moulds were put in sealed plastic bags to ensure a controlled water content for the setting process.

The sealed moulds were placed in a curing room controlled at 40°C and cured for 14 - 20 hours. The samples were then demoulded and returned to the curing room for an additional 7 - 10 days, in sealed plastic bags. A fully cured geopolymer sample is shown in Figure 3.1.



Figure 3.1: Sample of a fully cured reference geopolymer heated to 600°C compared to a New Zealand two-dollar coin

The top and bottom surfaces of the fully cured samples were ground flat and plane-parallel. These samples were the starting materials for further treatments described in the following sections.

3.5 Heat-treatment of geopolymers

Since heat-treatment of geopolymer samples is a possible means of reducing the alkalinity as mentioned in section 2.4.1, the cured samples were heated to 550°C and 600°C. The furnace was switched off and allowed to cool to room temperature with the door closed throughout.

For the heat processing, the pool of samples was divided three ways for each geopolymer composition, with one third of the samples remaining unheated. Due to variations in the compositions, some samples were found to require different heating rates to prevent cracking, but the maxi-

CHAPTER 3. EXPERIMENTAL

imum temperature remained the same for every geopolymer composition, as listed in Table 3.4.

Table 3.4: Heating schedules for heat-treatment to 550°C (top) and 600°C (bottom)

Sample	N1	N6	N11	N13	
T1 - T2 (°C)	time (min)	time (min)	time (min)	time (min)	heat rate (K/min)
RT - 100	70	70	70	70	1.1
100- 100	60	60	60	60	0.0
100 - 550	130	130	130	130	3.5
550 - 550	360	360	360	360	0.0

Sample	N1	N6	N11	N13	
T1 - T2 (°C)	time (min)	time (min)	time (min)	time (min)	heat rate (K/min)
RT - 100	70	70	70	70	1.1
100- 100	60	60	60	60	0.0
100 - 600	130	130	130	130	3.5
600 - 600	360	360	360	360	0.0

3.6 In-Vitro Studies

An accepted way to determine the bioactivity of substances is to expose them to simulated body fluid (SBF). SBF is a solution which reacts with materials to form the bone-like compound apatite $[(Ca, Mg, Na)_{10}(PO_4, CO_3)_6(OH)_2]$ [26]. The ion compositions and concentrations of SBF are chosen to be as identical to those of blood plasma as possible. Conventional simulated body fluid (1.5 SBF) was chosen because it has a very good (long term) stability at slightly elevated temperatures and is also highly active [26]. It also has the advantage that it does not form calcite when samples are exposed to it, although calcite may have already been present in some of the synthesised geopolymer samples.

Since a supplier of SBF could not be located, the SBF was synthesised, and stored according to published instructions [26] [27].

3.6.1 Synthesis of simulated body fluid (SBF)

The synthesis of the SBF requires a clean, dust free environment. Apparatus used for mixing, stirring and storage must be sterilised. The components of SBF are soluble salts and ultra pure water. Ultra pure water is demineralised water containing only H_2O that contains H^+ and OH^- in equilibrium. It is important to carefully add the ingredients in a particular order (Tab. 3.5).

Ultra-pure water in a suitable beaker is warmed to $36.5^\circ C$ and continuously stirred. The previously weighed compounds listed in Table 3.5 are carefully added one at a time and allowed to dissolve before the next

Table 3.5: *Ingredients and order of addition for 2000 ml of 1.5 SBF*

Order	Reagent	amount
0	Ultra-pure water	1500 ml
1	NaCl	23.988 g
2	NaHCO ₃	1.050 g
3	KCl	0.672 g
4	K ₂ HPO ₄ • 3H ₂ O	0.684 g
5	MgCl ₂ • 6H ₂ O	0.916 g
6	1 kmol/m ³ HCl	120 ml
7	CaCl ₂	0.834 g
8	Na ₂ SO ₄	0.214 g
9	(CH ₂ OH) ₃ CNH ₂	18.172 g
10	1 kmol/m ³ HCl	appropriate amount for adjusting pH to 7.4

is added. The pH is continuously checked using a pH meter. Addition of the tris-buffer (reagent 9) must be done little by little to avoid sudden pH increase. The pH is then adjusted to 7.4 using 1 kmol/m³ HCl delivered from a pipette. The prepared solution was transferred to a 2.0 litre volumetric flask and cooled to 20°C, then adjusted to 2000 ml using ultra-pure water and shaken well. This final solution is placed in polyethylene bottles and stored in a refrigerator at 5 to 10°C until required.

3.6.2 In vitro experiments

In vitro experiments were carried out using a temperature-controlled water bath, adjusted to $37.5^{\circ}\text{C} \pm 0.5^{\circ}\text{C}$ and checked frequently to ensure a stable temperature. No specific treatment of the samples was necessary, although it was important that they were free of dust or any other loose grinding material. The samples were placed in plastic sample jars and covered with approximately 50 ml of SBF. The containers were then closed and placed in the water bath for various times.

To determine whether the specimen had interacted with the SBF, samples of the specimen were taken out after various times and analysed. After removal from the solution, they were dried with a soft tissue and the XRD patterns of the exposed surfaces were recorded and described in section 4.1. The XRD results are reported in section 5.2.

Scanning electron microscopy (SEM) and electron dispersive spectroscopy (EDS) was also carried out using a JEOL microscope (see section 4.3) to determine alteration of the sample surface that may be undetectable by XRD. The SEM results are reported in section 5.6.

Solid state nuclear magnetic resonance spectroscopy (MAS NMR) (section 4.2) was used to monitor any changes in the ^{27}Al , ^{29}Si or ^{43}Ca environments during the in-vitro experiments.

The pH of the SBF during the experiments was recorded frequently using a portable pH-meter to determine the sample behaviour when exposed to SBF, as described in section 4.6.

Changes of the SBF composition during soaking were analysed by ICP (section 4.5) carried out by a commercial analytical laboratory.

Chapter 4

Characterisation Methods

This chapter introduces and briefly describes the analytical methods used to determine the properties of the samples e.g., strength, phase composition and structure.

4.1 X-ray Diffractometry

4.1.1 Introduction

X-ray diffractometry (XRD) is an important tool for the characterisation of crystalline materials. Using XRD, crystallographic phases can be identified and quantitatively determined in materials such as metals, clays, ceramics or mineral mixtures [28].

XRD is based on the diffraction of x-rays from crystalline phases containing long-range order; therefore it cannot be used as a characterisation method for amorphous phases with diffuse scattering patterns. Amorphous phases in such materials appear as broad humps and a raised background rather than well defined peaks. However, the presence of a broad amorphous hump allows this technique to indicate the presence of the amorphous inorganic polymers. Any partially reacted crystalline phases still present in inorganic polymers may also be detected as unusual peaks, or as peaks related to mineral phases present as impurities in the reactants.

4.1.2 Theoretical background

When an x-ray beam interacts with a crystalline substance the reflection of the beam results in a characteristic diffraction pattern of intensities at particular diffraction angles. Since each crystalline material produces its unique diffraction pattern, each crystalline phase can be identified or determined within a substance containing multiple crystalline phases. X-ray patterns of pure substances are thus like fingerprints.

XRD analysis is based on the principles of x-ray diffraction by a diffrac-

tion grating. Suitable “gratings” for x-ray beams are the planes of atoms in the crystal structures of crystalline phases. Without any diffraction effects, the incidence of a primary x-ray beam onto a sample volume would produce scattering in all directions. Diffraction redistributes intensity from the whole scattering field into distinct directions, between which the intensity drops drastically. The directions in which the reflections can be observed depend on the intervals between the lattice planes scattering x-ray beams and interference of the scattering by scattering from neighbouring lattice planes (Fig 4.1) [29].

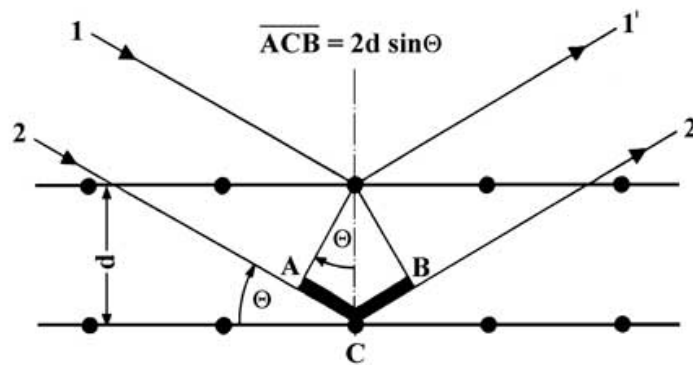


Figure 4.1: X-Ray diffraction by lattice planes [29]

Reflections can only occur where the path of the beam scattered by the lower of the two planes is longer by an integer number of wavelengths than the path length of the beam scattered by the upper plane, visualised in Figure 4.1. This is described by Bragg’s law (equation 4.1).

$$n\lambda = 2d \sin \theta \quad (4.1)$$

In which “ n ” is an integer, “ λ ” is the radiation wavelength, “ d ” is the distance between the planes and “ θ ” is half the angle through which the

incident beam is diffracted [28] [30].

4.1.3 XRD apparatus

The present samples were analysed using two slightly different diffractometers. One is used exclusively for powders whereas the other one may also be used for monolithic samples with flat surfaces. The sample preparation of both powder and monolithic specimens is described in section 4.1.4.

Diffractometer 1 is a Philips PW 1700 series Bragg-Brentano diffractometer with a PW 1729 generator, a PW 1050 goniometer of 173 mm radius, automatic divergence and 1 degree fixed anti scatter slits, a 0.2 mm receiving slit and graphite diffracted beam monochromator. The detector is a xenon-filled proportional counter.

Diffractometer 2 is a hybrid, but can be described as a Philips PW 3700 series Bragg-Brentano diffractometer with a PW 1729 generator, a PW 1050 goniometer of 173 mm radius and independent theta and two-theta drives, fixed 1 degree divergence and anti scatter slits, a 0.2 mm receiving slit and graphite diffracted beam monochromator. The detector is a xenon-filled proportional counter. A benefit of this machine is that monolithic samples may be analysed using special sample holders.

Both diffractometers use cobalt K alpha ($\text{Co K}\alpha$) radiation (weighted wavelength $\bar{\lambda} = 1.79026 \text{ \AA}$). The generator settings are a 40 kV excitation potential with a current of 35 mA for long fine focus tubes. Since $\text{Co K}\alpha$ radiation is used, the diffraction patterns presented in this thesis may not be compared directly with results published elsewhere using $\text{Cu K}\alpha$ radi-

ation.

The programs typically used were scans of 25 minutes or 5 hours and 25 minutes long, extending from 4 degrees to 80 degrees 2θ . For the 25-minute program, the counting time was one second per point, giving a sampling interval of 0.05 degrees whereas the longer program counted for 13 minutes per point with the same sampling interval. Both were “continuous” scans and therefore averaged over the 0.05 interval, assigning the count to the interval midpoint (thus the 4.00 degree point is actually an average from 3.975 to 4.025 degrees).

4.1.4 Sample preparation

Analysing a specimen to determine the phases present requires an even and flat sample surface on the diffractometer axis. Using the above diffractometers it is possible to analyse both powder and monolithic samples.

4.1.4.1 Monolithic sample preparation

Some experiments required the examination of sample surfaces for phases present after synthesis, or changes after a treatment. The surface to be exposed to the x-ray beam must be coplanar with the top of the sample holder. To achieve this, plasticine was used as a flexible fixing substance, with the benefits of easy height and angular adjustment of the sample and easy removal. Using this system and suitable sample holders, specimens of various heights and diameters may be analysed within the limitations of the diffractometer dimensions.

4.1.4.2 Powder sample preparation

Phase analysis of powders using x-ray diffraction requires thorough sample preparation. To prevent contamination of the samples and misleading results, it is essential to work in a clean environment. The starting materials may be solid pieces which must be powdered using a mortar. Ideally the particles should not be larger than about $5\ \mu\text{m}$; a good indication of sufficient fineness is when the powder feels floury. The sample holder was filled with a slight excess of powder which was then compressed using a clean glass microscope slide. It is important that the powder is only pushed down; sliding or turning the glass slide across the powder bed should be avoided to prevent preferred orientation of crystals. To check if the powder is attached to the holder, it can be gently tipped. If the powder remains in the sample holder with its surface coplanar, it is ready to be x-rayed.

If only a very small amount of sample is available, aluminium sample holders with a flat glass or quartz inlay are used but special sample preparation is necessary. Such samples are firstly ground, then suspended in a suitable liquid to create a slurry; distilled water was used for the present work but other liquids may also be applicable. The slurry is applied thinly to the top of the inlay of the sample holder. After drying, the sample is ready for the analysis.

4.2 Nuclear Magnetic Resonance Spectroscopy

4.2.1 Introduction

Solid state nuclear magnetic resonance spectroscopy (NMR) is a relatively new method for investigating solid materials. As a complementary technique to XRD analysis, NMR provides information not available from x-ray diffractometry especially for amorphous materials in which the atomic states of specific atoms can be examined.

NMR is a rf (radio frequency) spectroscopy and exploits the nuclear spin of specific nuclei to determine factors such as their coordination state and bonding to surrounding atoms. When nuclei with a nuclear spin are placed in a strong magnetic field, the energy levels of the different spin states separate. In the strong magnetic field, the nuclear spin has an associated magnetic moment and therefore the nucleus spins around an axis which precesses to the axis of the magnetic field at a specific frequency (Larmor frequency) characteristic of that nuclide. The sample is then irradiated with a pulse of plane polarised rf radiation at the Larmor frequency, causing a tipping of the spin system with respect to the magnetic field axis. At the end of the pulse, the spin system returns to its original axis with a characteristic time constant and the emission of a decaying pulse. Since the nucleus of an atom is shielded from the applied magnetic field by its surrounding electrons, this changes the emitted frequency slightly by an amount called the chemical shift. This emitted frequency is detected by

a coil surrounding the sample as a decaying voltage and is called free induction decay (FID) which is transformed from the time domain to the frequency domain using Fourier transformation (Fig. 4.2) [31].

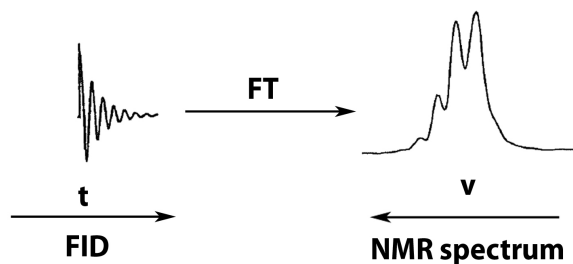


Figure 4.2: Fourier transformation of a free induction decay (FID) in the time domain to an NMR spectrum in the frequency domain [31]

Solid state NMR spectra are broadened due to a number of interactions including dipole moments and, in quadrupole nuclides, quadrupole moments [7]. Some of these broadening effects can be cancelled out by spinning the sample at high speeds (up to 20000 rev s^{-1}) at an angle of 54.7° to the magnetic field axis (called the “magic angle”). This technique is known as magic angle spinning - MAS and produces sharp peaks in the spectra of solids.

However, not all elements possess nuclei suitable for NMR spectroscopy. Nuclei to be analysed must have a nuclear spin and must occur with good natural abundance. The two main factors of the chemical environment affecting the resonance positions in NMR spectra are the coordination state and the nature of the coordinating ligand.

These environment changes can influence the chemical shifts signifi-

cantly. The ranges of chemical shifts of ^{29}Si and ^{27}Al in various environments are shown in Figure 4.3 [7] [31].

4.2.2 Sample preparation

NMR spectra are acquired using similar powder samples as used for x-ray diffraction. It is most important that the powders are ground fine and oven dried to 90°C . High spinning speeds and residual water cause the sample to solidify in the rotor. The powder is gently tamped into the rotor in layers and the rotor cap fitted.

4.2.3 NMR spectrometer

^{29}Si and ^{27}Al solid state nuclear magnetic resonance spectroscopy with magic angle spinning was carried out at 11.7 T using a BRUKER Avance 500 spectrometer and Doty MAS probes spun at approximately 6 kHz for ^{29}Si and 10 - 12 kHz for ^{27}Al . The experimental conditions used for ^{29}Si , ^{27}Al and ^{43}Ca were as follows:

^{29}Si NMR was carried out at a frequency of 99.926 MHz, using a $6\ \mu\text{s}$ ($\pi/10$) pulse and a 30 second delay, the spectra being referenced to tetramethyl silane (TMS).

^{27}Al NMR was carried out at a spectrometer frequency of 130.224 MHz, using a $1\ \mu\text{s}$ ($\pi/10$ pulse for solution) and a one second delay, the spectra being referenced to $\text{Al}(\text{H}_2\text{O})_6^{3+}$.

In the Physics Department, University of Warwick, UK, ^{43}Ca natural abundance MAS NMR spectra were acquired at 14.1 T using a Chem Mag-

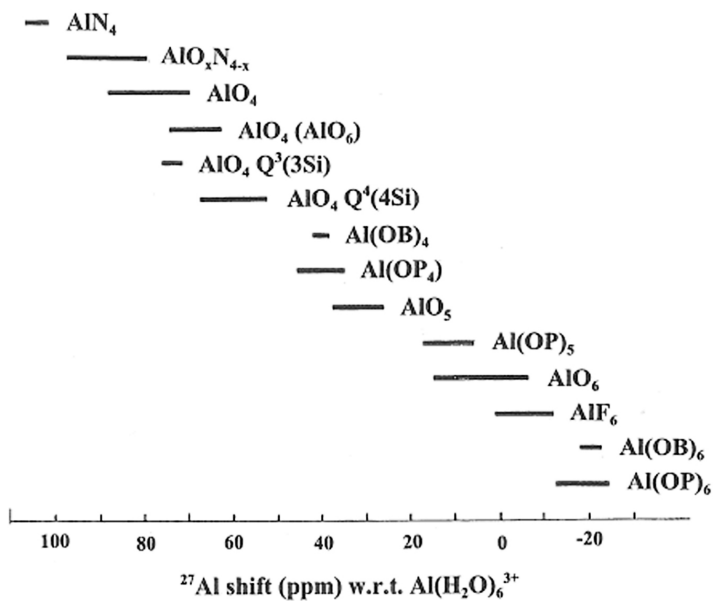
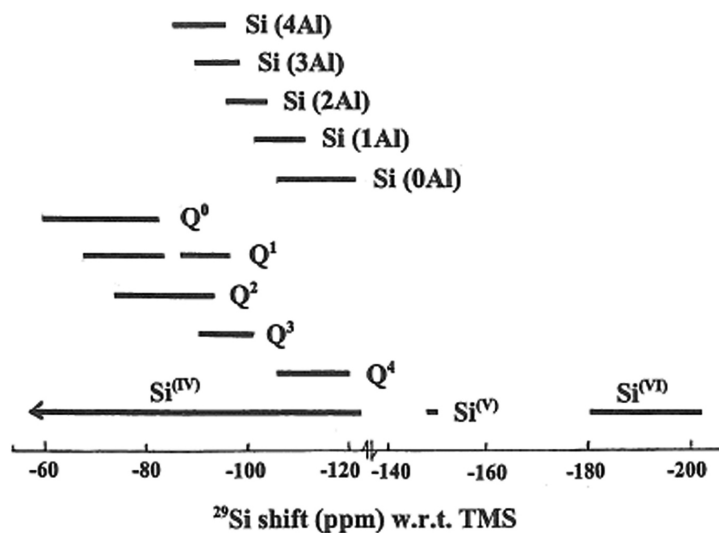


Figure 4.3: Chemical shifts of ^{29}Si and ^{27}Al in various coordination states and environments, [32], [33].

netics spectrometer. The spectrometer frequency was 40.388 MHz and the Varian 9.5 mm MAS probe was spun at 3.5 kHz for approximately 16 hours. A 3.5 - 4 μs ($\pi/9$ pulse for solution) RAPT single pulse sequence was used with a delay of 0.5 to 4 seconds whereas the delay of 0.5 seconds results in the best signal to noise ratio. The spectra were recorded with between 59,227 to 117,824 scans and referenced to saturated CaCl_2 solution.

4.3 Scanning Electron Microscopy

Electron microscopes using electron beams rather than light give an immense improvement in resolution. This improvement is due to the fact that the wavelength of electron beams is approximately 10^5 times less than the wavelength of light. Electrons can be influenced in their orbital characteristics by interaction with magnetic or electric fields. In electron microscopes such fields act as the refractive medium and function as the collector lenses (objective and condenser lens) in optical microscopes.

This technology has led to the development of transmission electron microscopy (TEM) and scanning electron microscopy (SEM). TEMs have a resolution barrier of about 0.1 to 0.2 nm and can provide information about the inner structure of translucent objects whereas SEMs have the potential to display solid surfaces in three dimensions. In terms of magnifications, scanning electron microscopes fill the gap between TEMs and optical systems. However, the actual resolution and the maximum magnification of TEMs and SEMs is strongly dependent on the samples and their preparation.

Scanning electron microscopes have a very good depth of field and can therefore deliver images of rough surfaces with good resolution. Due to the large depth of field, the images appear to be three dimensional. Nevertheless, sample preparation plays an important role if high magnification with high resolution is required. Because of its universal applicability, uncomplicated sample preparation and ease of interpreting the images, scanning electron microscopy is a very popular technique. In addition to displaying images, scanning electron microscopes provide the possibility of analysing micro areas. This technique is called energy dispersive x-ray fluorescence spectroscopy (EDS). Such analyses are carried out by scattering the sample surface with electromagnetic radiation that excites the atoms in the matter. Relaxation of the excited atoms leads to an emission of for each atom specific x-ray radiation that is detected to identify the atoms present in the specimen [34].

An important difference from optical microscopes is the way the image is produced. Optical systems provide direct imaging, but SEMs display indirect images; hence the signal production and signal processing systems are separated. SEM images are artificial copies of a sample surface arising from interactions of electrons with the specimen surface using a concentrated electron beam (the primary electron beam) which rasters the target. This produces secondary signals such as secondary and backscattered electrons which are used to control the brightness modulation of a cathode ray tube (CRT) on which the image appears. The scan coil in the microscope produces a line-by-line scanning of the target surface by the primary electron beam. Because of the interactions of primary electrons with the sample surface, secondary signals develop which are collected

by detectors. Line-by-line scanning therefore produces a copy of the sample surface as a row of signals transmitted serially. Areas emitting high concentrations of secondary electrons appear as bright spots on the screen whereas areas that provide only low secondary electron emission remain dark. The chronological separation of the electric signals allows the signal processing (“brightness” and “contrast”) to be altered. Thus, rough to very smooth surfaces can be displayed by adjusting the contrast and brightness.

Magnification of target surfaces arises from the fact that various size areas are rastered but the information gained from these areas are always projected on to the same screen size, e.g. 10×10 cm. Thus, a surface area of 5×5 mm results in a 20-times magnification, but a surface area of 10×10 μm would be magnified 10,000 times [34].

Analysis of geopolymer samples was carried out using SEM in various modes, including secondary electron imaging and backscattered mode.

4.3.1 Secondary electron imaging

Secondary electrons are excited by electrons incident on the sample. Since only a very small area generates such electrons, the image is hardly affected and therefore the best resolution can be obtained in this mode [35].

4.3.2 Backscattered electron imaging

The backscattered mode detects highly energetic electrons re-emitted from the sample surface after being scattered within the specimen. In this mode,

spots appear brighter or darker depending on the atomic number of the elements present. Generally speaking, the heavier the element or the higher the atomic number of the element, the brighter it appears on the screen [35].

Areas of interest of a sample are exposed to a focussed highly energetic beam of electrons, protons or x-rays. The atoms present have unexcited electrons (or electrons in ground state) in their electron shells. The highly energetic beam excites these electrons and forces them into a higher energy level (higher shell) which causes an electron gap. This gap is filled by another electron from a higher energy level (higher shell). The energy difference between these two shells is expressed by the emission of specific x-ray radiation characteristic of the energy difference. Every element has a specific x-ray radiation if its electrons are excited in this way which can therefore be used as a “fingerprint” or unique identifier.

4.3.3 SEM/ EDS apparatus

The scanning electron microscope used was a JEOL JSM-6500F with a Schottky-type field emission gun (T-FE gun) and a Zr/O tungsten emitter.

EDS conditions were used exclusively with an accelerating voltage of 15 kV, a probe current of 15 (coarse value approximately 5×10^{-9} A) and a working distance of 10 mm.

The backscattered electrons are detected using a retractable BE detector (JEOL SM-54031) and for EDS analysis a JEOL EX-23000BU ED x-ray analyser.

4.3.4 Sample preparation

Sample preparation of specimens for scanning electron microscopy involves coating the surface with an electrically conductive material that can be grounded to avoid surface charging by accumulation of a static electric charge. Conductive samples may not need special preparation other than cleaning but coating can improve the resolution, especially for elements of low atomic number.

Non-conductive materials such as ceramics or geopolymers require coating of their surfaces with an ultra-thin layer (few nm) of conductive material, for example, gold, platinum, silver or carbon. Depending on the coating substance, the layers are applied using low vacuum sputtering or high vacuum evaporation.

The coating material must be chosen to meet the specific demands of the sample. If high magnification with good resolution is the aim, carbon may not be satisfactory as it tends to form ball-shaped structures on sample surfaces. Commonly used materials for such purposes may be gold or platinum. Nevertheless, carbon is a good choice for analysis in the backscattered mode, since backscattered electrons can penetrate lighter materials.

Where EDS analysis is required, coating with heavy elements should be avoided since EDS mapping is done in the backscattered mode. When light elements are used as a coating material the electron beam can penetrate to the sample and interact to generate the signal. If heavy substances (e.g. gold) are used it is likely that a large number of secondary electrons will be generated within the coating layer, suppressing the secondary elec-

trons generated at greater depth i.e. at the sample surface.

The inorganic polymer samples were prepared and coated with carbon for backscattered electron imaging as well as for electron dispersive element analysis.

Gold and platinum coatings were used for high resolution imaging in the SEI-mode to display fine structure in the samples. The thickness of the platinum and gold coating layers was initially 8 nm but could be adjusted up to 18 nm depending on charging. The carbon coating layers were 6 nm initially but were increased to 16 nm to reduce surface charging.

4.4 Compression Testing (Brazil Test)

4.4.1 Introduction

The aim of implants is to replace bones or parts of bony structures, and therefore their major function is to support the body weight as bones do. However, specific applications require certain mechanical characteristics i.e. implants used for legs must withstand higher loads compared to implants used for ears.

To determine the mechanical strength of materials, several methods have been established, including 3 or 4-point bending, direct and indirect tensile strength measurements. Although these all measure tensile strengths, the results are not always comparable because different effective volumes and stress distributions may be involved. Thus, it should always be noted which method has been used when making comparisons with published results.

The diametral compression strength test or Brazil test was chosen for this study because it is commonly used to determine the tensile strength of brittle materials such as concretes or ceramics. The experimental setup is simple and similar to that used for axial compression. In addition, the sample shape can be kept very simple and specimens do not need to be attached to the testing machine. Compared with other test methods, only a small amount of the sample is exposed to the applied force. However, the maximum tensile strength is not limited to the surface of the sample and failure can be initiated from the internal areas [36], [37].

Tensile strength determination by the Brazil test is carried out on cylindrical samples with plane-parallel ends. The specimen is placed between two flat platens and compressed across its diameter, shown schematically in Figure 4.4 [37].

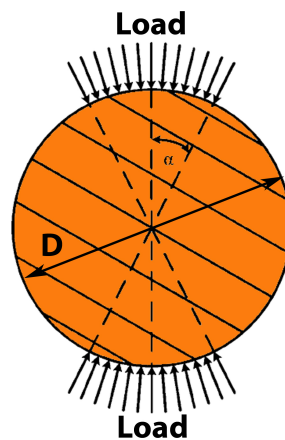


Figure 4.4: Schematic diagram of the test setup for diametral compression testing [37]

However, diametral tensile strength is limited to materials with mechanical properties such as linear elasticity, elastically isotropic, homogeneous and stronger in shear and compression than in tension. These

properties are characteristic of ceramics. If a material does not meet these requirements it is not suitable for examination by diametral compression because it may fail before the load which causes tensile failure can be applied.

The tensile strength is calculated using equation 4.2:

$$\sigma = \frac{2P}{\pi Dt} \quad (4.2)$$

Where, “ P ” is the applied load, “ D ” is the diameter and “ t ” is the thickness of the specimen [38].

Tests were carried out on cylindrical specimens with plane-parallel ends as illustrated in Figure 4.5 [37].

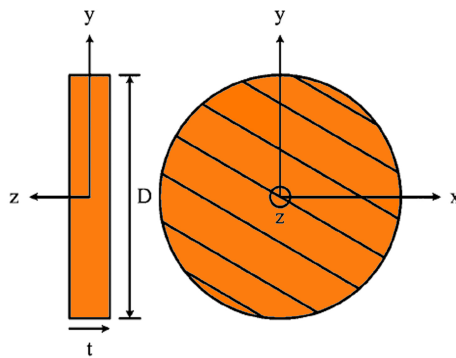


Figure 4.5: Requirements on the samples regarding the preparation [37]

The tests were carried out using a calibrated/ certified Instron Universal testing machine with a maximum load capacity of 250 kN. The load was applied with a cross-head speed of 1 mm/minute.

4.5 Inductively Coupled Plasma

Examination of composition changes of the simulated body fluid was carried out using inductively coupled plasma atomic emission spectroscopy (ICP-AES). This analytical spectroscopy uses the emission of electromagnetic radiation ($h\nu$) in the vacuum ultraviolet (VUV) range (120 - 185 nm) of excited atoms relaxing to the ground state, as shown in Figure 4.6 [39]. Due to their specific atomic mass, each atom emits its unique electromagnetic radiation. Detection of VUV radiation requires an environment free of air, commonly an argon atmosphere.

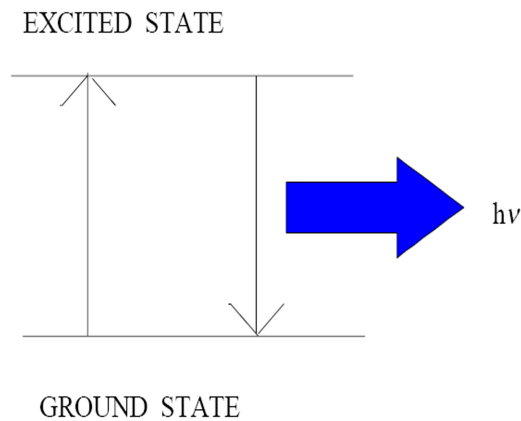


Figure 4.6: Emission of electromagnetic radiation after relaxing of an excited atom to its ground state [39].

ICP-AES is used to identify elements and to determine their concentrations in the sample. This involves three steps, the formation of the atoms, their excitation and the emission of electromagnetic radiation. However, before an atom is excited it must be separated from the other attached

atoms so it can emit its unique radiation.

The excitation source for ICP-AES analysis is an analytical plasma with a temperature between 600 - 8000 K, which is an electrically neutral, and highly ionised gas consisting of ions, electrons and atoms. Figure 4.7 illustrates the steps by which an aqueous phase is analysed by ICP-AES [39].

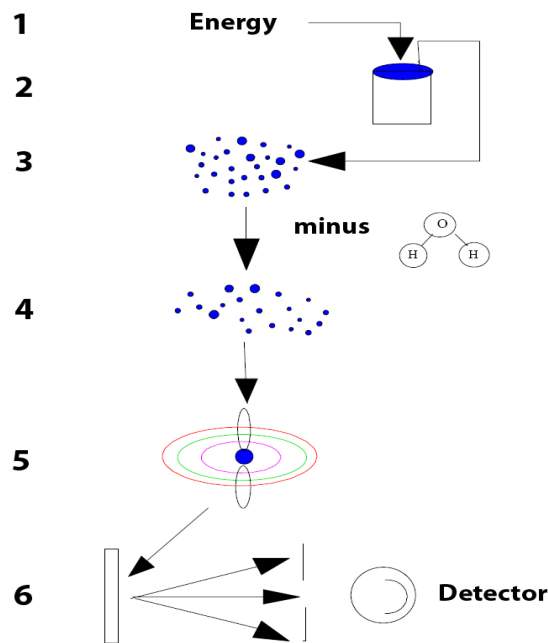


Figure 4.7: Steps in the analysis of an aqueous sample by ICP-AES [39]

The liquid sample is transformed to an aerosol (2), then water is driven off and the remaining solids and liquid compounds are converted to gases (3). In stage 4 atomisation occurs in a plasma by breaking the molecular bonds in gaseous molecules forming atoms. Excitation and emission of the characteristic wavelength takes place in step 5 and is detected in step 6 [39].

The accuracy of the results is $\pm 10\%$ of the measured values, the detection limits are listed in Table 4.1, both quoted by the analytical laboratory.

Table 4.1: ICP-AES detection limits

Aluminium	0.005 ppm
Calcium	0.01 ppm
Phosphorus	0.01 ppm
Potassium	0.01 ppm
Silicon	0.005 ppm

4.6 pH studies

An important part of this work was to determine pH changes in the simulated body fluid when geopolymers are soaked in it. Cured specimens in various states (unheated, heated to 550°C and 600°C) were exposed to SBF for various times and changes in the pH of the fluid were monitored by frequent measurements. Within the first two hours measurements were made every five to 10 minutes, then the intervals increased to 30 minutes between two and four hours, that followed by a further increase of the measurement intervals to hourly and twice daily intervals throughout the rest of the experiment.

The pH measurements were carried out using a portable pH-meter (RS V5969, accuracy: $\pm 0.03\text{pH}$) which was calibrated with buffer solutions of pH 7 and pH 9.

Chapter 5

Results and Discussion

5.1 Strength measurement results

Diametral compression strength measurements were carried out only on the initial fully cured samples, namely, unheated, heated to 550°C and 600°C. Specimens exposed to SBF were not tested because of the small number of samples available which would have led to statistically unsatisfactory results.

The average measured tensile strengths of the tested specimens are shown in Table (5.1).

Table 5.1: Tensile strength measurement results of geopolymer samples, (values) are standard deviations

	unheated	heated 550°C	heated 600°C
Sample	Tensile strength (MPa)	Tensile strength (MPa)	Tensile strength (MPa)
Reference	2.49 (0.19)	2.05 (0.90)	1.22 (0.68)
Ca-hydroxide	3.97 (0.99)	0.64 (0.38) ¹	1.46 (0.69)
Ca-silicate	1.00 (0.39)	— ²	1.38 (0.32)
Ca-phosphate	2.86 (0.44)	4.17 (1.21) ³	1.73 (0.77)

¹: samples had small surface cracks

²: samples broke during the heat-treatment

³: result of only 6 measurements

The highest mean strengths of the unheated samples were shown by the calcium hydroxide-containing samples, measured on 10 samples, followed by the calcium phosphate-containing samples and reference geopolymers (3.97, 2.86 and 2.49 MPa) respectively. The weakest samples were

those containing calcium silicate, with a tensile strength of 1 MPa.

The results of samples heated to 550°C should be viewed with caution, especially for the geopolymers containing calcium hydroxide and calcium silicate. Strength tests on calcium silicate-containing samples heated to 550°C could not be carried out because they broke during the heat-treatment. Heating of the geopolymers to 550°C and 600°C removes the structural (hydroxyl) water content. This typically leads to shrinkage of the material that may cause internal stresses. If the materials are hydrophilic - as in the present work - an exposure to air and therefore humidity causes reabsorption of water. This can lead to a critical expansion of the samples and may involve mechanical failure including crack development or even destruction of specimens.

The lowest tensile strengths (0.64 MPa) are shown by the samples containing calcium hydroxide possibly because the samples had developed surface cracks prior to testing. The reference geopolymer samples showed tensile strengths of 2.05 MPa, while 4.17 MPa was recorded for the samples containing calcium phosphate; however, these values are based on only 5 samples. All other strength tests were carried out on 14 to 18 samples.

A possible explanation for the higher strengths of the calcium phosphate-containing sample is because of phosphate bonding, known to occur in alumina ceramics and cements [40]. It has been reported that phosphorus can be incorporated in the network structure of geopolymers and may lead to higher strengths of the geopolymers [1] [22].

Strength measurements on the samples heated to 600°C show a relatively narrow distribution. The results range from 1.22 to 1.73 MPa for the reference and the calcium phosphate-containing geopolymers respec-

tively, whereas the calcium hydroxide and calcium silicate-containing samples show tensile strengths of 1.46 and 1.38 MPa respectively.

A clear trend of the strength measurements with heating temperature is shown only by the reference geopolymer, which becomes weaker with increasing temperature. The strengths of the other samples fluctuate according to their calcium compounds and heating temperature, possibly because the samples were examined within different periods after removal from the furnace or curing room. The unheated geopolymers were tested almost immediately after removal from the curing room whereas the heat-treated geopolymers were not tested directly after being taken out of the furnace. Since the as-synthesised geopolymers appear to be hydrophilic, they were kept in sealed plastic bags to avoid rehydration until required for testing.

Table 5.2 shows the a collection of the tensile strengths of other bio-ceramics and bone compared with one of the results measured in this project.

Table 5.2: Comparison of the tensile strengths of various bio-ceramics and bone, test method unknown unless labelled [†].

Material	Tensile strength (MPa)	Reference
Bone	60 - 160	[41]
Cancellous bone	3	[42]
Hydroxyl apatite	80	[42]
Bioglass®	42	[42]
Bioglass®	5.54 (SD 0.529)	[43] [†]
Bioglass®/ polyethylene*	10.15	[42]
Bioglass®/ polysulfone*	1.5	[42]
Apatite-wollastonite glass-ceramic / polyethylene*	14.87	[42]
Ca-phosphate geopolymer (H550)	4.17 (SD 1.21)	†

[†]: Diametral compression testing

*: 40% ceramic, 60% polymeric phase

Direct comparison of the tensile strengths of the materials listed in Table 5.2 is still inappropriate because of the unknown nature of the testing method. As mentioned in section 4.4, there are various methods for determining the tensile strengths of materials in which the tested volume of the specimen and hence the results can vary, e.g. the two values for Bioglass® shown in Table 5.2 are very different. The result from the unknown testing method [42] is much higher than that from the diametral compression test (DCT) [43] (42 and 5.54 MPa respectively). Therefore, it is likely that dissimilar methods were used and that the Brazil test (DCT) used in this work provides generally lower strength measurements.

Extending these observations to the geopolymer results shown in Table 5.1 and 5.2 suggests that their strengths results comparable with those of the materials known to have been determined by DCT. Specifically, the strength of Bioglass® [43] and the calcium phosphate-containing geopolymer, both measured using diametral compression testing do not differ greatly, although the geopolymer shows a slightly lower value.

The strongest samples (calcium phosphate-containing geopolymer heated to 550°C) has a tensile strength comparable to that of Bioglass® tested by the same method, although the lower strengths of the other calcium-containing geopolymers are still comparable with those of Bioglass®/ polysulfone composite.

5.2 XRD results

5.2.1 XRD patterns of the raw materials

The raw materials were examined by XRD to determine whether or not they change during the setting process i.e. undergo reaction, or if they remain in the product structure after synthesis.

The XRD diffraction pattern of calcium phosphate (Fig. 5.1) shows it to be a purely crystalline material consisting of calcium hydrogen phosphate hydroxide (PDF No. 00-046-0905) and calcium phosphate phases (PDF No. 00-017-0499). Peaks labelled CP/CPH are present in both phases, calcium phosphate and calcium hydrogen phosphate hydroxide.

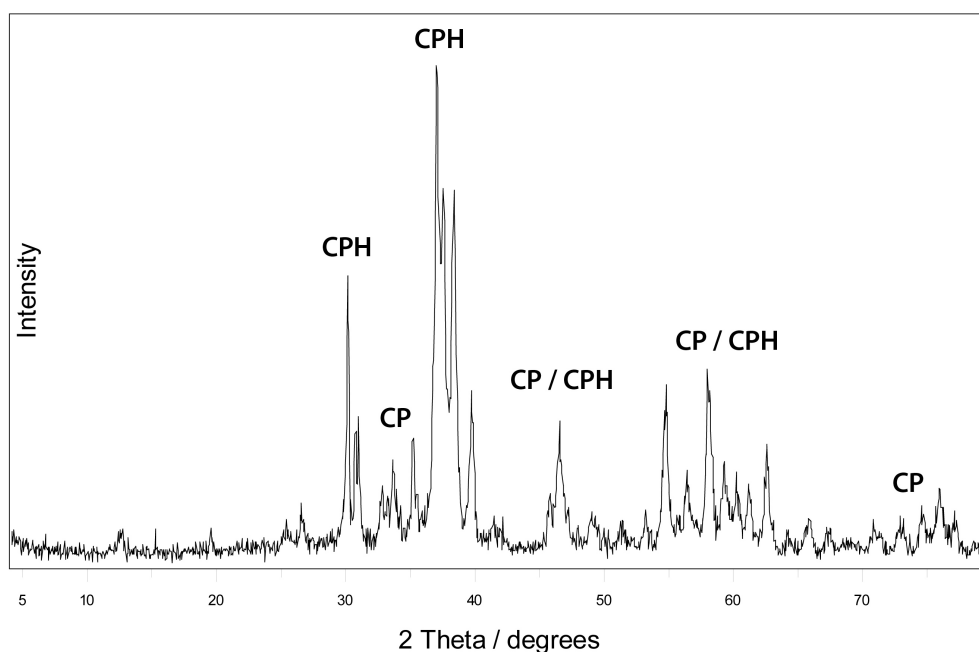


Figure 5.1: XRD pattern of calcium phosphate; CPH = calcium hydrogen phosphate hydroxide, CP = calcium phosphate

XRD shows the nano-structured calcium silicate starting material to contain poorly crystalline calcium silicate hydrate (PDF No. 00-033-0306) (Fig. 5.2).

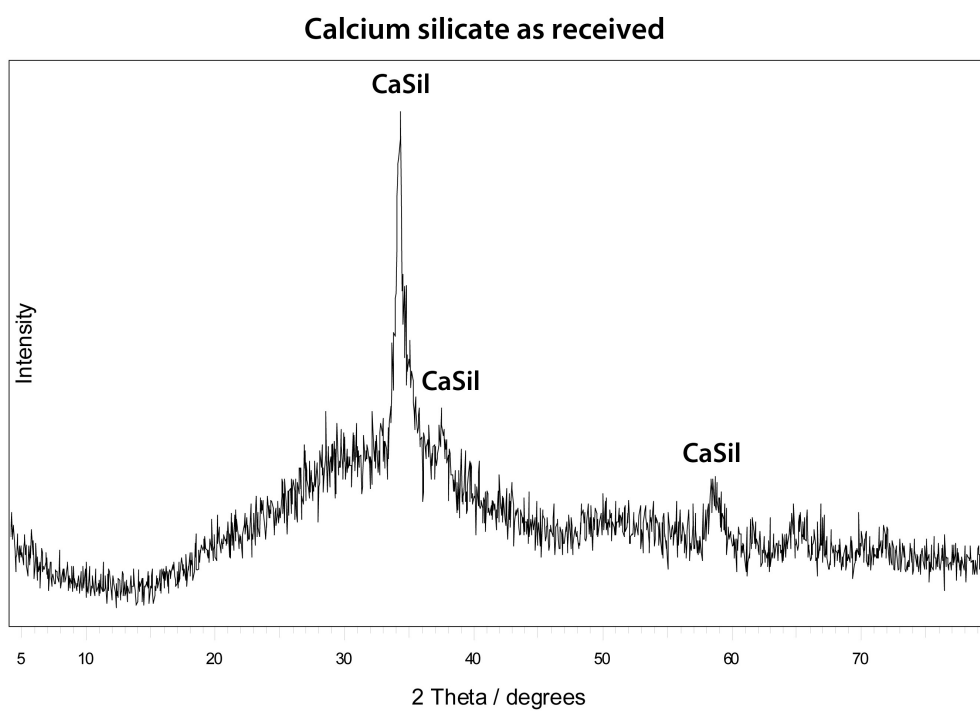


Figure 5.2: XRD pattern of calcium silicate; CaSil = calcium silicate

The x-ray diffraction pattern of the calcium hydroxide starting material, Figure 5.3, shows it to be highly crystalline calcium hydroxide, portlandite (PDF No. 00-44-1481).

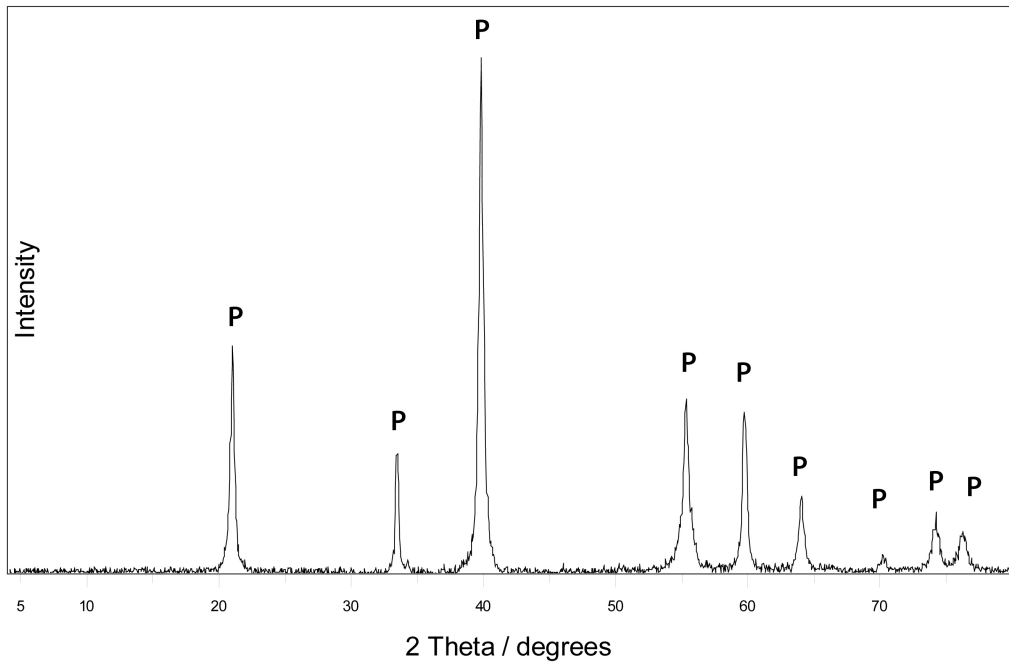


Figure 5.3: XRD pattern of calcium hydroxide; P = portlandite

Dehydroxylation of the halloysite results in the destruction of the clay structure (Fig. 5.4).

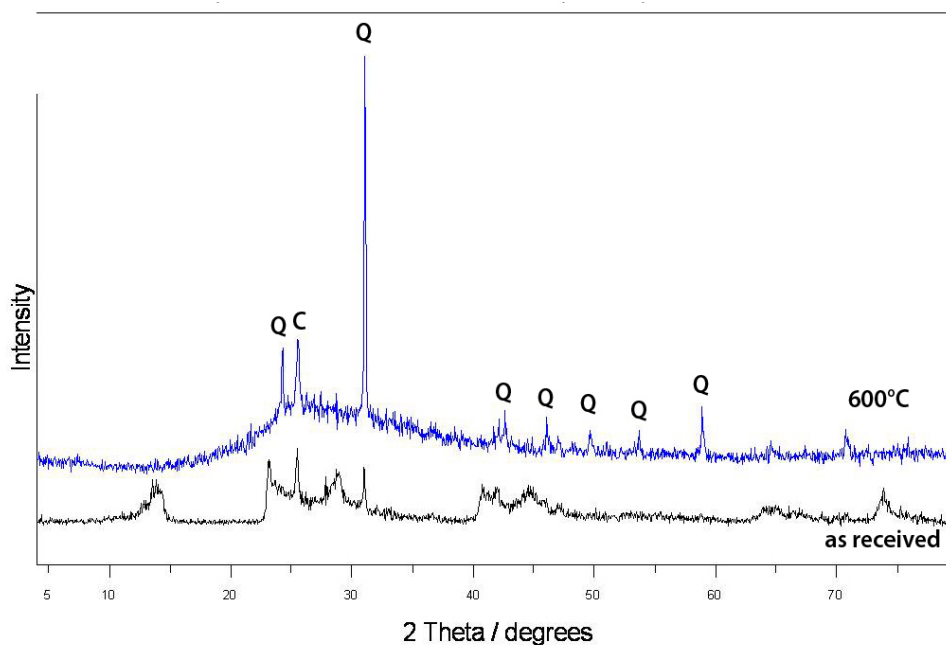


Figure 5.4: XRD patterns of halloysite as received (bottom) and after dehydroxylation (top), Q = quartz, C = cristobalite

Quartz (PDF No. 00-046-1045) and possibly cristobalite (PDF No. 00-039-1425) are probably impurities in the original halloysite, although some of the quartz could be converted to cristobalite upon heating. The unlabelled peaks of the lower pattern (as received) indicate the halloysite prior to dehydroxylation.

Thus, the dehydroxylated halloysite and calcium silicate starting materials are more or less x-ray amorphous, but contain some crystalline phases, (Fig. 5.2 and 5.4), whereas the calcium hydroxide and calcium phosphate show sharp, well-defined peaks (Fig. 5.1 5.3).

5.2.2 Reference geopolimer

The x-ray diffraction patterns of the geopolimer without added calcium compounds, unheated and heated to 550°C and 600°C do not show significant differences, apart from a small unidentified peak appearing at about 36 2 θ /degrees after heating at 600°C (Fig. 5.5). The only crystalline peaks present are impurities from the dehydroxylated halloysite, the quartz (PDF No. 00-046-1045) and cristobalite (00-039-1425).

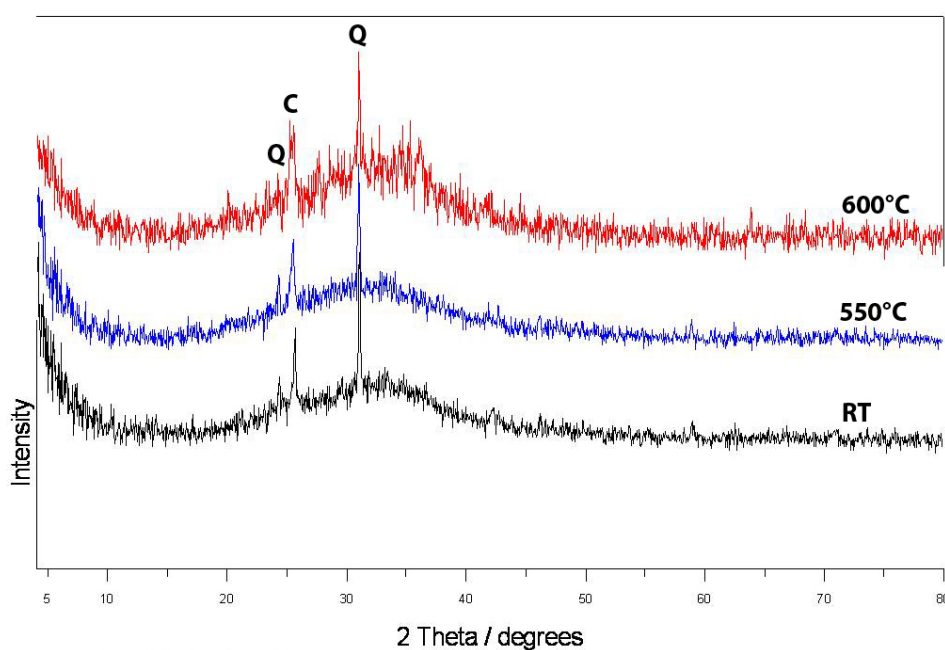


Figure 5.5: XRD patterns of the reference geopolimer before and after heating, Q = quartz, C = cristobalite

Exposure of these geopolymers to SBF produces no change in the XRD patterns.

5.2.3 Calcium hydroxide geopolymers

The synthesised calcium hydroxide-containing geopolymers in general show the x-ray amorphous XRD patterns typical of geopolymers, both before and after heating. The added crystalline calcium hydroxide could not be detected by XRD diffractometry, however it is still present in the material in the form of x-ray amorphous nano-crystals shown by SEM and EDS analysis in section 5.6.2.

The calcium hydroxide-containing geopolymers after synthesis and heating to 550°C show similar XRD patterns whereas the XRD pattern of the sample heated to 600°C is slightly different (Fig. 5.6).

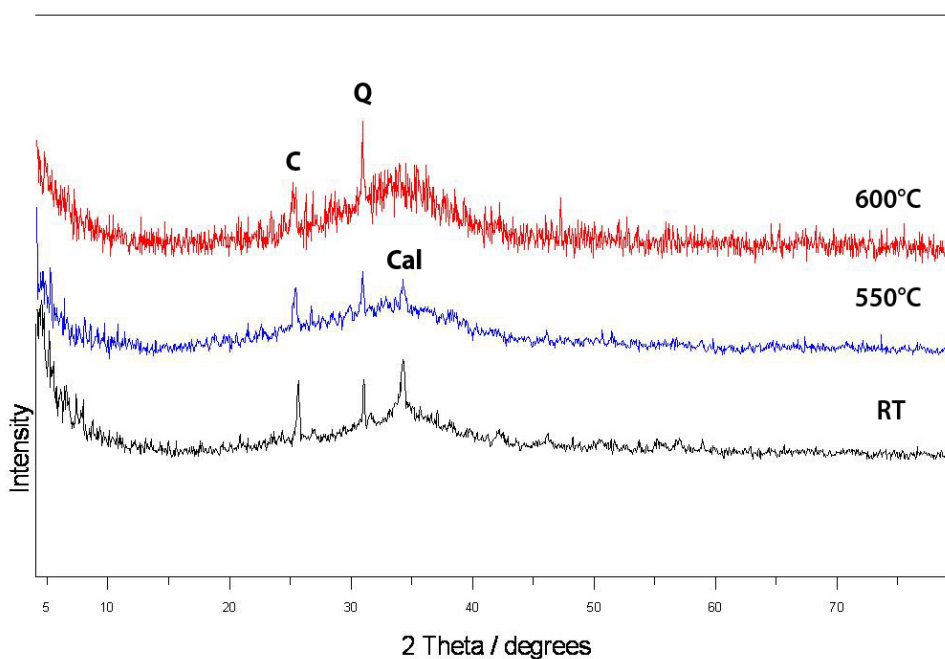


Figure 5.6: XRD patterns of calcium hydroxide-containing geopolymers before and after heating. Q = quartz, C = cristobalite, Cal = CaCO₃

All the samples contain residual quartz (PDF No. 00-046-1045)) and

cristobalite (PDF No. 00-039-1425) whereas heating to 600°C leads to an increase of the amorphous phase, indicated by the increased size of the hump at 34 2θ /degrees and the loss of the calcite peaks (PDF No. 01-072-1937) which are present in the samples unheated and heated to 550°C (Fig. 5.6). The calcite probably arises from atmospheric carbonation forming nano-structured particles. The continuous degradation of the calcite with increasing of the heating temperature may be explained by the thermal destruction of nano-structured calcite at lower temperatures with reduced activating energy compared with bulk calcite, reported by Yue et al. [44], and thus very finely divided invisible for x-ray diffractometry.

X-ray diffraction of an unheated calcium hydroxide-containing geopolymer after exposure to SBF for four weeks (Fig. 5.7) presents a much larger and sharper calcite peak (PDF No. 01-072-1937).

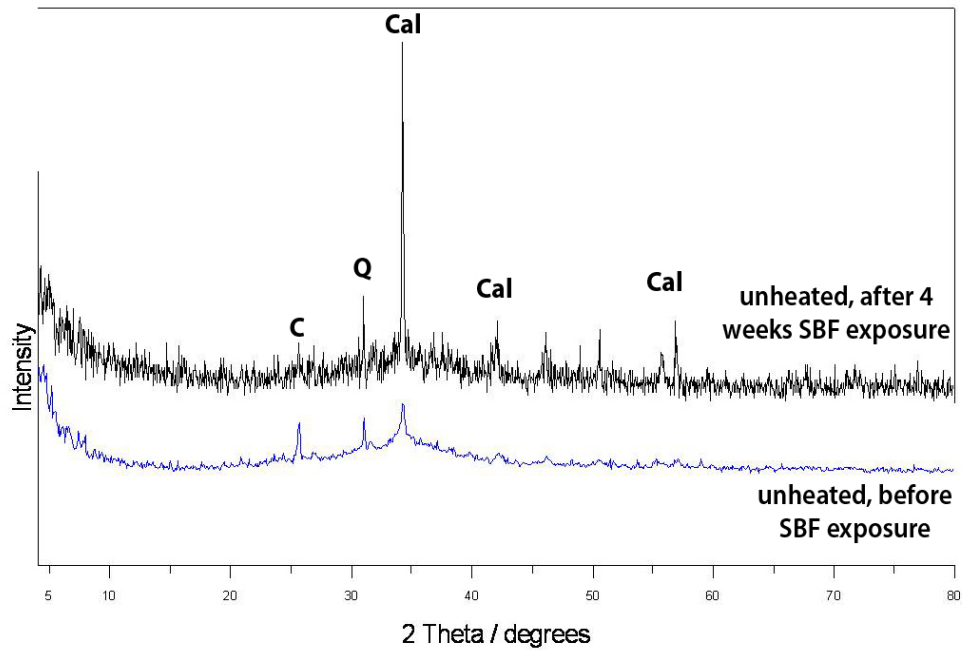


Figure 5.7: XRD spectra of calcium hydroxide-containing geopolymers before and after SBF exposure. *Q* = quartz, *C* = cristobalite, *Cal* = calcite

The Calcite in this case probably arises from reaction with the sodium bicarbonate ions in the simulated body fluid.

The calcium hydroxide-containing samples heated to 550°C (Fig. 5.8) and 600°C (Fig. 5.9) have similar XRD patterns before and after the in-vitro exposure experiments.

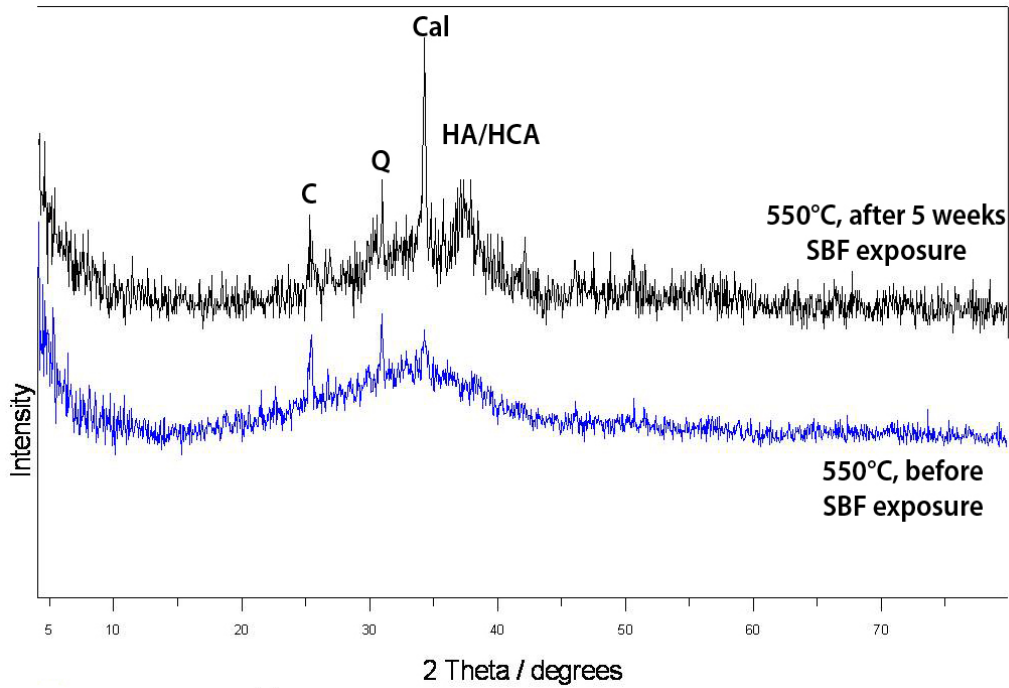


Figure 5.8: XRD patterns of calcium hydroxide-containing geopolymer (550°C) before and after SBF exposure. Q = quartz, C = cristobalite, Cal = calcite, HA = hydroxyl apatite, HCA = hydroxyl carbonate apatite

Both show evidence of reaction with the SBF to form hydroxyl apatite (PDF No. 00-009-0432) and hydroxyl carbonate apatite (PDF No.00-019-0272) phases after an exposure time of four weeks (Fig. 5.9) and five weeks (Fig. 5.8). The two crystalline impurity phases cristobalite and quartz remain unchanged by the heating and exposing to SBF. The specimen heated to 550°C (Fig. 5.8) contains well-crystallised calcite in addition to the two other poorly crystalline phases HA and HCA, all of which have formed

during the in-vitro exposure experiment.

The XRD patterns of a calcium hydroxide-containing sample heated to 600°C before and after exposure to simulated body fluid are shown in Figure 5.9. The formation of HA and HCA in this sample upon exposure is more advanced, as induced by the greater intensity of the representative x-ray peak and the lack of a calcite reflection. Thus, this sample appears to be a good candidate for a bioactive geopolymer.

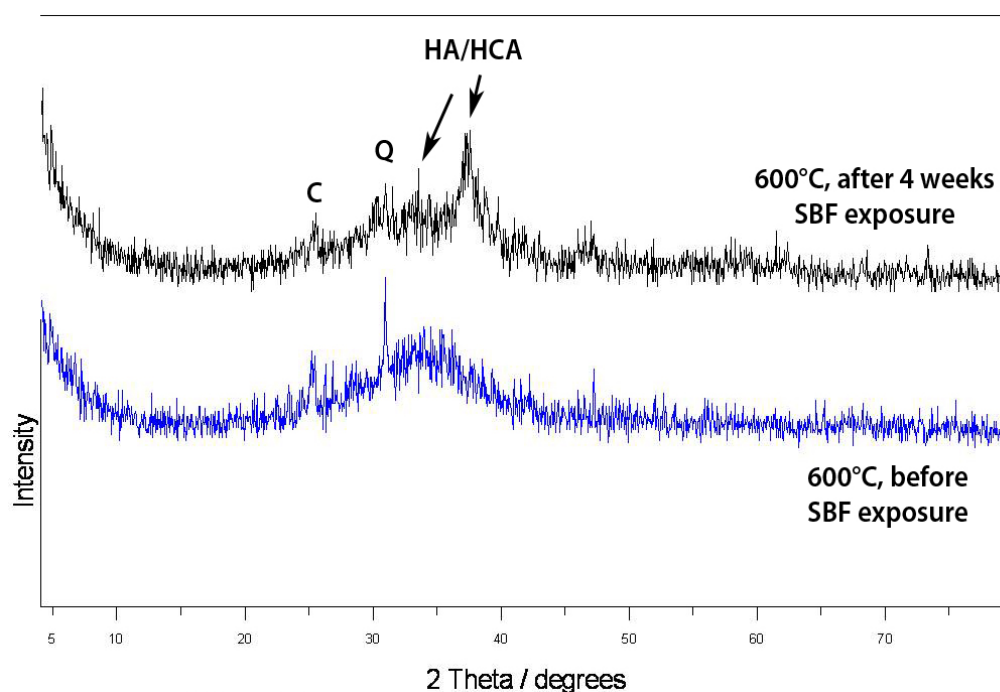


Figure 5.9: XRD spectra of calcium hydroxide-containing geopolymers (600°C) before and after SBF exposure. Q = quartz, C = cristobalite, Cal = calcite, HA = hydroxyl apatite, HCA = hydroxyl carbonate apatite

5.2.4 Calcium silicate geopolymers

The calcium silicate-containing geopolymers show very similar XRD patterns regardless of the heat-treatment. They all containing the broad hump typical of a geopolymer together with crystalline quartz and cristobalite impurity phases (Fig. 5.10).

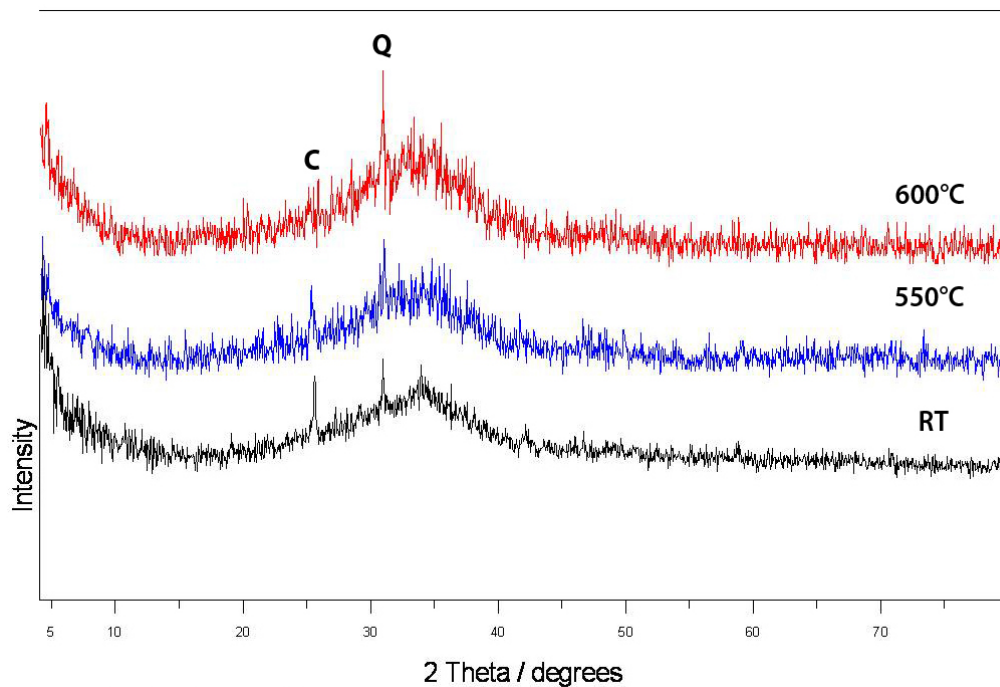


Figure 5.10: XRD patterns of calcium silicate-containing geopolymers before and after heating. Q = quartz, C = cristobalite

In-vitro exposure experiments of samples, both unheated and heated to 550°C, show no change after exposure to simulated body fluid.

Specimens heated to 600°C show the formation of two possible forms of poorly crystalline hydroxyl apatites (PDF No. 01-082-1944 and 01-089-4405) after four weeks of SBF exposure (Fig. 5.11), quartz and cristobalite impurities are still present.

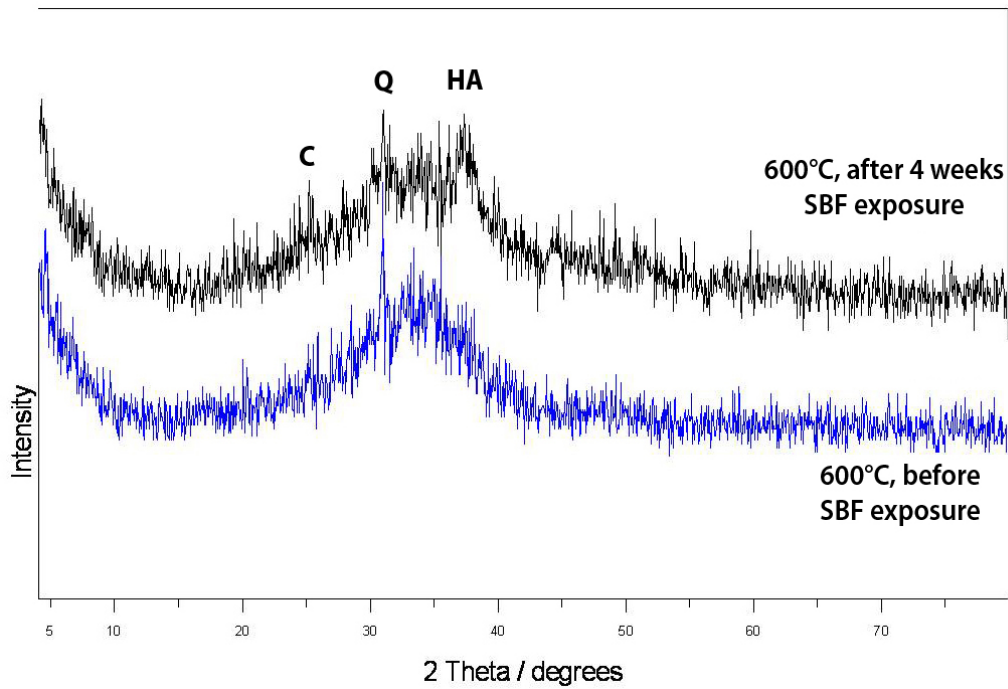


Figure 5.11: XRD patterns of calcium silicate-containing geopolymers (600°C) before and after SBF exposure; Q = quartz, C = cristobalite, HA = hydroxyl apatite

5.2.5 Calcium phosphate geopolymers

The geopolymers containing calcium phosphate all show typical x-ray amorphous geopolymer diffraction patterns, in both heated and unheated samples (Fig. 5.12).

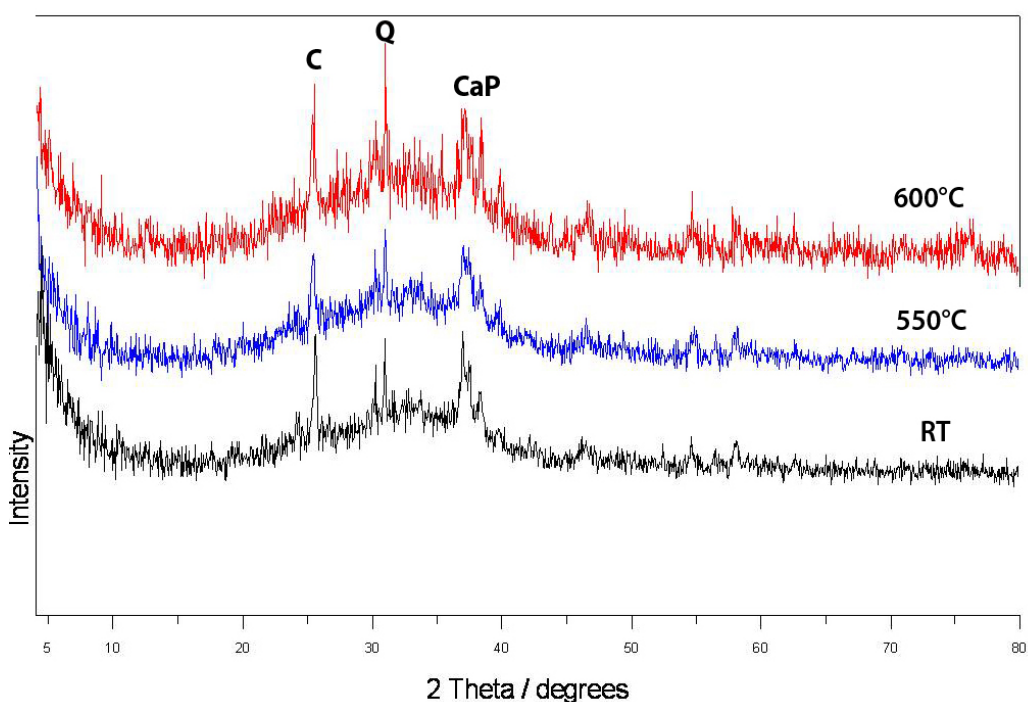


Figure 5.12: XRD patterns of calcium phosphate-containing geopolymers before and after heating. Q = quartz, C = cristobalite, CaP = calcium hydrogen phosphate hydroxide

In addition to the amorphous geopolymer feature, all the patterns contain sharp peaks of quartz and cristobalite impurities and calcium hydrogen phosphate hydroxide (PDF No. 00-046-0905). The in-vitro exposure experiments produce no new peaks in the XRD patterns. However, in the pattern of the geopolymer heated to 600°C, the CaP peaks appears slightly more intense possibly due to formation of another calcium phos-

phate phase, such as hydroxyl apatite or carbonate hydroxyl apatite. Analysis of this sample by SEM showed the formation of small crystals after 7 weeks of SBF exposure, section 5.6.4.

To summarise the XRD results, all the samples show the x-ray amorphous feature of a typical geopolymer, with superimposed crystalline phases corresponding to quartz and cristobalite impurities, and the calcium compounds where these are present. Heating to 550°C and 600°C produces little change in the XRD pattern, apart from the loss of calcite from the calcium hydroxide-containing sample at 600°C.

After exposure to SBF, the geopolymers containing calcium hydroxide and calcium silicate heated to 550°C and 600°C show the formation of the bioactive phases hydroxyl apatite and carbonate hydroxyl apatite. The hydroxyl apatite or carbonate hydroxyl apatite are not detected by XRD as they may be present in insufficient quantities or be of very poor crystallinity (x-ray amorphous).

In-vitro exposure experiments of the reference geopolymer without calcium compounds produced no evidence of the formation of bioactive compounds regardless of the heat-treatment. Neither the heated or unheated calcium phosphate-containing geopolymers show any obvious changes in the XRD patterns, after in-vitro SBF exposure experiments. However, under the alkaline conditions of geopolymerisation, the added calcium phosphate is identified by XRD as calcium hydrogen phosphate hydroxide. Since the XRD patterns of hydroxyl apatite and carbonate hydroxyl apatite and calcium hydrogen phosphate hydroxide are practically indistinguishable, the possible formation of hydroxyl apatite or hydroxyl carbonate apatite during the in-vitro experiments cannot be ruled out.

Thus, bioactive compounds are shown by XRD to be formed under in-vitro conditions in samples containing calcium hydroxide and nano-structured calcium silicate, especially in the former sample heated to 600°C. The similarity of the XRD patterns of the phosphate compound formed in the geopolymers containing calcium phosphate before SBF exposure and hydroxyl apatite or hydroxyl carbonate apatite makes it impossible to determine whether the sample has interacted with the SBF. Geopolymers without added calcium compounds do not form bioactive compounds with SBF. These findings are summarised in Table 5.3.

The presence of calcium is important for effective bioactivity. According to a personal communication [45], it was stated that the most recent information is that both, calcium and silicon play an essential role in activating the genes that turn on the body's regenerative processes. The optimum concentration for calcium is 60 ppm and for silicon is 20 ppm [45].

Table 5.3: Presence of bioactive phases (HA/ HCA) found in geopolymers after SBF exposure.

Geopolymer	heating temperature	HA / HCA
Reference	unheated	absent
	550°C	absent
	600°C	absent
Calcium hydroxide	unheated	absent
	550°C	present
	600°C	strongly present
Calcium silicate	unheated	absent
	550°C	absent
	600°C	present
Calcium phosphate	unheated	*
	550°C	*
	600°C	*

*: Cannot be determined (see text)

5.3 MAS NMR results

5.3.1 ^{27}Al and ^{29}Si MAS NMR results

5.3.1.1 Reference geopolymer

The ^{27}Al MAS NMR spectrum of the unheated reference geopolymer (Fig. 5.13) is very similar to the samples heated to 550°C and 600°C. In-vitro exposure experiments for seven weeks does not change the ^{27}Al MAS NMR spectrum of these materials.

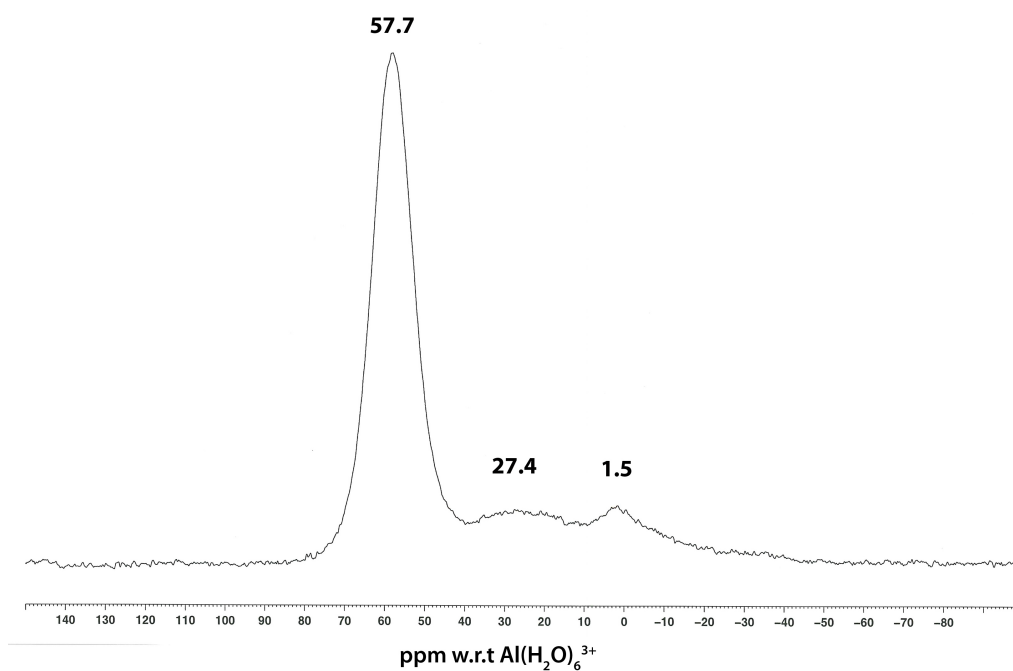


Figure 5.13: 11.7T ^{27}Al MAS NMR of the reference geopolymer, unheated.

The major ^{27}Al peak at 57.7 ppm arises from tetrahedral AlO_4 and the peaks at 27.4 and 1.5 ppm correspond to aluminium in 5-coordination (AlO_5) and 6-coordination (AlO_6) respectively. These sites are typically

found in the meta-halloysite starting material, and hence probably due to a small amount of unreacted meta-halloysite, indicating an incomplete geopolymerisation process eventually due to insufficient amounts of alkaline materials or water, or both.

The ^{29}Si MAS NMR spectra (Fig. 5.14) are all very similar. They all containing a major peak at about -92 ppm arising from tetrahedral silicon in predominantly $\text{Q}_4(3\text{Al})$ units and a shoulder at -106 ppm arises from unreacted quartz impurity, indicating $\text{Q}^4(0\text{Al})$.

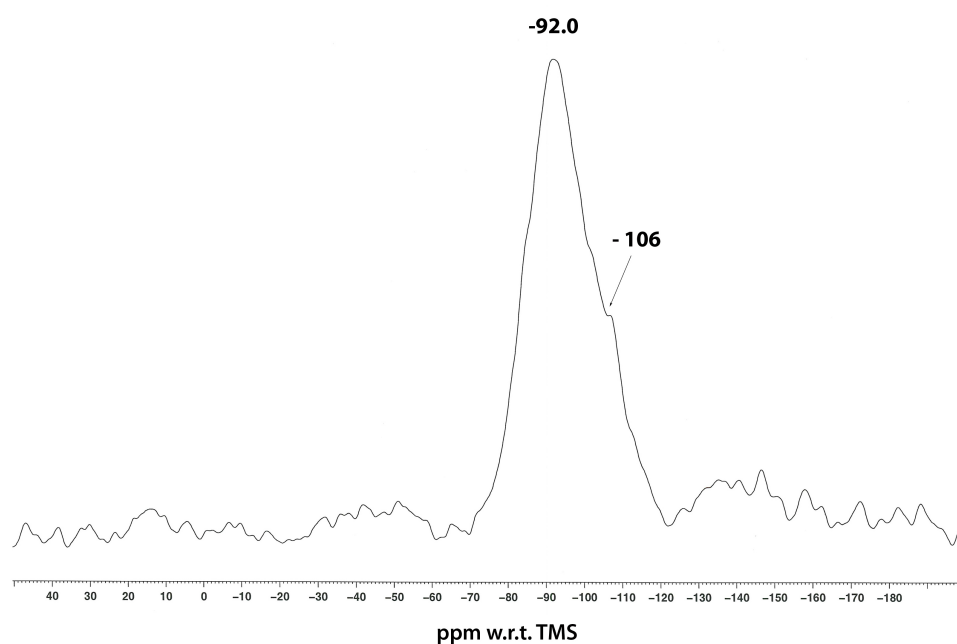


Figure 5.14: 11.7T ^{29}Si MAS NMR spectrum of the reference geopolymer, unheated.

The ^{29}Si spectrum of the sample heated to 550°C differs in that the shoulder is absent (Fig. 5.15), and that the main peak at -92.8 is relatively broad, suggesting that other Q^4 Si-units such as $\text{Q}^4(4\text{Al})$ and $\text{Q}^4(2\text{Al})$ are present under the spectral lineshape.

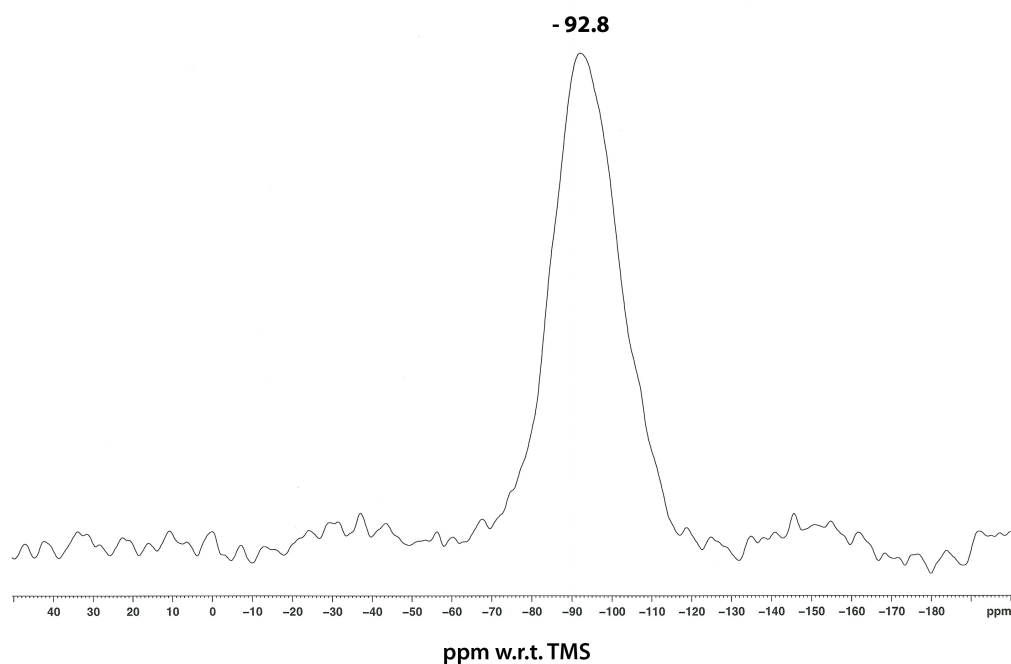


Figure 5.15: $11.7\text{T } ^{29}\text{Si}$ MAS NMR spectrum of the reference geopolymer heated to 550°C .

5.3.1.2 Calcium hydroxide geopolymers

Figure 5.16 shows the ^{27}Al MAS NMR spectrum of an unheated calcium hydroxide-containing geopolymer.

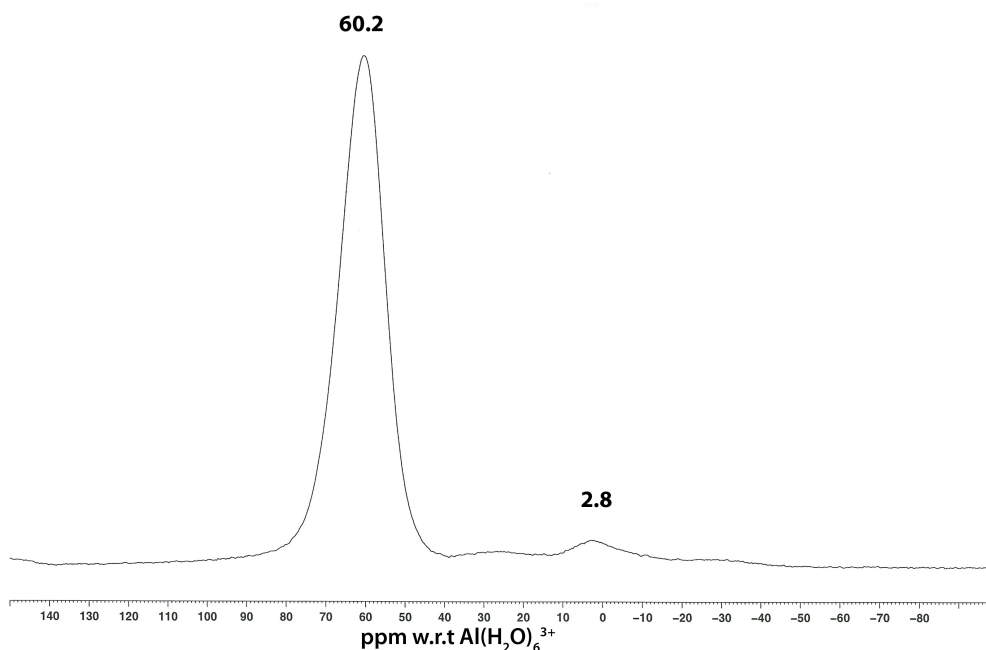


Figure 5.16: 11.7 T ^{27}Al MAS NMR spectrum of the 10wt% calcium hydroxide-containing geopolymer, unheated.

The ^{27}Al spectrum of the sample before and after the exposure to simulated body fluid remains unchanged, both spectra being shown in Figure 5.16.

The major peak at 60.2 ppm arises from the presence of aluminium in tetrahedral sites (AlO_4), and the small hump visible at 2.8 ppm shows that a small amount of 6-coordinated aluminium (AlO_6) is also present in the geopolymer, probably due to unreacted meta-halloysite. The small feature at 28 ppm is in the correct position for (AlO_5), but is too minor to

be significant.

Heating the calcium hydroxide-containing geopolymers to 550°C and 600°C changes the ^{27}Al MAS NMR spectra only slightly. The broad octahedral feature is no longer visible, the major peak at 58.3 ppm indicating only tetrahedral aluminium (Fig. 5.17), indicating an improved ideal geopolymer structure due to the absence of 5- and 6- coordinated aluminium. In-vitro exposing experiments do not change these ^{27}Al MAS NMR spectra.

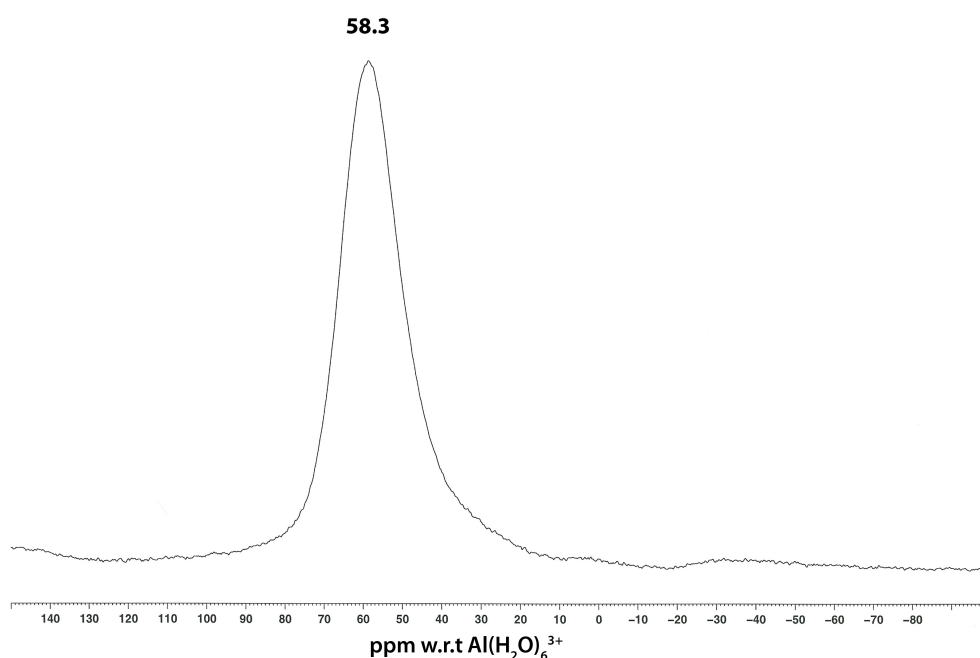


Figure 5.17: $11.7\text{ T } ^{27}\text{Al}$ MAS NMR spectrum of the 10wt% calcium hydroxide-containing geopolymer heated to 550°C.

The ^{29}Si spectrum of the unheated calcium hydroxide-containing geopolymers is shown in Figure 5.18.

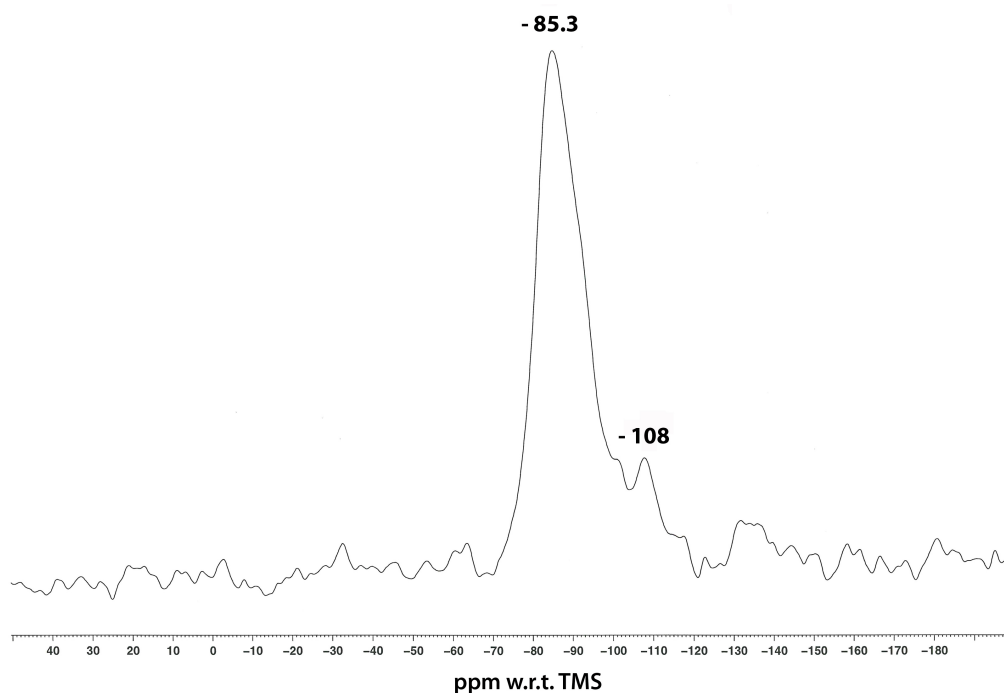


Figure 5.18: 11.7 T ^{29}Si MAS NMR spectrum for the 10wt% calcium hydroxide-containing geopolymer cured at room temperature.

The major peak at -85.3 ppm is in the general vicinity of a typical ^{29}Si geopolymer resonance (-90 ppm), normally assigned to $\text{Q}^4(3\text{Al})$ units [24]. The small downfield shift of this resonance has also been reported in geopolymer samples containing calcium hydroxide [24] and may be due either to the effect of the calcium or to a greater degree of saturation by aluminium, producing $\text{Q}^4(4\text{Al})$ and $\text{Q}^4(3\text{Al})$ units. The small peak at -108 ppm is due to the unreacted SiO_2 (quartz) impurity and arises from silicon in $\text{Q}^4(0\text{Al})$. The ^{29}Si spectrum of the unheated calcium hydroxide-containing geopolymer is unchanged by the in-vitro experiments.

Calcium hydroxide-containing geopolymers heated to 550°C and 600°C (Fig. 5.19) show variations in their ^{29}Si MAS NMR spectra.

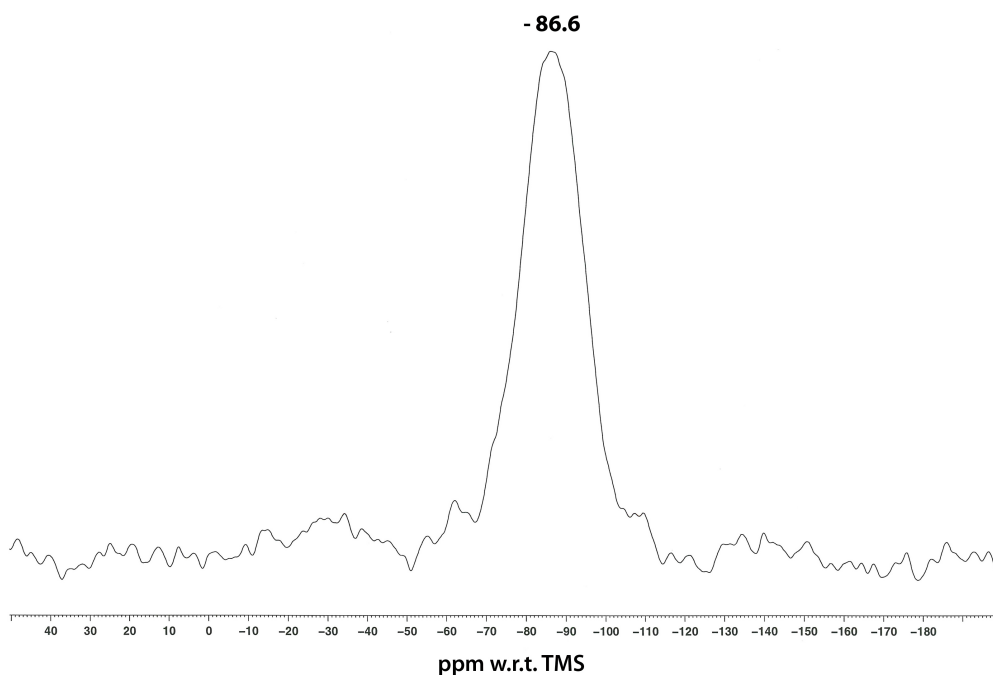


Figure 5.19: 11.7 T ^{29}Si MAS NMR spectrum of the 10wt% calcium hydroxide-containing geopolymer heated to 550°C.

Compared to the unheated geopolymer the main ^{29}Si -NMR peak at -86.6 ppm of the samples heated to 550°C and 600°C appears to be broader. Thus, the shoulder arising from quartz at -108 ppm, if present in Fig. 5.18, is obscured by the noise. However, in Fig. 5.19 because of the broadening effect the present quartz impurity at -108 ppm only appears as a small shoulder and not as a proper peak but is still there.

The major peak at -86.6 ppm (Fig. 5.19) indicates tetrahedral silicon in $\text{Q}^4(4\text{Al})$ and possibly $\text{Q}^4(3\text{Al})$. In-vitro exposing to SBF does not change the ^{29}Si MAS NMR spectra significantly, and their major peak is probably

again due to $Q^4(4Al)$ and $Q^4(3Al)$ units. Thus, both the ^{27}Al and the ^{29}Si MAS NMR spectra of the calcium hydroxide-containing geopolymers are consistent with those of normal geopolymers, and are unchanged by either heating or exposure to SBF.

5.3.1.3 Calcium silicate geopolymers

Calcium silicate-containing geopolymers cured at room temperature without additional heat-treatment have similar ^{27}Al MAS NMR spectra to that of shown in Figure 5.20, both before and after the in-vitro exposing experiments.

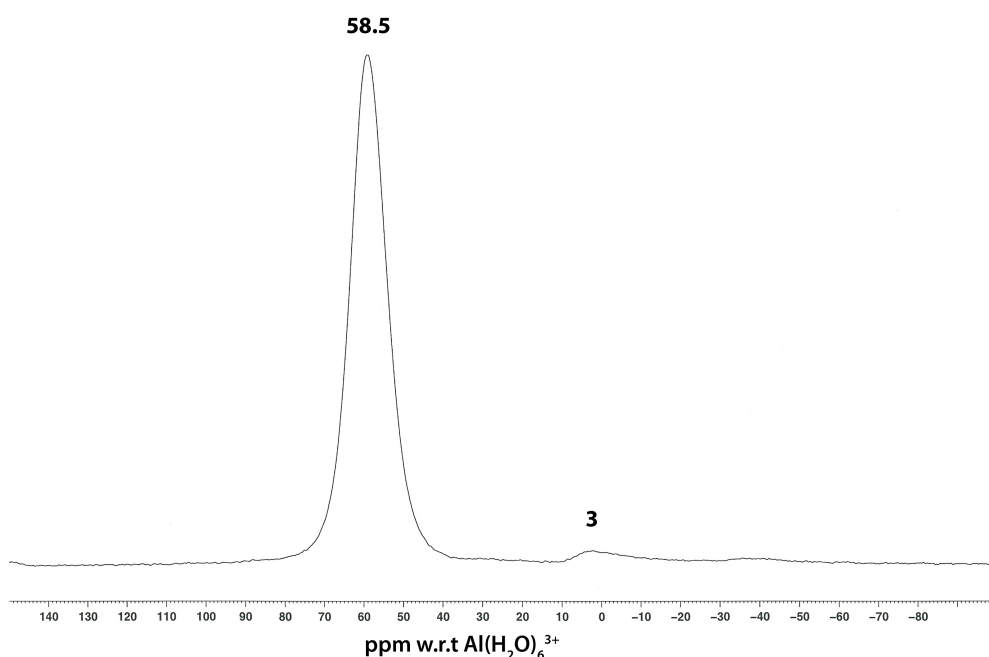


Figure 5.20: 11.7 T ^{27}Al MAS NMR spectrum of a 10wt% calcium silicate-containing geopolymer cured at room temperature.

The sharp peak at 58.5 ppm arises from tetrahedral aluminium (AlO_4),

while the small hump at 3 ppm arises from a very small amount of 6-coordinated aluminium (AlO_6) arising from unreacted meta-halloysite.

The ^{27}Al MAS NMR spectra of geopolymers containing calcium silicate after heating to 550°C and 600°C are very similar and are represented by Figure 5.21 (spectrum of the sample heated to 550°C). They show only a sharp peak at about 57 ppm, indicating aluminium in solely tetrahedral coordination. The absence of 5- and 6-coordinated aluminium indicates an improvement of the ideal geopolymer structure after heating.

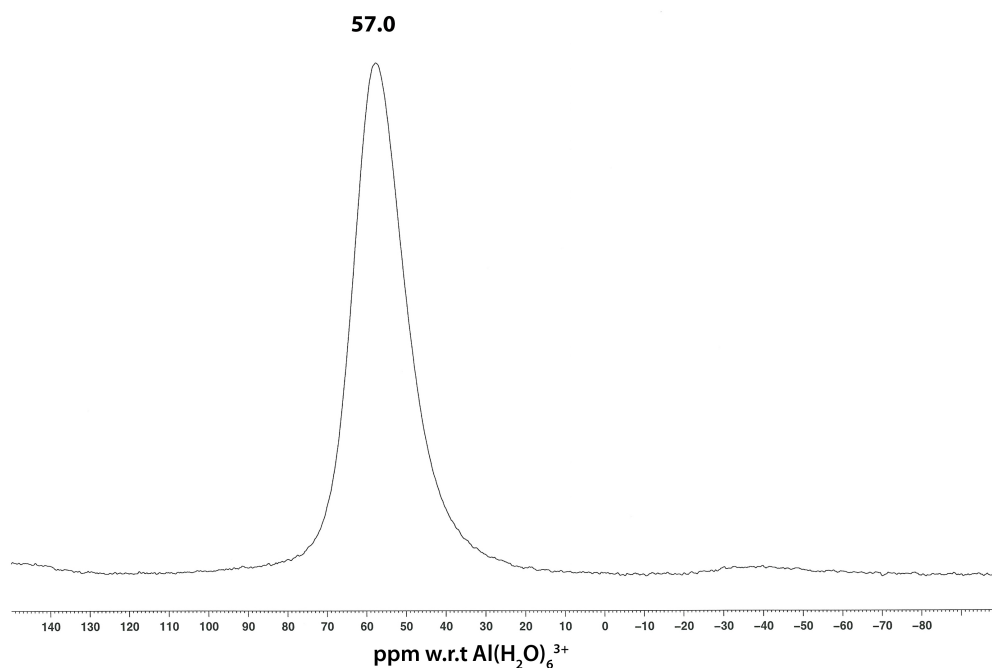


Figure 5.21: 11.7 T ^{27}Al MAS NMR spectrum of a geopolymer containing 10wt% calcium silicate, after heating to 550°C .

Exposure to simulated body fluid does not change the coordination state of the aluminium which remains tetrahedral (AlO_4), similar to the

spectrum shown in Figure 5.21.

The ^{29}Si MAS NMR spectra of geopolymers containing nano structured calcium silicate unheated, heated to 550°C and 600°C prior to the in-vitro exposure experiments show comparable results, regardless of the heating temperature. A similar spectrum is shown also by the unheated calcium silicate geopolymer after the in-vitro exposure to SBF. Figure 5.22 is representative of those spectra, showing a major peak at -90.2 ppm typical of a geopolymer with silicon in $\text{Q}^4(3\text{Al})$ and possibly $\text{Q}^4(4\text{Al})$ sites.

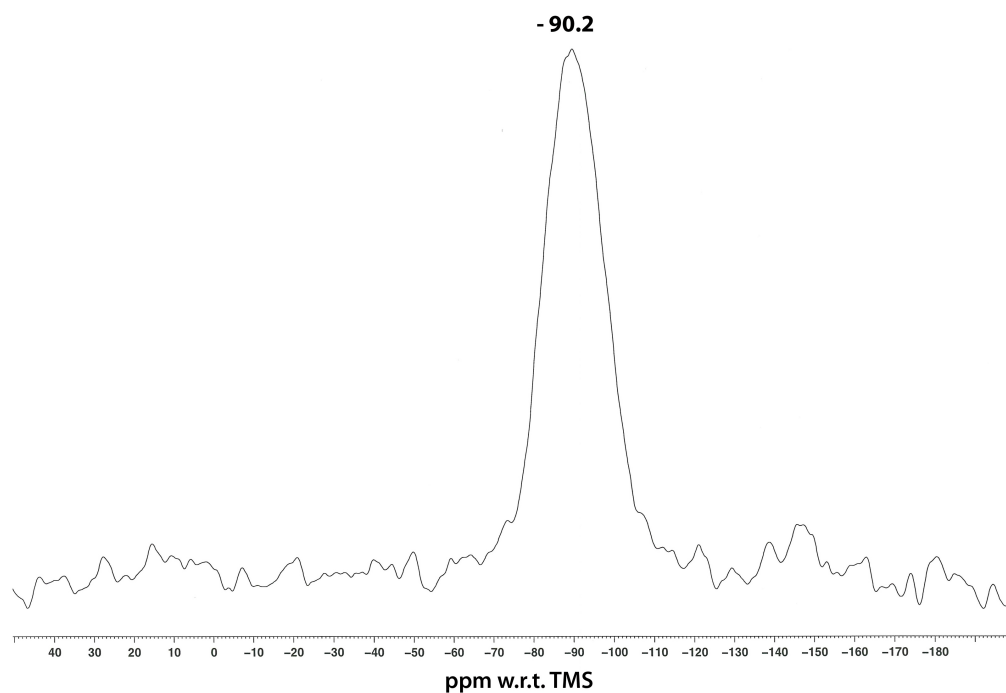


Figure 5.22: $11.7\text{ T }^{29}\text{Si}$ MAS NMR spectrum of a $10\text{wt}\%$ calcium silicate-containing geopolymer heated to 550°C .

Geopolymers containing calcium silicate heated to 550°C and 600°C show slightly altered ^{29}Si MAS NMR spectra after exposure to SBF for 5 and 7 weeks, with evidence of shoulders at -94 and -104 ppm (Fig. 5.23). The large peak at about -90.6 ppm is typical of a geopolymer $\text{Q}^4(3\text{Al})$ or ($\text{Q}^4(4\text{Al})$) environment. The shoulder at -94 ppm is due to a silicon unit less saturated in aluminium, such as $\text{Q}^4(2\text{Al})$, and the shoulder at -104 ppm may arise from $\text{Q}^4(1\text{Al})$ units containing even less aluminium coordinated in the aluminosilicate units.

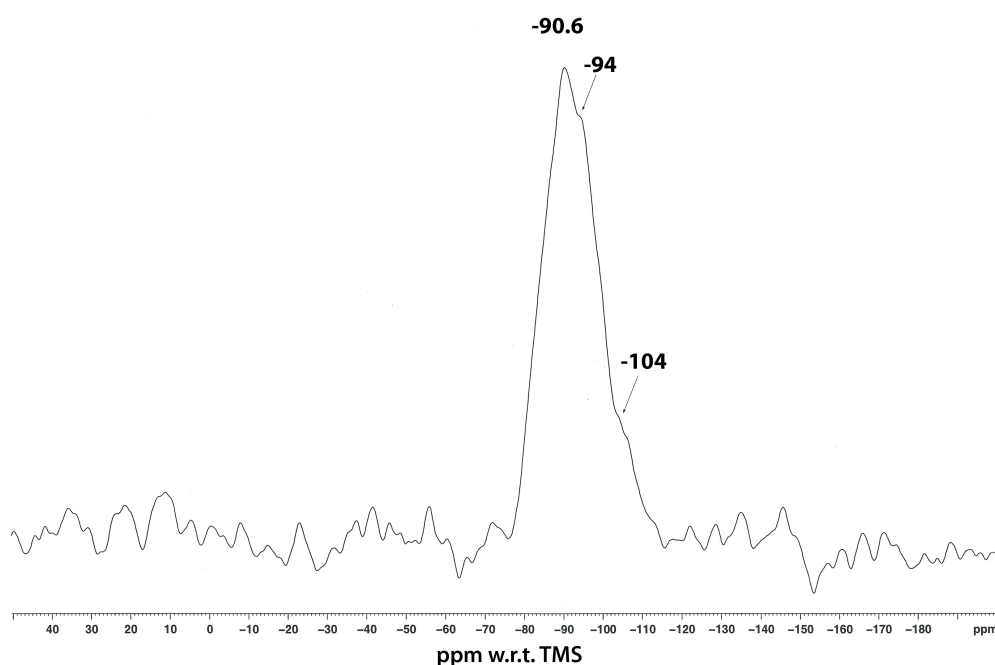


Figure 5.23: 11.7T ^{29}Si MAS NMR spectrum of a 10wt% calcium silicate-containing geopolymer heated to 600°C, after 7 weeks SBF exposure.

5.3.1.4 Calcium phosphate geopolymers

A typical ^{27}Al MAS NMR spectrum of an unheated geopolymer containing 10wt% calcium phosphate both before and after in-vitro exposure to simulated body fluid is shown in Figure 5.24.

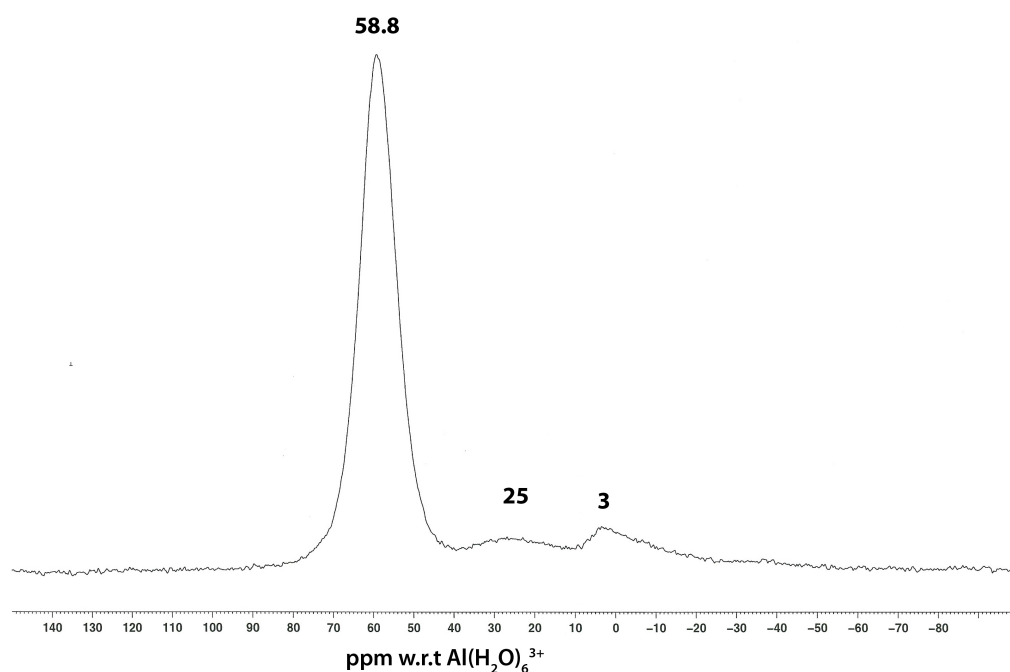


Figure 5.24: 11.7T ^{27}Al MAS NMR spectrum of an unheated 10wt% calcium phosphate-containing geopolymer.

The large peak at 58.8 ppm is due to tetrahedral aluminium (AlO_4) and the two smaller features at 25 and 3 ppm arise from small amounts of 5- and 6-coordinated aluminium, probably from unreacted meta-halloysite.

The ^{27}Al spectra of 10wt% calcium phosphate-containing geopolymers heated to 550°C and 600°C are unchanged by the in-vitro exposure experiments. A typical spectrum is shown in Figure 5.25.

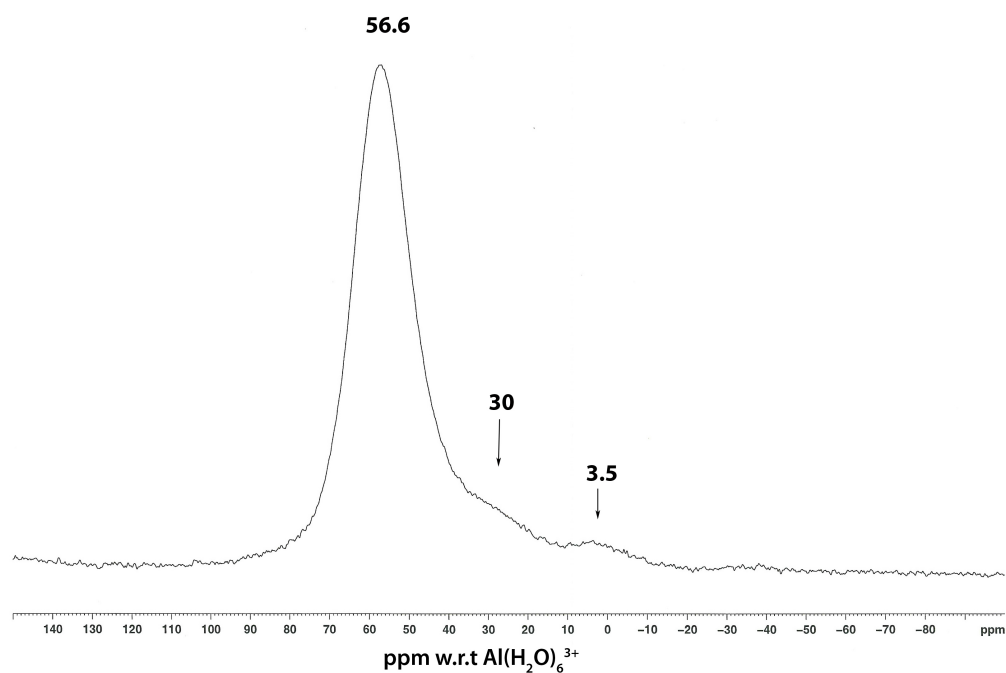


Figure 5.25: 11.7T ^{27}Al MAS NMR spectrum of the 10wt% calcium phosphate-containing geopolymer heated to 550°C.

The main peak at 56.6 ppm due to 4-coordinated aluminium appears to be broader with a small downfield shift compared to the main peak in Figure 5.24. This probably arises from the still incomplete reaction of the meta-halloysite, indicated by the poorly resolved peaks at 30 and 3.5 ppm. The broadening effect is probably due to an aluminium-phosphate phase ($\text{Al}(\text{PO}_4)$).

The ^{29}Si MAS NMR spectrum of the unheated sample (Fig. 5.26), has its major peak at -90.5 ppm indicating 4-coordinated silicon in $\text{Q}^4(3\text{Al})$ units typical of a geopolymer. The small peak at about -107 ppm arises from unreacted silica ($\text{Q}^4(0\text{Al})$ and $\text{Q}^4(1\text{Al})$ sites), probably due to the quartz impurity. The shoulder on the major peak at about -100 ppm may indicate the presence of silicon in $\text{Q}^4(1\text{Al})$ and $\text{Q}^4(2\text{Al})$ sites. Similar results were found for samples both before and after exposure to SBF, which show ^{29}Si spectra similar to Figure 5.26.

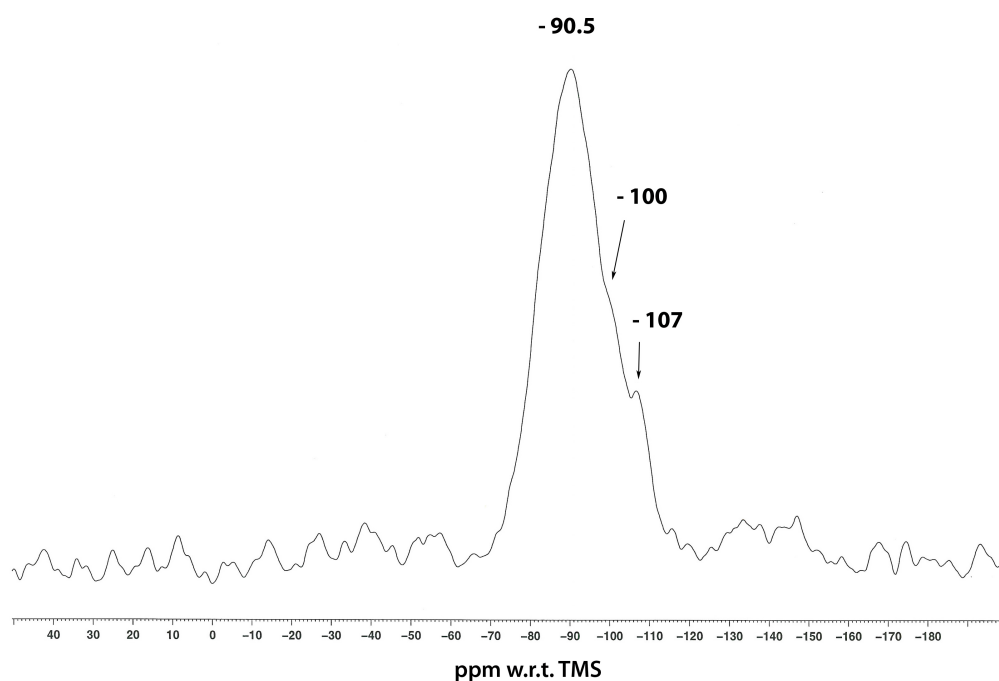


Figure 5.26: 11.7T ^{29}Si MAS NMR spectrum of a geopolymer containing 10wt% calcium phosphate.

The ^{29}Si MAS NMR spectra of calcium phosphate-containing geopolymers heated to 550°C and 600°C prior to exposure to simulated body fluid (Fig. 5.27), are slightly different to the ^{29}Si MAS NMR spectrum of the unheated sample (Fig: 5.26).

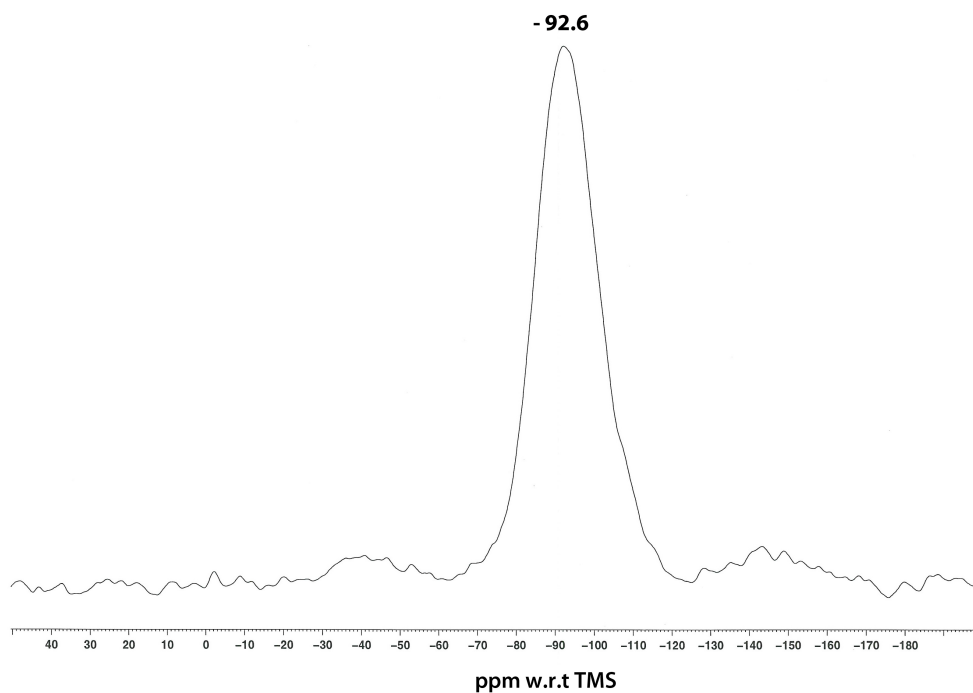


Figure 5.27: 11.7T ^{29}Si MAS NMR spectrum of the geopolymer containing 10wt% calcium phosphate heated to 550°C.

The single peak at -92.6 ppm is typical of predominantly $\text{Q}^4(3\text{Al})$ geopolymer units. A similar ^{29}Si MAS NMR spectrum is found for the sample heated to 550°C after exposure to SBF.

However, as shown in Figure 5.28, after the in-vitro exposure experiments of the calcium phosphate-containing geopolymer heated to 600°C, the ^{29}Si MAS NMR spectrum appears slightly different from that of the unexposed geopolymer, showing a sharp peak at -93.7 ppm and slight shoulders at -100 ppm and -107 ppm. These features indicate the presence of silicon in predominantly $\text{Q}^4(3\text{Al})$ sites, together with some unreacted meta-halloysite and quartz impurities (silicon in $\text{Q}^4(2\text{Al})$, $\text{Q}^4(1\text{Al})$ and $\text{Q}^4(0\text{Al})$), .

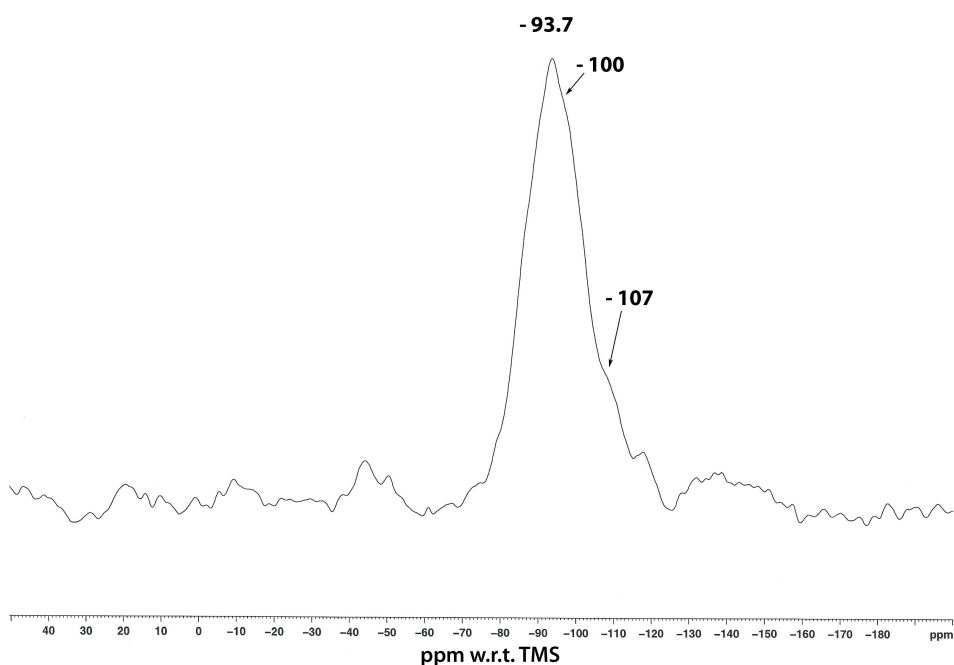


Figure 5.28: 11.7T ^{29}Si MAS NMR spectrum of the 10wt% calcium phosphate-containing geopolymer heated to 600°C, after seven weeks SBF exposure.

Summary

- ^{27}Al MAS NMR and ^{29}Si MAS NMR of all the geopolymers show the presence of tetrahedral aluminium and silicon.
- Heating the samples to 550°C and 600°C to lower their pH does not affect the geopolymer structure.
- Exposure to simulated body fluid does not change the geopolymer structure of any of the samples.

5.3.2 ^{43}Ca MAS NMR of calcium phosphate geopolymers

This section presents the natural abundance ^{43}Ca MAS NMR results for all the geopolymers containing 10 wt% of calcium phosphate, including the unheated sample, samples heated to 550°C and 600°C, and these samples after the in-vitro exposure experiments. The ^{43}Ca MAS NMR spectra are shown in Figure 5.29, and the peak positions and additional information listed in Table 5.4.

Table 5.4: ^{43}Ca MAS NMR shifts of the centre-of-gravity (δ_{COG}) of calcium phosphate-containing geopolymers, uncertainties in brackets.

Sample	δ_{COG} (ppm)	peak width (Hz)	no. of scans
unheated	-11 (4)	1260 (100)	59227
unheated, 4 weeks SBF exposure	-11 (4)	1600 (100)	108585
heated 550°C	-4 (4)	1500 (100)	117824
heated 550°C, 4 weeks SBF exposure	-4 (4)	1000 (100)	113617
heated 600°C	-7 (4)	1400 (100)	116903
heated 600°C, 4 weeks SBF exposure	-7 (4)	unmeasured	106798

All the ^{43}Ca MAS NMR spectra show almost identical results before SBF exposure. However, there are slight variations in the peak positions (Tab. 5.4); the ^{43}Ca peak of the unheated geopolymer is at about -5 ppm

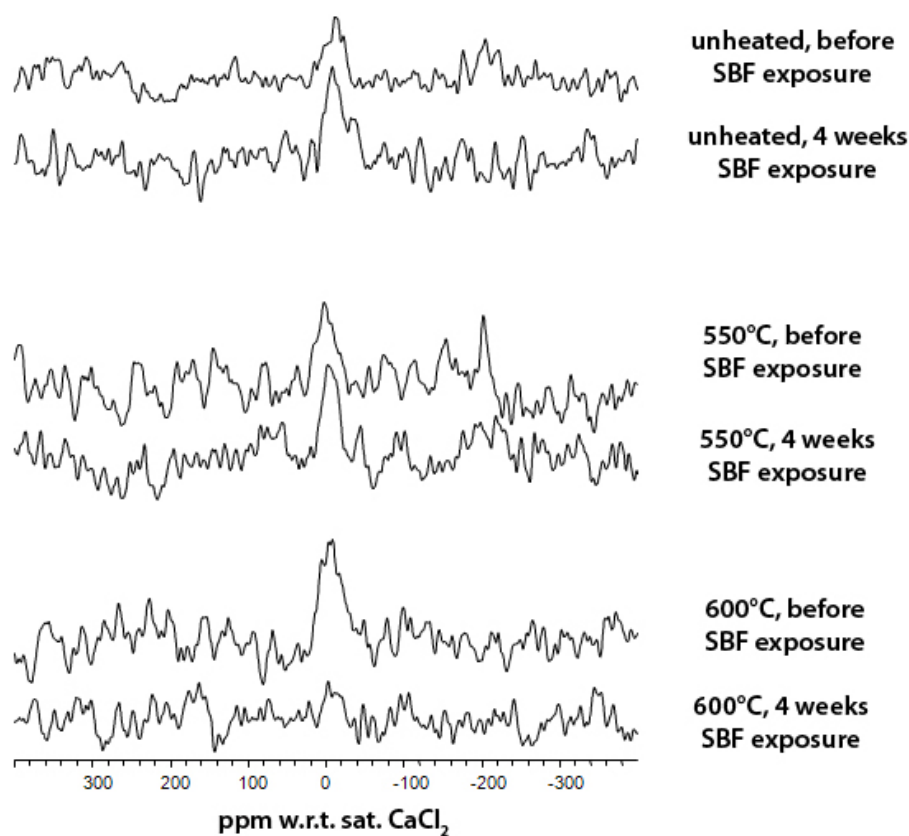


Figure 5.29: $14.1T$ ^{43}Ca MAS NMR spectra of calcium phosphate-containing geopolymers before and after SBF exposure

while it is about -10 ppm in both the heated samples. The quality of these spectra (noise and broadness) reflects the extreme difficulty in obtaining natural abundance ^{34}Ca NMR spectra (the natural abundance of ^{34}Ca is 0.135%). Therefore, these peak positions represent the centre-of-gravity (δ_{COG}) of the resonance. These peak positions are very similar to those previously published for samples containing 30 and 50wt% calcium phosphate (-6 to -7 ppm [24]).

Since the number of scans in each case is very similar, the peak heights

should provide an approximate indication of the amount of calcium detected in each sample. These show that apart from the sample heated to 600°C and exposed to SBF, the amounts of calcium (and their peak positions) are unchanged by heating or SBF exposure. In the case of the sample heated to 600°C and exposed to SBF, the absence of calcium suggests it must have leached out of the material. Another possible reason for its disappearance is that it is distributed over a large number of sites corresponding to a number of environments, as in a gel. This gel is not calcium-silicate-hydrate (C-S-H) gel, however, since this has a peak of similar widths to the present spectra, but centred at 14.6 ppm [24].

This result is peculiar and cannot be explained by ICP analysis nor by SEM/ EDS observations. ICP analysis (section 5.5) shows that the calcium phosphate-containing geopolymer absorbs the calcium of the simulated body fluid. EDS analysis of an identical sample shows the presence of calcium, distributed mostly homogeneously (section 5.6.4).

5.4 Alteration of the pH of the SBF

The pH values of the simulated body fluid, during the in-vitro exposure experiments, changed significantly within the first four hours of all experiments, then became stable. All the in-vitro experiments began at pH of 7.4.

5.4.1 Behaviour of the reference and calcium phosphate geopolymers in SBF

Exposure to SBF of the reference geopolymer and calcium phosphate-containing geopolymer samples resulted in similar pH-development patterns, shown in Figure 5.30 for the reference geopolymer and Figure 5.31 for the calcium phosphate-containing geopolymer.

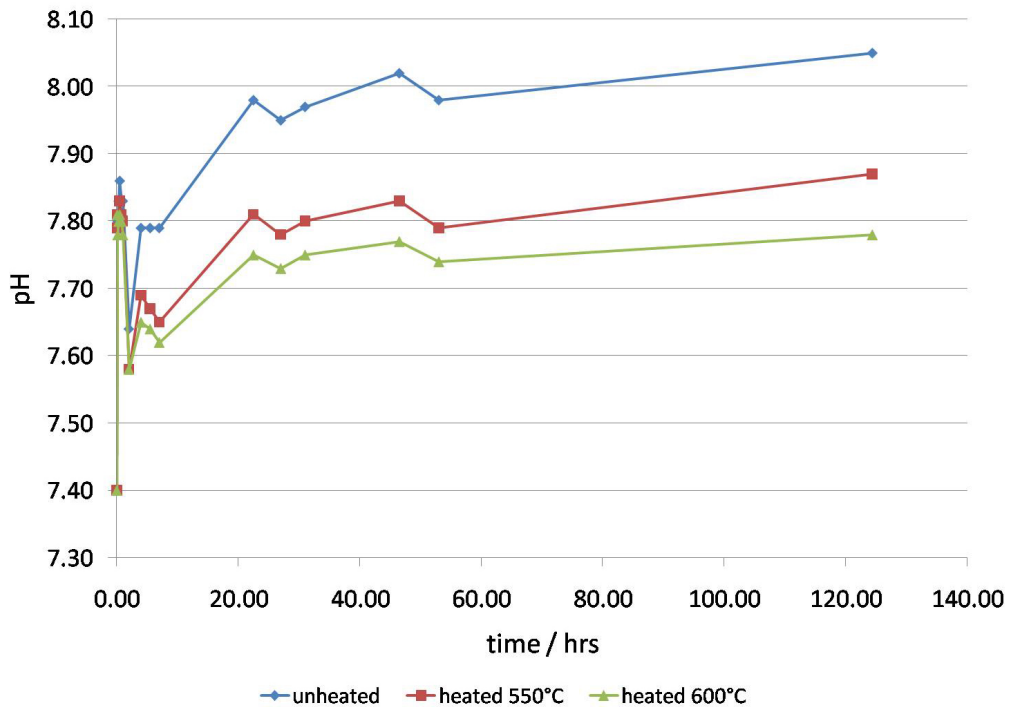


Figure 5.30: Changes of the pH of the SBF during exposure of the reference geopolymers.

The highest pH values of the SBF solution were recorded for the unheated reference and calcium phosphate-containing samples (≈ 8 and 8.2 respectively). In-vitro exposure experiments on the reference and calcium phosphate-containing geopolymers heated to 550°C produced pH values

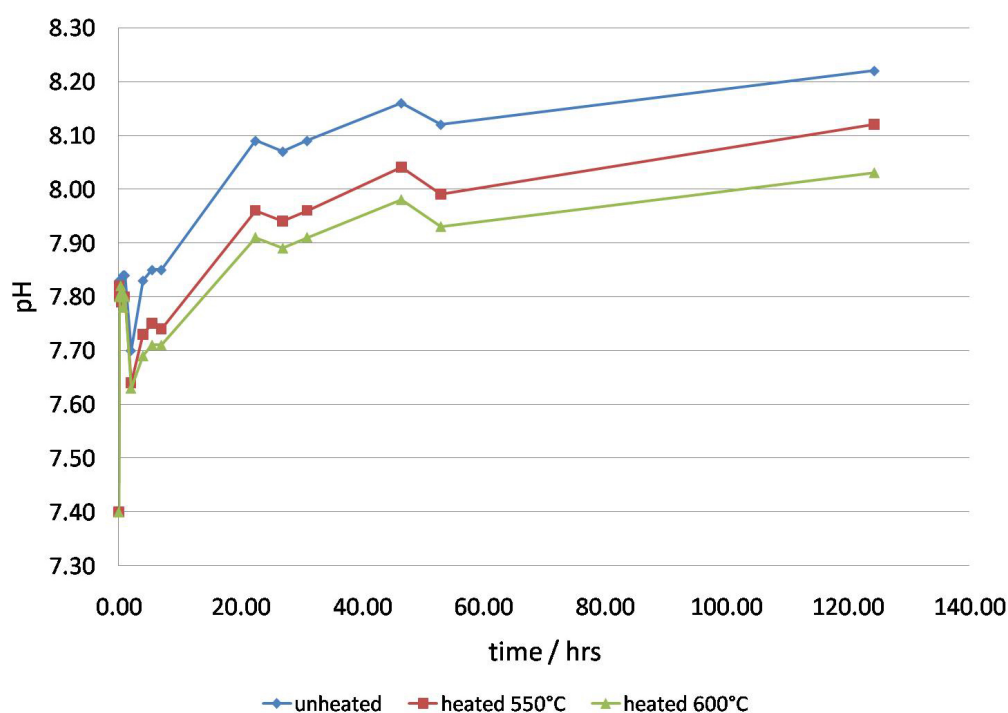


Figure 5.31: Changes of the pH of the SBF during exposure of the calcium phosphate-containing geopolymers.

of 7.9 and 8.1 respectively. The measured pH of the solution containing samples heated to 600°C decreased only slightly by pH of 0.1. All these solutions showed a slight increase in the pH between 4 and 30 hours. Thereafter, the pH of the simulated body fluid of the reference geopolymer heated to 600°C remained stable (≈ 7.8), but all the other fluids showed a further small increase of the pH of approximately 0.1 units until the end of the experiments after 125 hours.

5.4.2 Behaviour of the calcium hydroxide geopolymers in SBF

The pH of the simulated body fluid during in-vitro exposure experiments of calcium hydroxide-containing geopolymers is shown in Figure 5.32.

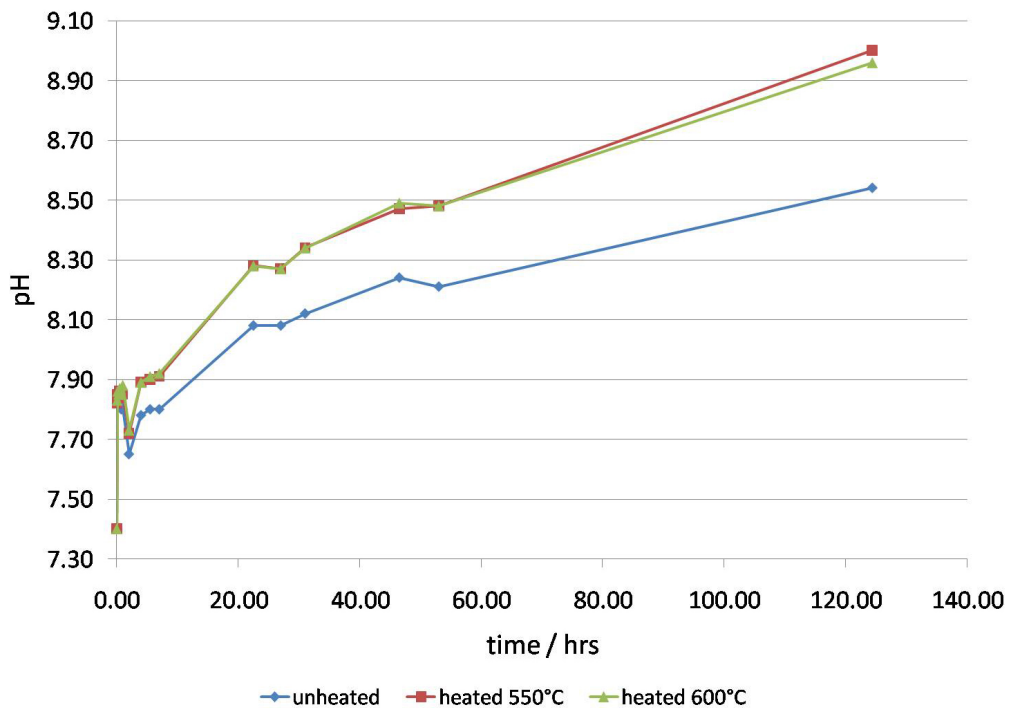


Figure 5.32: Changes of the pH of the SBF during exposure of the calcium hydroxide-containing geopolymers.

Samples heated to 550°C and 600°C affected the solution equally and produced slightly higher pH values (≈ 9) compared with the unheated sample (≈ 8.5). The curves are almost parallel in the early stages and increase more steeply during the first 24 hours to pH 8 and 8.3 for the unheated and heated samples respectively. This is followed by a steady

increase of the pH, reaching values of ≈ 9 and 8.5 after 125 hours, when the experiments were stopped.

5.4.3 Behaviour of the calcium silicate geopolymers in SBF

The pH changes of the SBF during in-vitro exposure experiments of calcium silicate-containing geopolymers are shown in Figure 5.33.

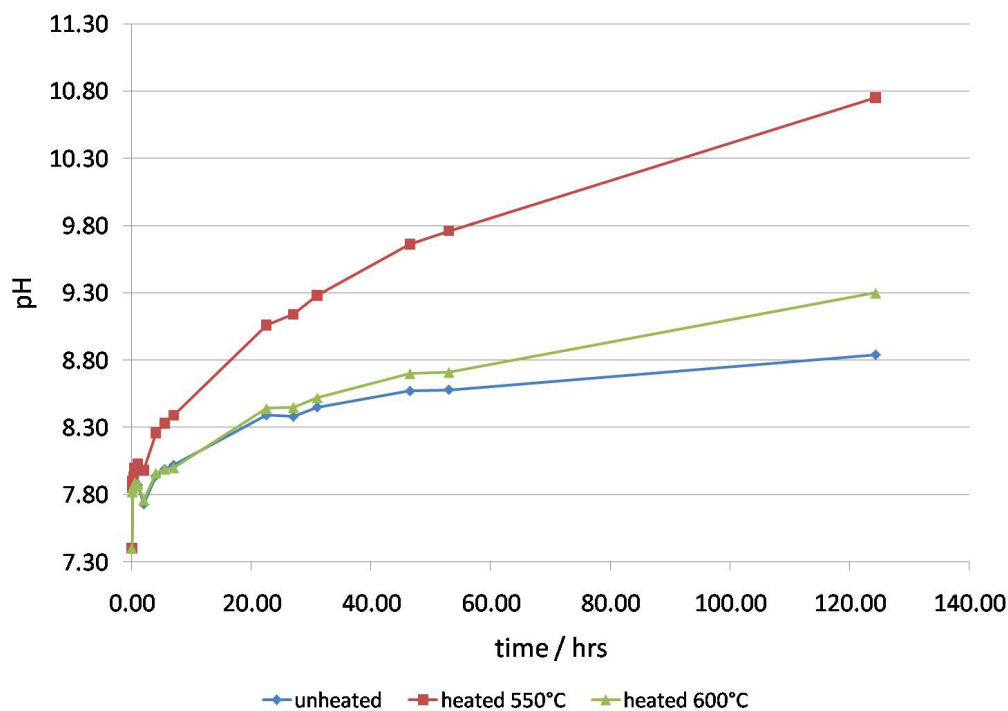


Figure 5.33: Changes of the pH of the SBF during exposure of the nano structured calcium silicate-containing geopolymers.

The unheated sample and the sample heated to 600°C behave similarly, producing pH values of approximately 8.8 and 9.3 respectively, after 125

hours. The solution of these exposed samples produce a significant increase in the pH within the first 24 hours followed by a slower increase until the experiments were ended after 125 hours. The pH of the SBF solution containing the sample heated 550°C behaves differently, showing a steadily increasing pH to 9.8 after 53 hours of exposure, followed by a slower pH increase to ≈ 10.8 until the ending of the experiment. However, this pH behaviour might be due to the fact that the sample broke into two pieces when initially exposed to the SBF.

All the diagrams of the pH-measurements presented in this section show minor fluctuations in the pH during the experiments. These trends can probably be referred to the re-calibration of the pH-meter before each measurement. The fluctuations are within the pH-meter's accuracy (± 0.03 pH) and can be left unattended. This phenomenon is most noticeable in Figures 5.30 and 5.31 due to the pH-scale used here.

Immersion of all the geopolymers in SBF led to reaction between the material and the solution. The samples containing calcium hydroxide and nano-structured calcium silicate underwent the most obvious reaction. The calcium hydroxide-containing geopolymers released a considerable quantity of gas, which was possibly air present in the pores of the samples being displaced by the SBF solution. This led to the development of minor cracks whereas the geopolymers containing calcium silicate not only released gas bubbles but fell to pieces. Minor gas release without cracking of the sample was noticed for the reference geopolymer and the geopolymer containing calcium phosphate after their immersion in simulated body fluid.

These observations may explain the higher pH values measured for the samples containing calcium hydroxide and calcium silicate, since cracking of the samples leads to an increased sample surface and thus a larger area exposed to the SBF. The significantly higher alkalinity of the SBF produced by the exposure of the calcium silicate-containing geopolymers may also be explained by the higher content of alkaline potassium hydroxide (section 3.3.1).

The lower pH values measured when calcium phosphate geopolymers were exposed can also be explained by the solubility of the calcium phosphate in alkaline conditions in aqueous media reported by Hench [16]. He quoted that the stable calcium phosphate phase at $\text{pH} > 4.2$ is hydroxyl apatite. Unhydrated, high-temperature calcium phosphate phases, such as tri-calcium phosphate, interact with water, or body fluids at 37°C to form hydroxyl apatite. Thus, the solubility of a tri-calcium phosphate (TCP) surface approaches the solubility of hydroxyl apatite and decreases the pH of the solution [16].

According to these results, the reference geopolymer and the calcium phosphate-containing geopolymer both show that an increase in the heating temperature results in a lowering of the pH. Similar results have been reported previously showing that pH-values of approximately 7 can be achieved in geopolymers heated to 500°C (Oudadesse et al. [11], [3]). However, different geopolymer powder compositions and distilled water were used for their experiments, which are therefore not directly comparable.

The reference and the calcium phosphate-containing geopolymer heated to 600°C showed the best results, in terms of both pH and material

stability when exposed to SBF. Both materials provide the lowest pH of all the samples (≈ 8). The calcium-phosphate containing geopolymer was chosen for further studies by ^{43}Ca MAS NMR (section 5.3.2).

5.5 ICP analysis of the SBF after exposure of the geopolymers

Results of inductively coupled plasma analysis are shown in this section. The simulated body fluid to which geopolymers heated to 600°C were exposed was chosen for this work. It should be noted that the simulated body fluid was renewed every two weeks but was analysed weekly. The analysed elements were calcium (Ca), phosphorus (P), silicon (Si), aluminium (Al) and potassium (K).

5.5.1 Phosphorus analysis

As shown in Figure 5.34, all samples absorb the phosphorus present in the simulated body fluid during the in-vitro experiment.

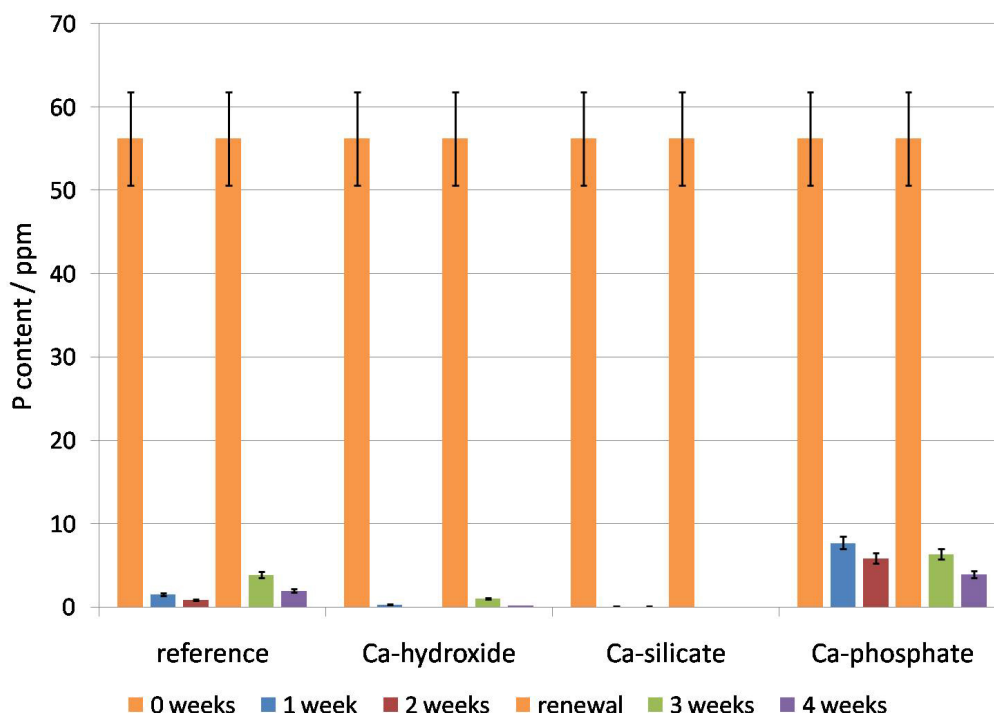


Figure 5.34: ICP results of phosphorus content in SBF after various exposure times.

The original content of phosphorus in the simulated body fluid is drastically reduced after one and two weeks exposure time regardless of the calcium compound in the geopolymer. In the first two weeks, the calcium hydroxide and calcium silicate geopolymer composites absorbed almost all of the phosphorus, but 1 - 6 ppm of phosphorus remained in the solution to which the reference and the calcium phosphate geopolymer were exposed. After renewal of the SBF, the phosphorus present after the second two weeks of exposure is slightly higher than the amount of phos-

phorus absorbed in the first two weeks, but the rate of absorption is also slightly higher than in the first two weeks; the phosphorus present in the SBF decreased by at least 50% to 60% in the second exposure period by comparison with a 25% to 30% decrease during the first two weeks. This increase in the absorption of phosphorus may be due to changes in the material during the first exposure period. The possibility of a change in the structure, cannot be excluded e.g. an increase in the porosity or the formation of a calcium phosphate phase (section 5.2.3 and 5.2.4) which would deplete the phosphorus in solution. However, the formation of new phases in the reference geopolymer and the calcium phosphate-containing geopolymer was not confirmed by x-ray diffraction.

5.5.2 Aluminium analysis

The results of the ICP analysis for the aluminium contents of the simulated body fluid are shown in Figure 5.35.

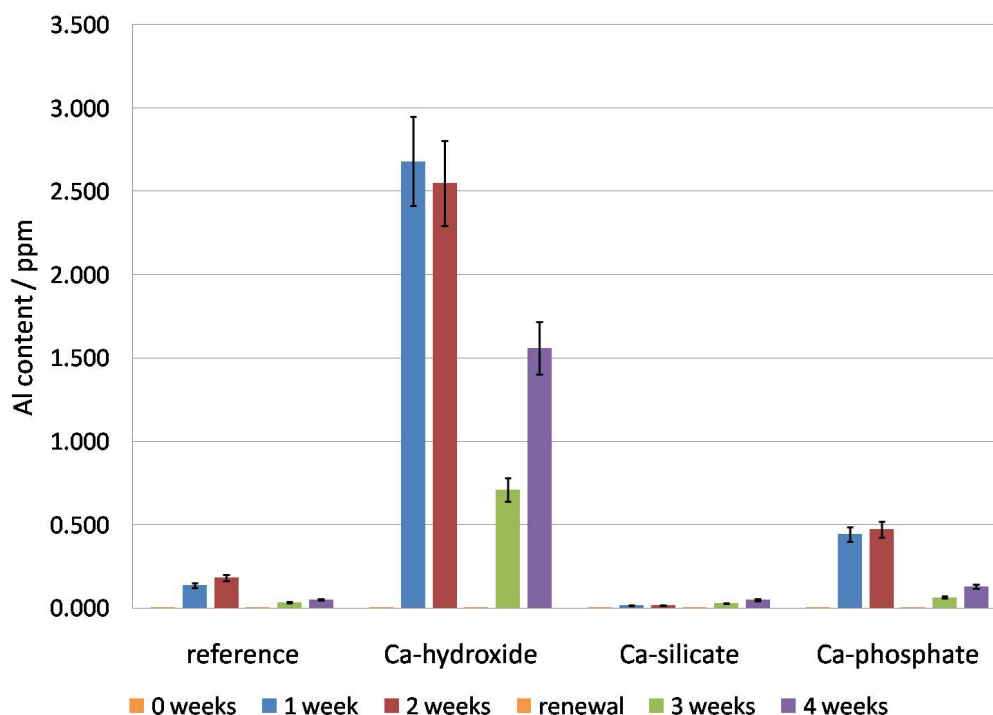


Figure 5.35: Aluminium concentration in SBF after exposure of the various geopolymers for various times.

This shows all the geopolymers release some aluminium during exposure, and although aluminium is not detectable in the SBF (orange bar absent) the calcium hydroxide geopolymer releases considerably more aluminium than the other geopolymers. In case of the calcium hydroxide geopolymer, more aluminium is released into the SBF after the first week (≈ 2.7 ppm) than during the second week (≈ 2.5 ppm). This drop in the aluminium content may be due to reabsorption by the geopolymer. How-

ever, renewing the SBF after the second week produces a steady increase in the aluminium released, a trend also seen in the other geopolymers.

The lowest results in terms of aluminium release were found for the calcium silicate-containing geopolymers, in which traces of aluminium, (0.015 and 0.016 ppm) could be detected after one and two weeks exposure time, respectively. However, renewal of the SBF led to the leaching of slightly higher amounts of aluminium (0.027 and 0.049 ppm) during the following two weeks.

Similar trends are seen in the behaviour of the reference geopolymer and the calcium phosphate-containing geopolymer. Most aluminium is released after the first two weeks, only slight differences being seen after one week. After replacement of the SBF, the aluminium concentrations increased only slightly possibly because most of the soluble aluminium was removed within the first two-week period.

The aluminium concentrations removed from these samples by the SBF are relatively low. However, it has been reported by Hantson that aluminium concentrations of less than 0.1 ppm in cerebrospinal fluid (CSF), after use of an aluminium-containing cement led to serious brain diseases [21]. Thus, because it has also been reported by Yap that minor release of aluminium is beneficial for new bone formation and to determine the biocompatibility, the literature on aluminium toxicity in humans is contradictory [19].

5.5.3 Calcium analysis

The results of the Ca analysis of the SBF are shown in Figure 5.36.

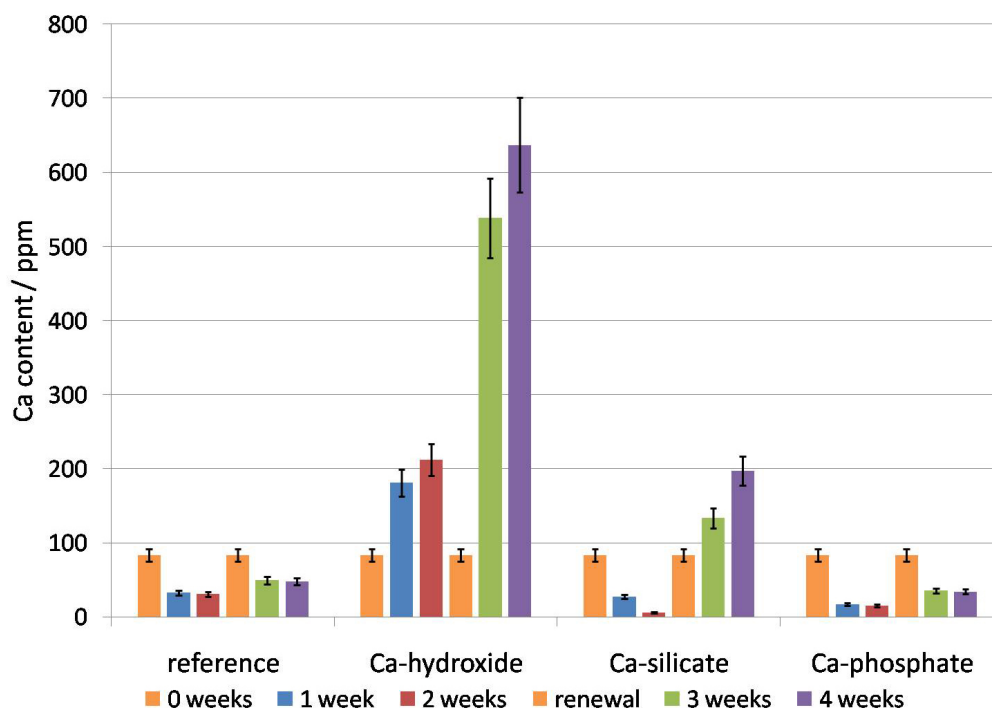


Figure 5.36: Calcium concentration in SBF after exposure of the various geopolymers for various times.

The calcium silicate-containing geopolymer absorbs calcium during the first two weeks of the in-vitro experiment, indicated by the reduced calcium concentration in the SBF. After renewing the solution, the same geopolymer apparently re-releases calcium to the solution, evidenced by the relative increase of the calcium content of the SBF. This unusual behaviour could indicate the formation of an insoluble calcium compound or x-ray amorphous gel on the surface of the sample (or the absorption of Ca^{2+} from the solution by the geopolymer during the initial exposure

period. When the concentration of Ca^{2+} is subsequently increased by the renewal of the SBF, the equilibrium is disturbed and the reaction is reversed.

Exposure of calcium hydroxide containing geopolymers leads to an increase of calcium in the SBF throughout the experiment. Replacing the SBF leads to an even quicker increase in the calcium concentration, the calcium content was about 200 ppm after one to two weeks, increasing to > 500 - 600 ppm after one and two weeks since the solution was changed.

The reference geopolymer and the calcium phosphate-containing geopolymer both show similar behaviour when exposed to simulated body fluid. The calcium concentration in the solution decreases throughout the experiment, although the geopolymer containing calcium phosphate takes up more calcium. During the first two weeks before the replenishment of the SBF, the calcium concentrations decreased to 30 and 15 ppm for the reference and the calcium phosphate-containing geopolymers respectively. The concentrations of calcium in the SBF during the second stage of the exposure experiments dropped to 48 and 34 ppm for the reference geopolymer and the geopolymer containing calcium phosphate respectively. Thus, the reference sample and that containing calcium phosphate both remove calcium from the SBF, whereas the geopolymer containing calcium hydroxide releases calcium to the SBF. The behaviour of the geopolymer containing calcium silicate is intermediate between these extremes initially removing the calcium from the SBF, then releasing it when the Ca^{2+} content is renewed.

5.5.4 Silicon analysis

The results of ICP analysis of the simulated body fluid for silicon show that 4.4 ppm of silicon is present in the original SBF solution (Fig. 5.37).

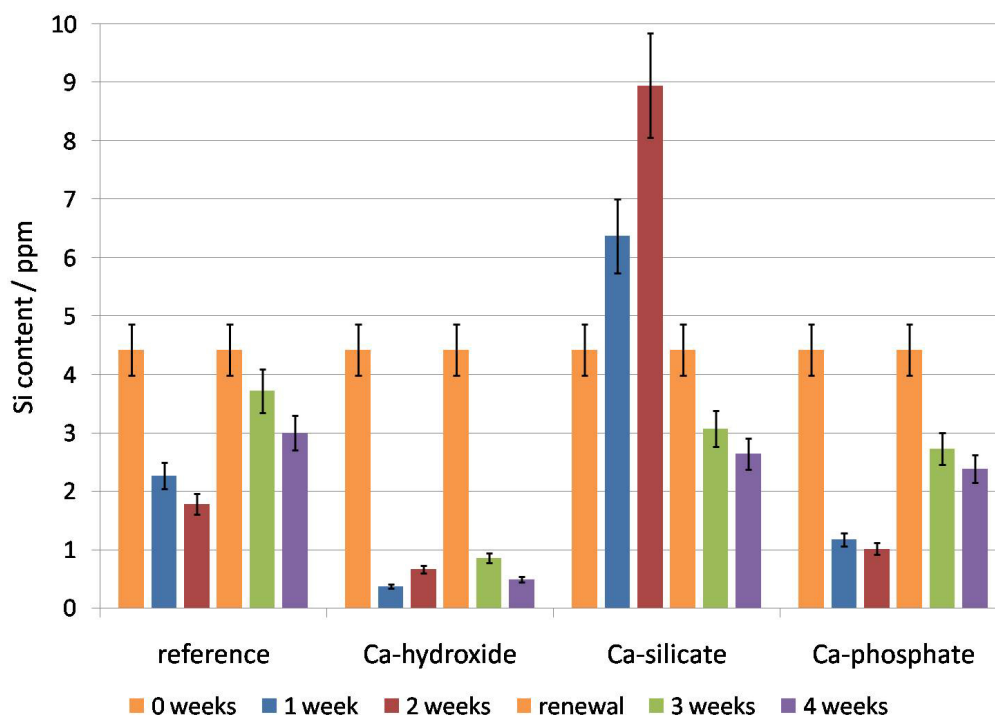


Figure 5.37: Silicon concentration in SBF after exposure of the various geopolymers for various times.

Since silicon is not part of the original formulation of the SBF, this must be an impurity, either present in one of the reagents or leached from the glass volumetric flask used to adjust the SBF volume.

Apart from the calcium silicate-containing sample, all samples absorb silicon from the solution, evidenced by the decreased amount of silicon. However, this absorption varies between the samples, the calcium hydroxide geopolymer taking up the most silicon and leaving < 1 ppm silicon,

regardless of whether or not the SBF was changed.

The reference geopolymer and the calcium phosphate-containing geopolymer show similar results whereas the calcium phosphate geopolymer absorbs about 1 ppm more silicon. Both geopolymers absorbed less silicon after the SBF had been changed, showing values of 3 and 2.3 ppm for the reference and the calcium phosphate-containing geopolymer respectively, two weeks after the SBF change. This reduced absorption might be due to an increased saturation of silicon in the geopolymer sample.

The calcium silicate geopolymer releases silicon to the SBF, increasing the silicon concentration to about 6.3 and 9 ppm after one and two weeks respectively. Changing the SBF led to the absorption of silicon during the second stage of the experiment, during which the silicon concentration dropped from 4.4 ppm to about 3.1 and 2.6 ppm one and two weeks after the change of the solution.

Thus, of all geopolymers, only that containing nano-structured calcium silicate releases silicon to the SBF, possibly due to the presence of leachable silicate in this sample. The other samples are stable to silicon-containing solutions, but will absorb small amounts of available silicon, possibly by surface absorption.

Solubility data for HA and HCA in SBF at this pH are unavailable, neither has the solubility of calcium silicate in SBF been reported in the literature. However, an indication that the extent of leaching of both Ca and Si from the inorganic polymer materials is provided by the present experimental elemental concentrations in the SBF after the leaching experiment.

5.5.5 Potassium analysis

The ICP results of the potassium analyse of the simulated body fluid are shown in Figure 5.38.

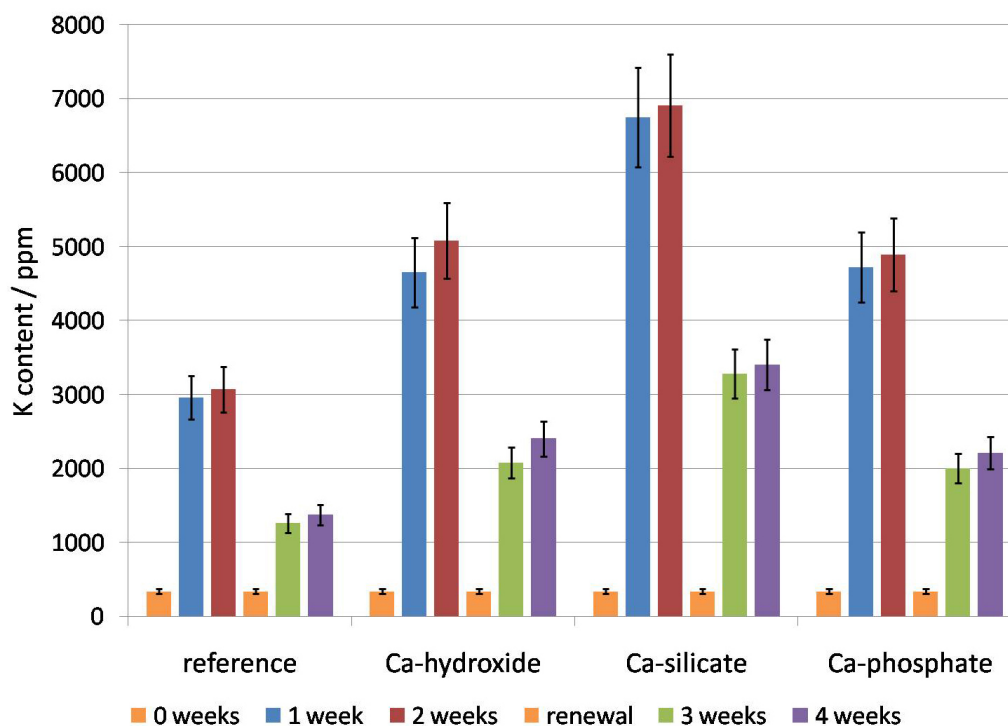


Figure 5.38: Potassium concentration in SBF after exposure of the various geopolymers for various times.

Potassium is leached from all the geopolymers increasing the potassium concentration of the SBF from its original value of about 340 ppm. After the change of simulated body fluid, the release of potassium drops by at least 50%.

The highest amount of potassium is released by the calcium silicate-containing geopolymer during the first two weeks. During this period,

the potassium concentration reduced about 6800 - 6900 ppm dropping to 3300 and 3400 ppm 1 - 2 weeks after the change of SBF.

The geopolymers containing calcium phosphate and calcium hydroxide show almost identical results. Both geopolymers increased the potassium concentration in the SBF up to about 5000 ppm after the first two weeks but this concentration then decreased to about 2300 ppm two weeks after renewal of the SBF.

The lowest level of potassium into the SBF occurred with the reference geopolymer. Only 3000 ppm potassium was leached out during the first two weeks, dropping further to about 1400 ppm after change of the simulated body fluid.

Since potassium is associated with the presence of alkalinity in the geopolymers, these results correlate with the pH measurements presented in section 5.4. The pH measurements showed that the calcium silicate-containing geopolymer produced the highest alkalinity, followed by the calcium silicate and calcium phosphate-containing geopolymers and the reference geopolymer respectively. Although the calcium hydroxide and the calcium phosphate geopolymers show almost identical leaching of potassium, the pH of the calcium hydroxide is slightly higher than that of the former (pH 8.9 and 8 respectively) possibly due to the additional content of the alkaline compound calcium hydroxide.

5.6 SEM results

In this section, scanning electron images of geopolymers heated to 600°C, before and after in vitro experiments are presented and interpreted.

Secondary electron imaging (SEI) was used for high resolution with a large depth of field whereas backscattered electron imaging (COMPO) was used for EDS analysis.

Generally, imaging of the synthesised geopolymers was often difficult as many of the specimens were charging causing a bright appearance of the sample without contrast. To minimise these issues various coating materials such as platinum, carbon and gold, and coatings of several layers were tried.

Carbon coating (12 nm thickness) was found not to be helpful in the SEI mode but was used for EDS analysis and imaging in backscattered mode. One of the better solutions for imaging in SEI mode was to use a relative thick layer of platinum or gold (18+ nm thickness).

5.6.1 Reference geopolymer

5.6.1.1 Before SBF exposure

Scanning electron microscopy images of the reference geopolymer prior to SBF exposure show a typical geopolymer micro structure [46], [8]. Figure 5.39 gives an overview of an area of the sample surface after heating at 600°C, the bright area on the right indicating charging problems. The few scratches on the surface remain after the grinding process.

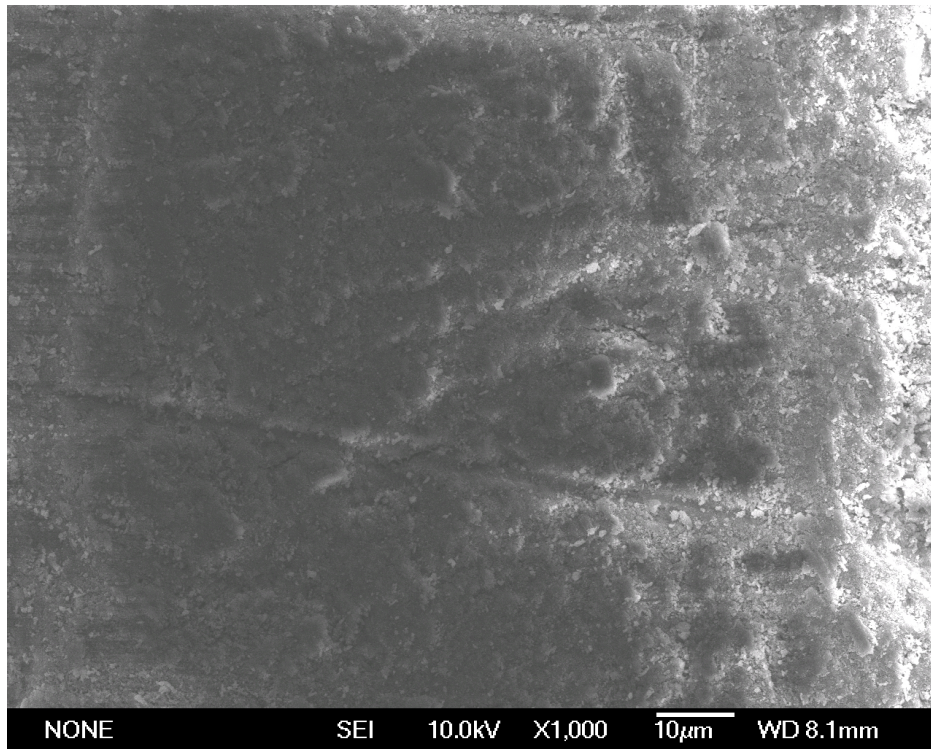


Figure 5.39: SEM micrograph of the reference geopolymer heated to 600°C , x 1000.

At higher magnifications (Fig. 5.40), a nanoporous structure and fine ball-like agglomerates become visible. The agglomerates vary in sizes between < 100 nm to > 1 μ m. The bright spots are due to charging of the sample.

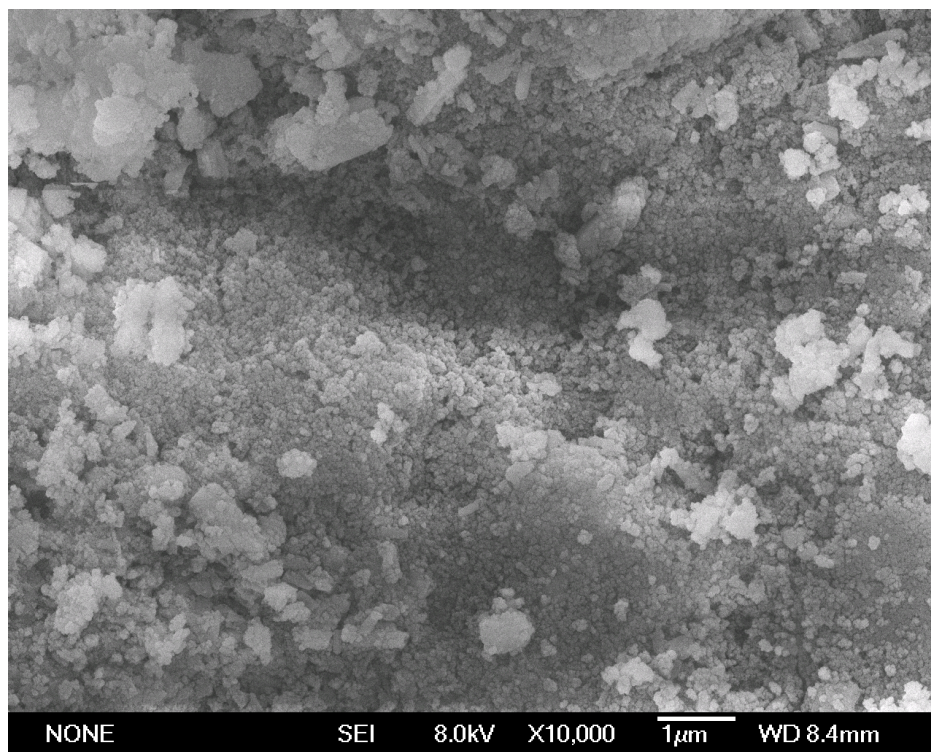


Figure 5.40: SEM micrograph of the reference geopolymer heated to 600°C, x 10k.

At a still higher magnification ($\times 30,000$) (Fig. 5.41) small ball shaped particles and a fine porous network can be seen. The single particles forming the agglomerates are sized 20 - 50 nm whereas the main pore network consists of pores < 10 nm but with a few larger pores of 100 to 200 nm.

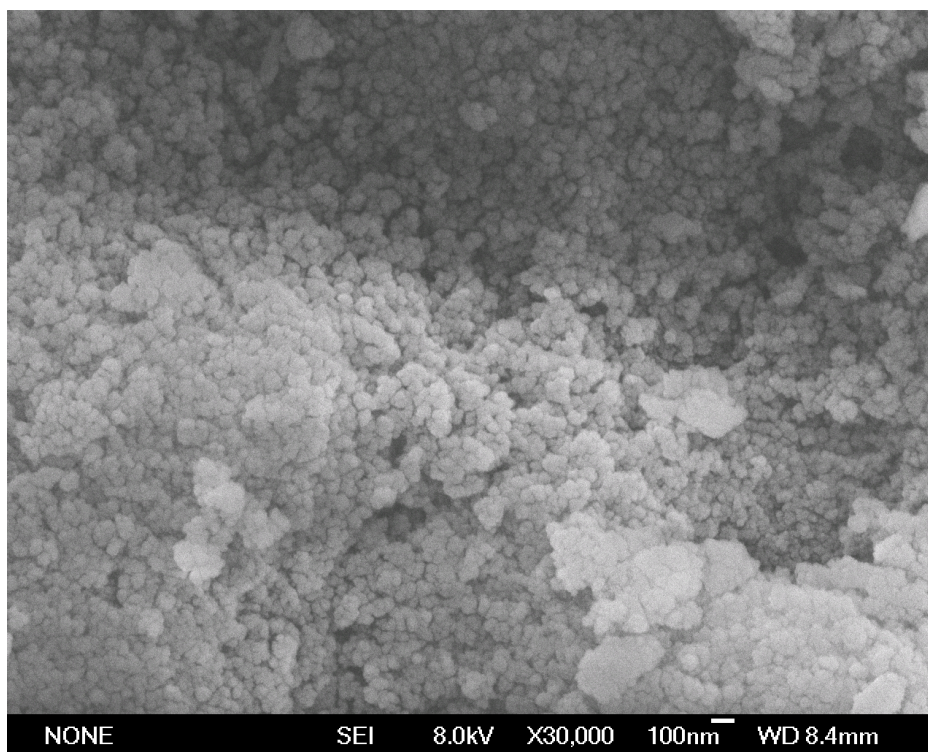


Figure 5.41: SEM micrograph of the reference geopolymer heated to 600°C , $\times 30k$.

EDS analysis of the reference geopolymer sample (Fig. 5.42) shows the presence of some areas with higher potassium concentrations. Aluminium and silicon are well distributed throughout the material. The concentrations of potassium are difficult to explain because the potassium-compounds were completely dissolved before the other reagents were added, followed by thorough stirring to a homogeneous paste. This result suggests a separation of the potassium from the aluminosilicate and the sep-

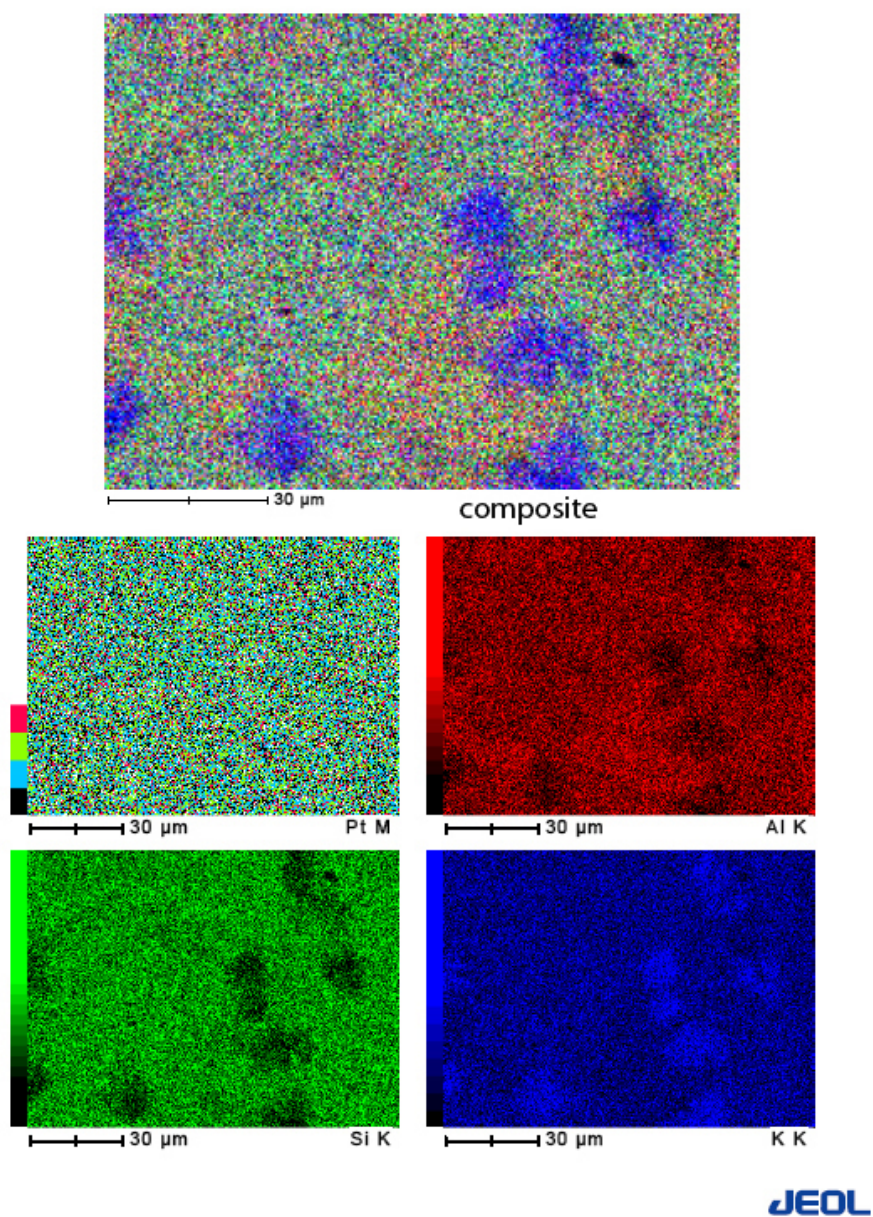


Figure 5.42: EDS element maps of the reference geopolymer heated to 600°C, x 1000.

aration of a potassium-rich phase on heating. The precise composition of this phase is unknown as no EDX analyses of these potassium-rich regions

were made.

5.6.1.2 After SBF exposure

Exposure of the heated reference geopolymer to SBF affects the micro structure slightly, as illustrated in the following images.

Figure 5.43 shows large 40 to 50 μm agglomerates (marked 1), together with smaller ($< 10 \mu\text{m}$) agglomerates (marked 2). The cracks developed during the in-vitro exposure experiment because they were not present prior to exposure to simulated body fluid.

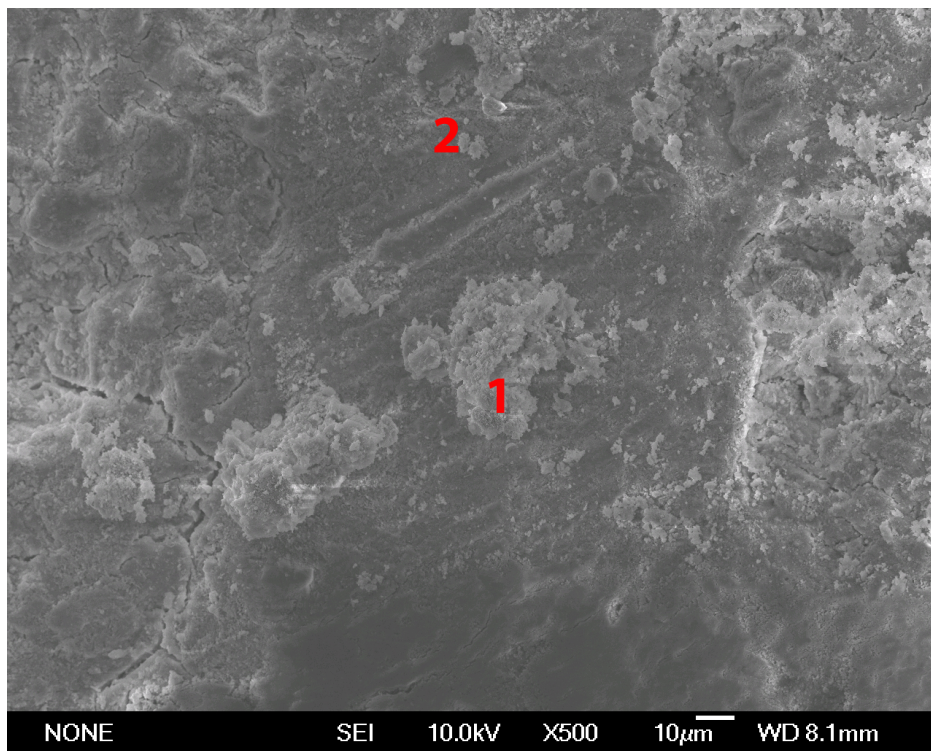


Figure 5.43: SEM micrograph of the reference geopolymer heated to 600°C, 7 weeks SBF exposure, $\times 550$.

Images taken at higher magnifications (Fig. 5.44 and 5.45) show that, in addition to the agglomerates, crystals (marked 3) have formed. These crystals are up to $1.5\ \mu\text{m}$ in length and are thin and spiky. They are randomly distributed, but absent from parts of the sample.



Figure 5.44: SEM micrograph of the reference geopolymer heated to 600°C , 7 weeks SBF exposure, $\times 5000$.

In the areas where crystals are present the material structure seems to have changed; the surface of the agglomerates and the areas surrounding the crystals appear completely disordered. However, other areas are not affected by exposure of the geopolymer to simulated body fluid and remain unchanged.

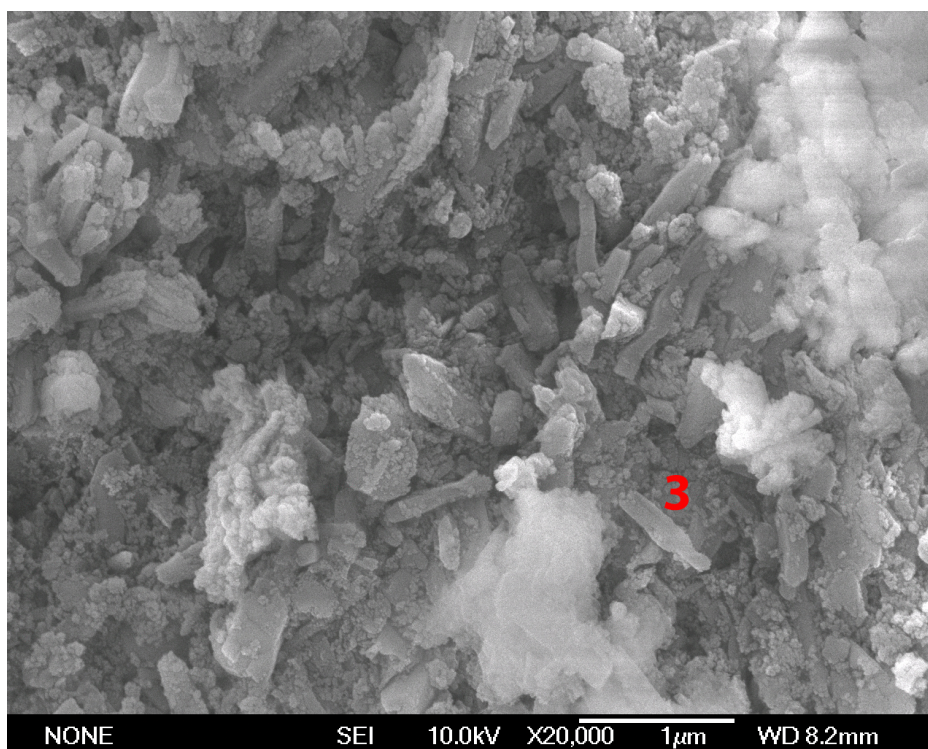


Figure 5.45: SEM micrograph of the reference geopolymer heated to 600°C, 7 weeks SBF exposure, $\times 20k$.

EDS mapping of the reference geopolymer after the in-vitro experiment is shown in Figure 5.46. Phosphorus (blue), silicon (green) and aluminium (red) are homogeneously distributed throughout the whole sample. However, the newly formed crystals could not be analysed by EDS because all areas where such crystals were present appeared to be in an unfavourable position for the electron beam. Since the reference geopolymer absorbs both calcium and phosphorus from the simulated body fluid it is possible that the needles are composed of a calcium phosphate phase, but this could not be confirmed by EDS nor by x-ray diffraction.

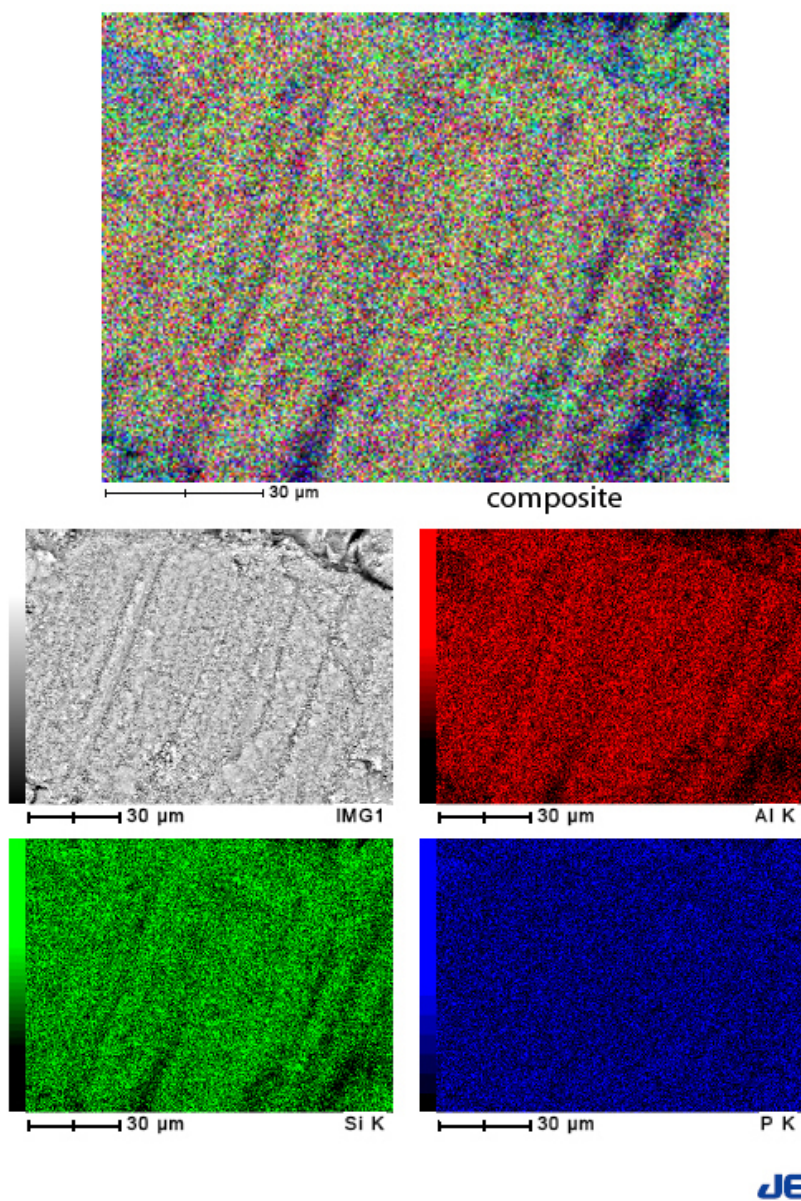


Figure 5.46: EDS element maps of the reference geopolymer heated to 600°C, 7 weeks SBF exposure, $\times 1000$.

5.6.2 Calcium hydroxide geopolymer

5.6.2.1 Before SBF exposure

Scanning electron micrographs and element mappings of the calcium hydroxide-containing geopolymer heated to 600°C prior to in-vitro exposure to SBF are shown in this section.

Main features of the calcium hydroxide-containing geopolymer are variously sized thin needles (marked 1 in Fig. 5.47), pores and agglomerations (marked 2). The needles are randomly ordered and are 100 - 200 nm long, and 1 - 10 nm thick.

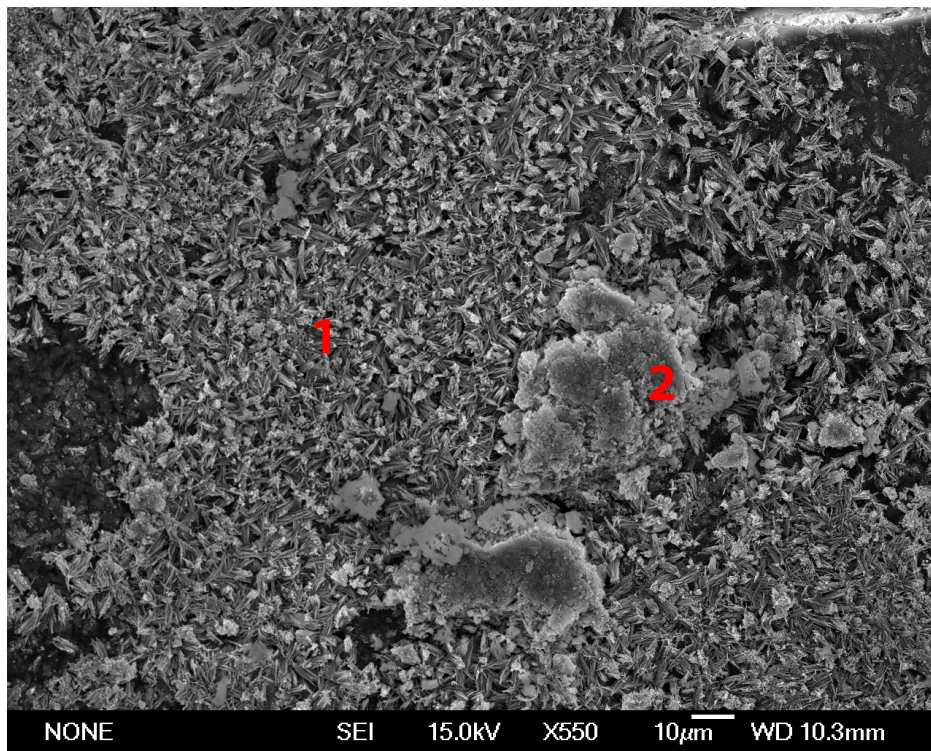


Figure 5.47: SEM micrograph of calcium hydroxide geopolymer, heated to 600°C, x 550.

At higher magnification ($\times 15,000$), a needle-rich area (Fig. 5.48) shows the presence of longer and shorter needles together with other random morphologies. The agglomerated regions look like clusters of ball-shaped material and appear much more dense than the surrounding needles.

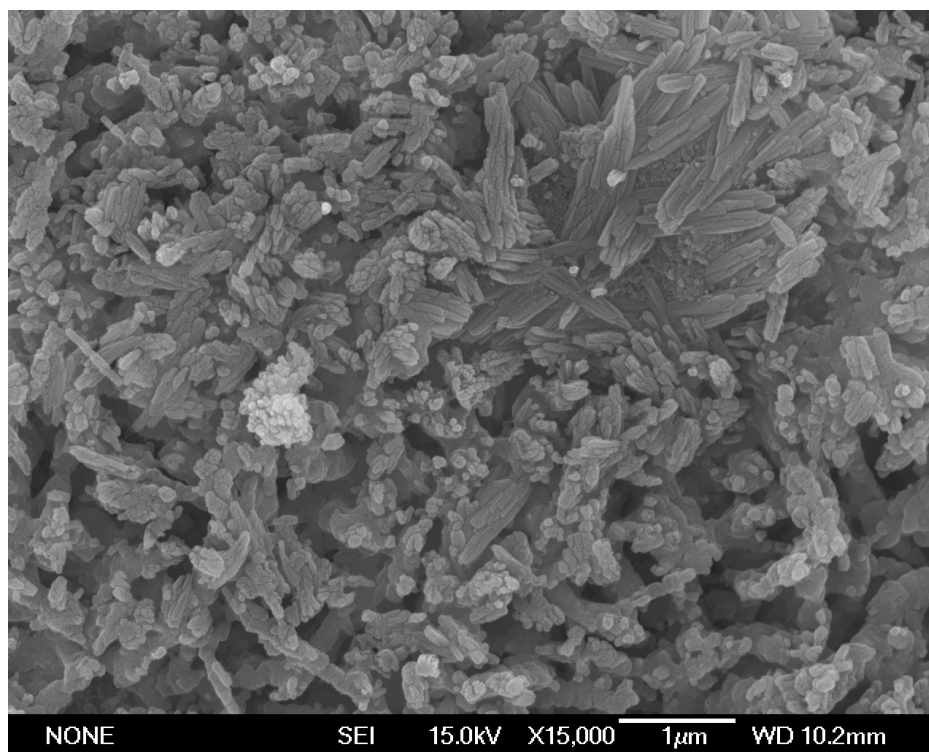


Figure 5.48: SEM micrograph of calcium hydroxide geopolymer, heated to 600°C, $\times 15k$.

EDS analysis of the sample area of Figure 5.49 shows that the needles are rich in calcium (blue) whereas the agglomerated areas contain silicon and aluminium, indicated by the yellow coloured areas in the top image. Although there are areas rich in elements typical of geopolymers, together with other calcium rich areas, the calcium is homogeneously distributed throughout the material.

XRD patterns of the calcium hydroxide-containing geopolymers show

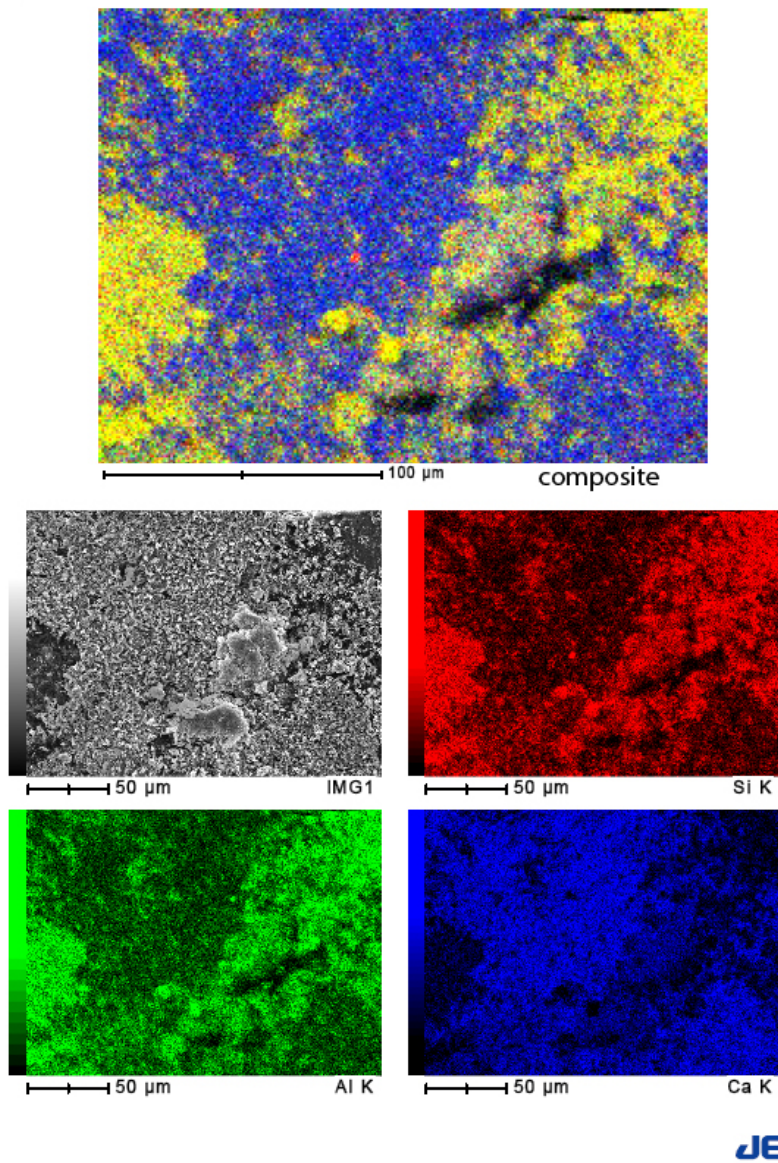


Figure 5.49: EDS elemental maps of calcium hydroxide geopolimer, heated to 600°C.

them to be more amorphous after heating to 600°C. SEM observations of the same type of specimen (Figs. 5.47, 5.48) show that there are fine, randomly ordered nano-crystals present. Thus, heating to 600°C may have

lead to a formation of x-ray amorphous nano-crystals which may explain their more amorphous nature, since the formation of the nano-crystals takes place upon heating to 600°C but not at lower temperatures.

5.6.2.2 After SBF exposure

The calcium hydroxide geopolymer after exposure to simulated body fluid for seven weeks shows different SEI and EDS results. The micro structure appears much finer and more homogeneous after the exposure to SBF (Fig. 5.50).

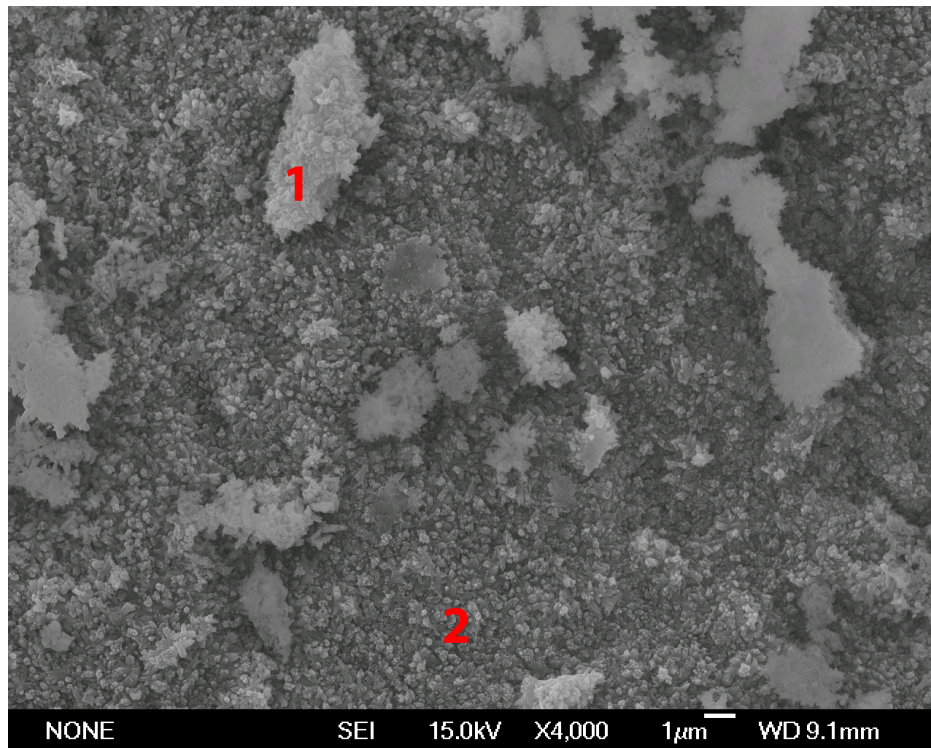


Figure 5.50: SEM micrograph of calcium hydroxide geopolymer, heated to 600°C, 7 weeks SBF exposure x 4000.

The number of crystal needles (2) appear to be reduced and the agglomerated regions (1) have been transformed and covered in a crystalline substance.

Figure 5.51 shows that two types of structures are present; larger flaky crystals and small agglomerates. The pores seem to be more homogeneously distributed and appear to be internally connected.

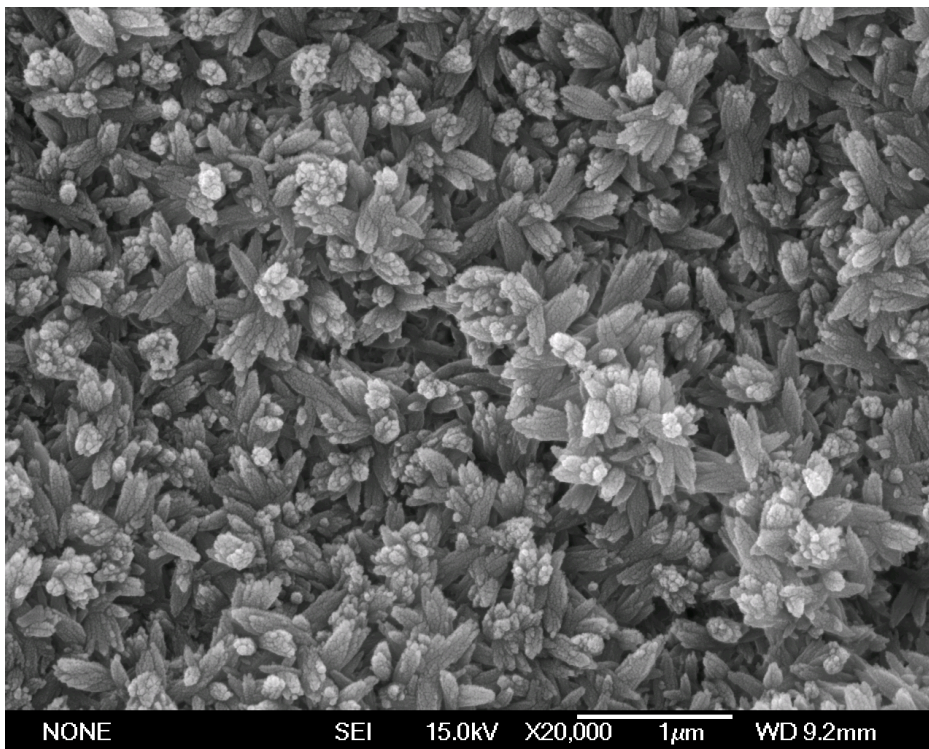


Figure 5.51: SEM micrograph of calcium hydroxide geopolymer, heated to 600°C, 7 weeks SBF exposure, x 20k

The flaky crystals are between 0.2 - 0.6 μm long and $\approx 0.1 - 0.2 \mu\text{m}$ thick and of spiky shape. The smaller crystals have a more ball-shaped structure and are less than 0.2 μm in size. The pores-size is difficult to judge, as the sample is not polished and the pores are internally connected. However,

the visible pores range in sizes from about $0.5\ \mu\text{m}$ to less than $100\ \text{nm}$.

EDS analysis of the area of Figure 5.50 is shown in Figure 5.52.

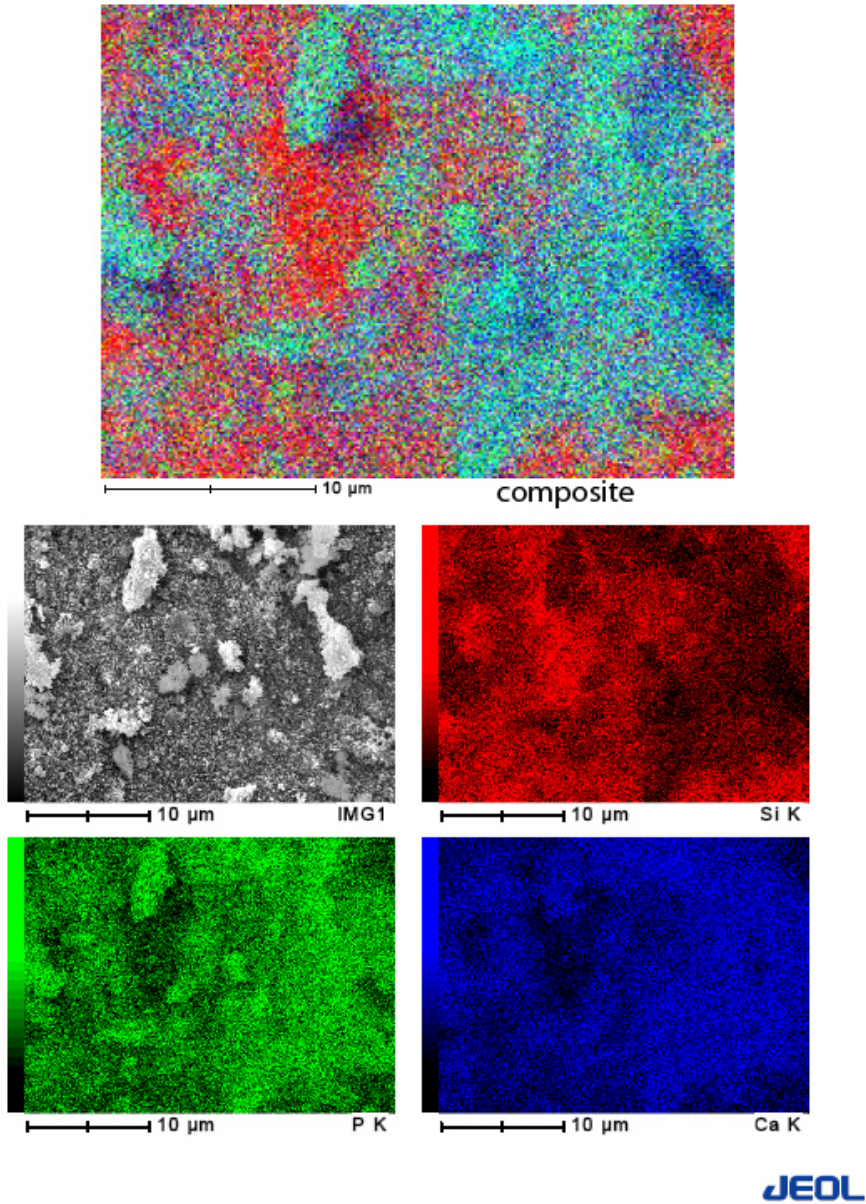


Figure 5.52: EDS elemental map of calcium hydroxide geopolymer, heated to 600°C , 7 weeks SBF exposure

The calcium and phosphorus (blue and green areas respectively in the elemental map) are well distributed throughout the sample. Further, the larger composite image shows that calcium and phosphorus occur together (greenish blue areas) whereas there are still areas dominated by the geopolymer (red).

Since the phosphorus was not initially present in the material, it has been absorbed from the simulated body fluid. ICP analysis (section 5.5) shows that the calcium hydroxide-containing geopolymers absorb almost all of the phosphorus present in the simulated body fluid. Since calcium and phosphorus are present in the same regions it appears that a calcium phosphate phase has formed during the exposure time to simulated body fluid. X-ray diffraction (section 5.2) confirmed that the two calcium phosphate phases formed after four weeks exposure to simulated body fluid were hydroxyl apatite and hydroxyl carbonate apatite, both bioactive calcium phosphate phases.

5.6.3 Calcium silicate geopolymer

5.6.3.1 Before SBF exposure

The SEM micrograph shows that the micro structure of calcium silicate-containing geopolymers (Fig. 5.53) is relatively fine and porous. Two different types of material structures are visible; one looks like large agglomerations of large particles whereas the other shows a very fine porous texture (Fig. 5.53).

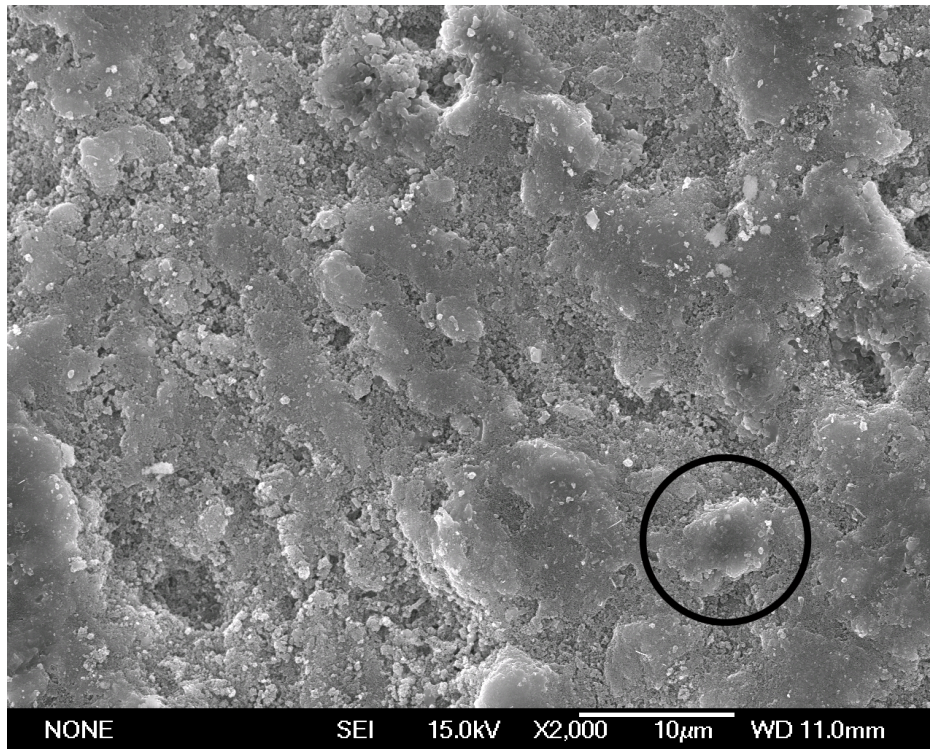


Figure 5.53: Calcium silicate containing geopolymer heated to 600°C , x2000

At higher magnifications (Fig. 5.54), it can be seen that the pores are in the nanometer range and are homogeneously distributed throughout the material. The artefact in the center of this image is one of the agglomerations, circled in the previous image and seems to be slightly different from the surrounding material, being 5 - 6 μm in diameter and apparently less porous. EDS analysis (Fig. 5.56) shows that the circled area is rich in calcium whereas the surrounding areas are rich the elements aluminium and silicon, typical of geopolymers.

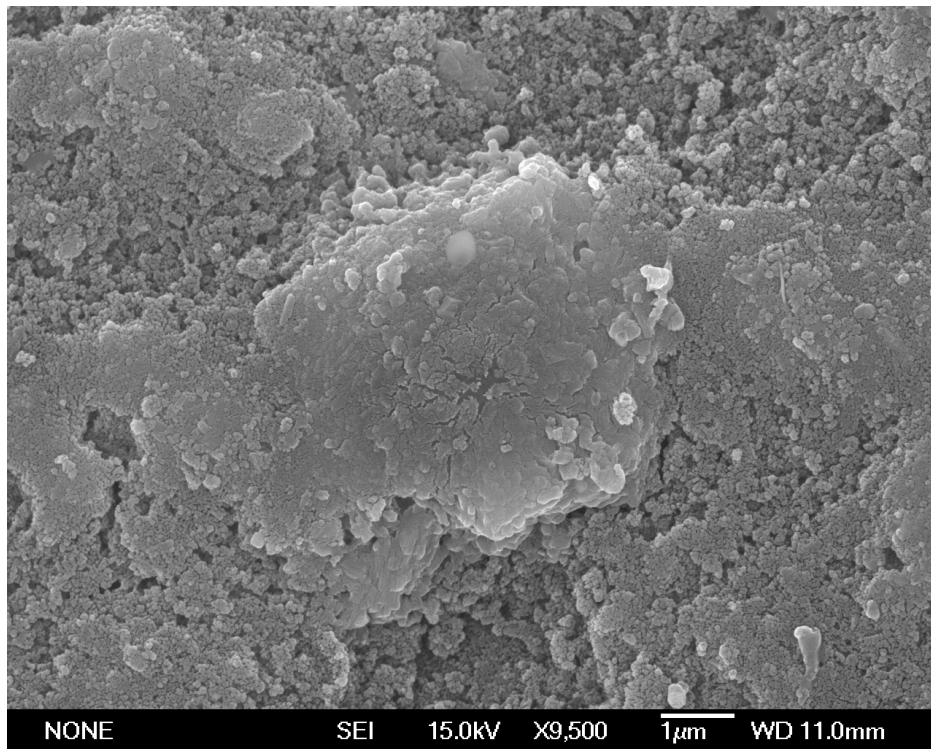


Figure 5.54: SEM micrograph of calcium silicate-containing geopolymer heated to 600°C, \times 9500

At still higher magnifications (x20,000), the areas rich in aluminium and silicon (Fig. 5.55) show a nano-porous network with pore sizes of 10 - 100 nm. The geopolymer particles range in size between 10 - 150 nm. The brighter parts visible in the image are due to charging of the sample surface.

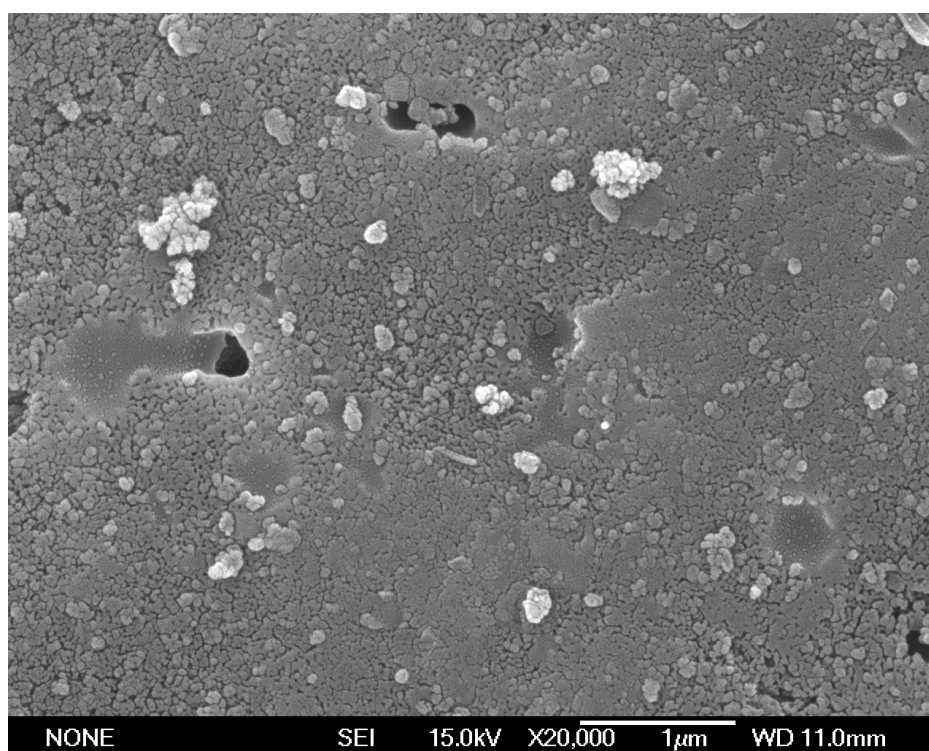
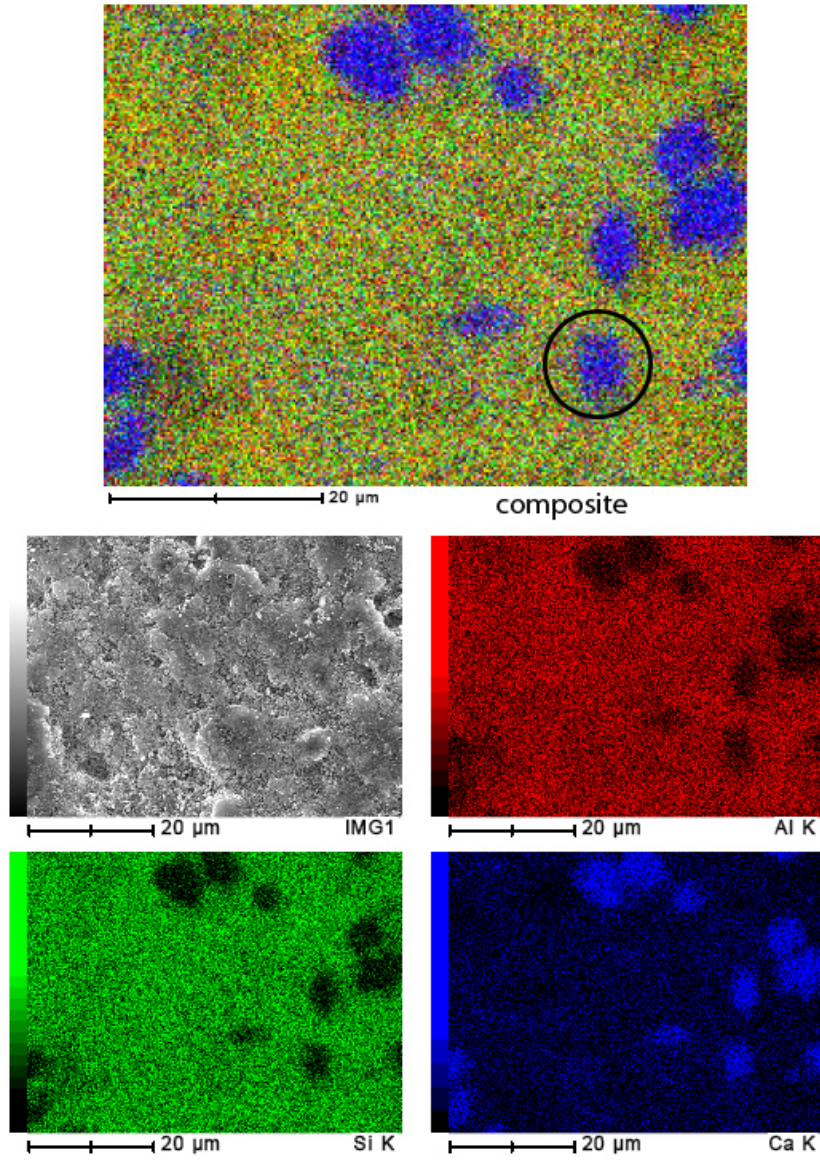


Figure 5.55: SEM micrograph of calcium silicate-containing geopolymer heated to 600°C, x 20k

EDS analysis of the area shown in Figure 5.53 is shown in Figure 5.56.



JEOL

Figure 5.56: EDS elemental maps of calcium silicate-containing geopolymer heated to 600°C, x2000

The distribution of calcium throughout the sample is not homogeneous, the blue spots in the top image indicating calcium rich areas. However, because calcium silicate was the additive to the geopolymer, calcium and silicon rich areas should occur in conjunction, rather than areas rich in calcium alone. Because only calcium is concentrated in certain parts of the sample, the silicon may have entered the geopolymer structure. This possibility is supported by the NMR results (section 5.3.1.3). The calcium rich areas may therefore correspond to calcium hydroxide.

5.6.3.2 After SBF exposure

Exposure of the calcium silicate-containing geopolymer to simulated body fluid for seven weeks produced clear changes in the micro structure. The SEM image taken at 4000 times magnification (Fig. 5.57) shows that regular square shaped-crystals (1) have formed and partially cover the sample surface. The crystals range in size from 0.3 - 5 μm . Sponge-like structures (2) and agglomerated areas (3) are also present, similar to those in the sample prior to exposure to simulated body fluid.

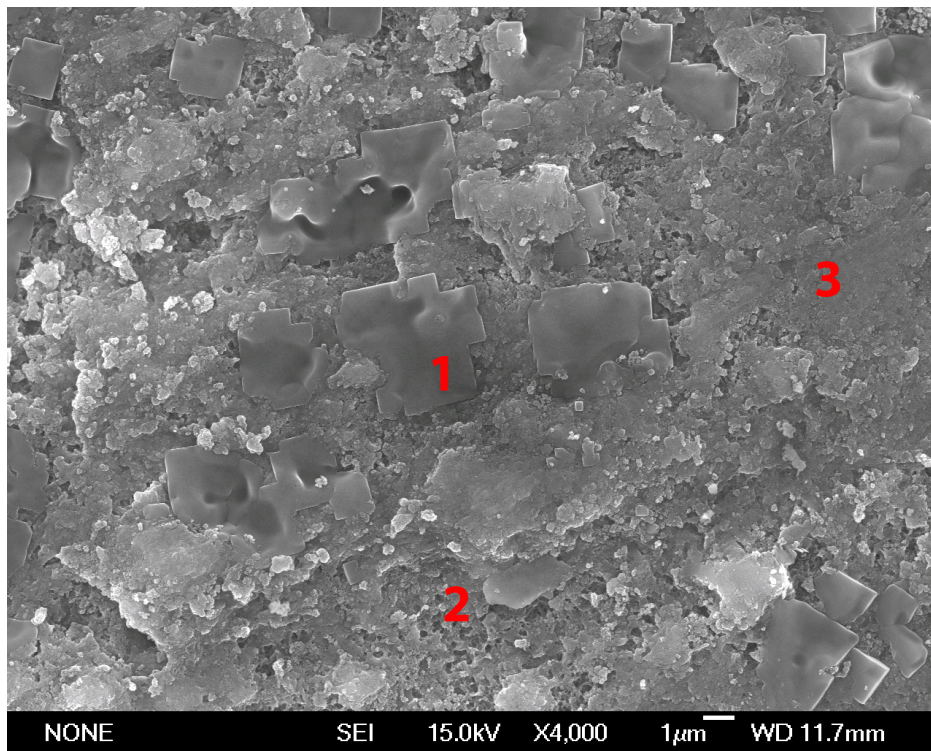


Figure 5.57: SEM micrograph of calcium silicate-containing geopolymer heated to 600°C, 7 weeks SBF exposure, x 4000

At higher magnifications (Fig. 5.58), the sponge-like texture contains intra-connected pores and agglomerated small round particles. The pores range in size from 50 - 0.5 μm whereas the agglomerated particle size range between 100 nm and 1 μm .

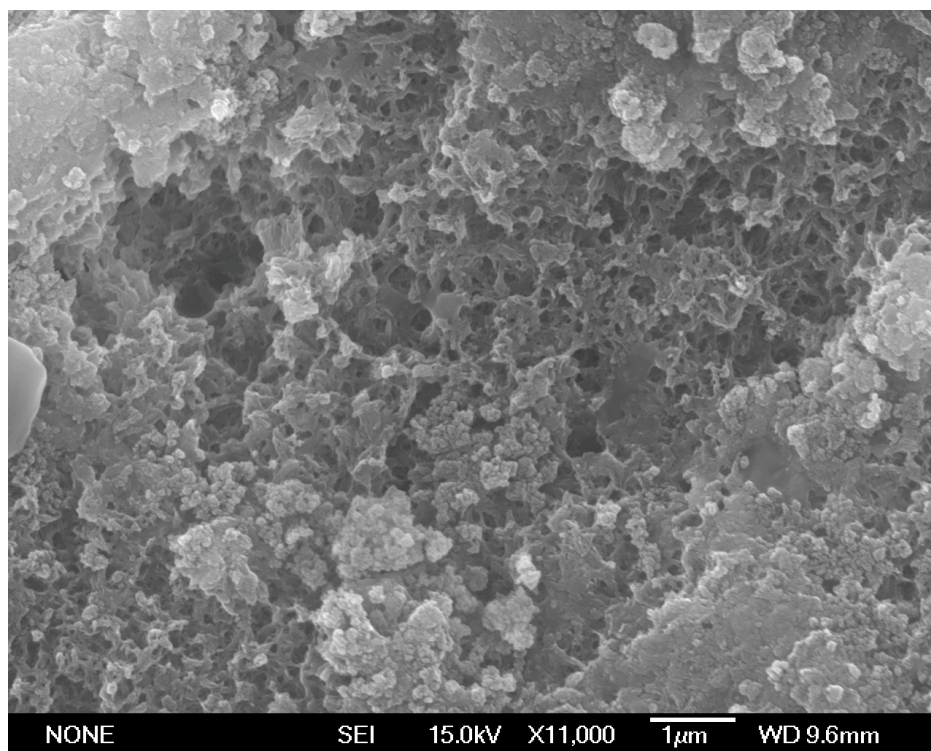


Figure 5.58: SEM micrograph of calcium silicate-containing geopolymer heated to 600°C, 7 weeks SBF exposure, x 11k

A more detailed image of an agglomerated area is shown in Figure 5.59, revealing fine particles 20 - 300 nm in size that comprise the agglomerates. These particles contain very small white dots whose origin could not be determined.

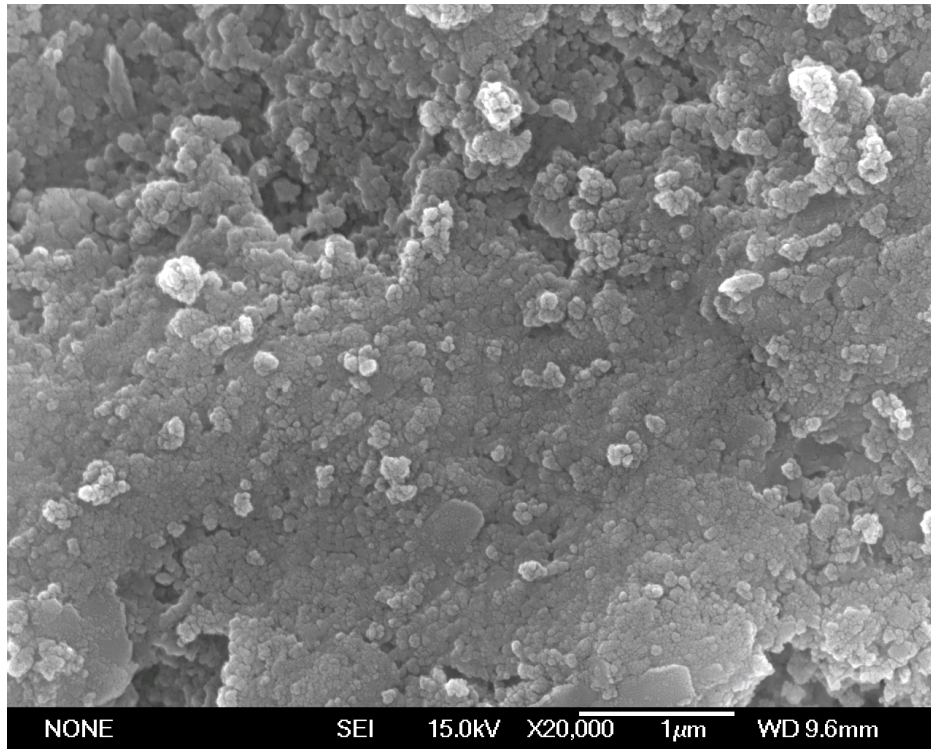
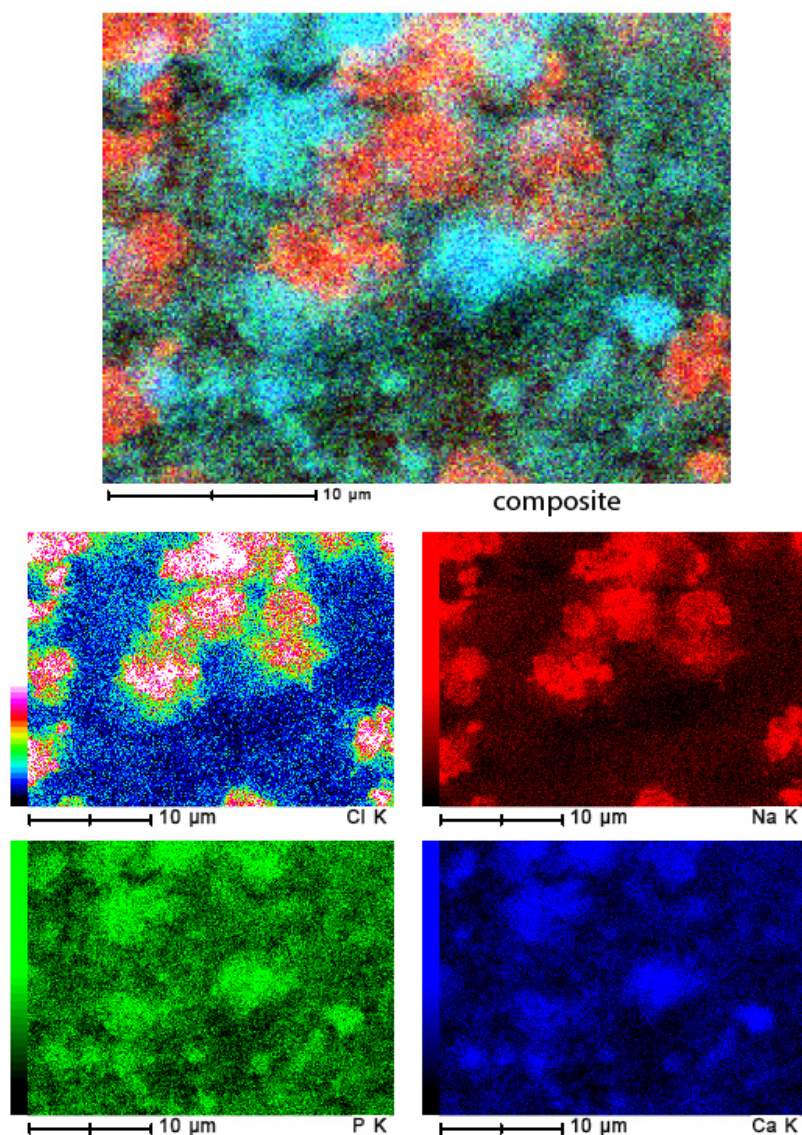


Figure 5.59: SEM micrograph of calcium silicate-containing geopolymer heated to 600°C, 7 weeks SBF exposure, x 20k

EDS analysis of of the sample area of Figure 5.57 is shown in Figure 5.60.



JEOL

Figure 5.60: Element maps of calcium silicate-containing geopolimer heated to 600°C, 7 weeks SBF exposure, x 4000

Chlorine is imaged in multicolour whereas sodium, calcium and phosphorus are displayed in red, blue and green respectively. The EDS mapping identifies the square-shaped crystals as sodium chloride (indicated in red in the composite image). The greenish blue areas representing calcium phosphate and the darker parts of the composite image are the geopolymer elements (silicon and aluminium). The sodium chloride has crystallised from the SBF, nucleating on the underlying crystal aggregates.

To summarise, the calcium silicate added to the geopolymer mixture appears to have added silicon to the geopolymer structure during the setting process. The resulting calcium rich regions become associated with phosphorus during exposure to simulated body fluid, forming calcium phosphate identified as hydroxyl apatite by x-ray diffraction. Hydroxyl apatite is a material which is well known for its bio-compatibility and as a resorbable biomaterial [16] whose formation could explain the microstructural changes observed here. ICP analysis shows that the phosphorus in the simulated body fluid is almost completely assimilated by the geopolymer whereas calcium is firstly absorbed but then released. This behaviour might be explained by the initial formation of a resorbable calcium phosphate phase such as hydroxyl apatite, followed by the degradation of this phase when the Ca^{2+} concentration is increased upon the addition of fresh SBF.

5.6.4 Calcium phosphate geopolymer

5.6.4.1 Before SBF exposure

Geopolymer samples containing calcium phosphate heated to 600°C analysed by SEM at relatively low magnifications show darker and lighter regions (Fig. 5.61). The lighter regions arise from charging of the sample.

The scratches visible in this micrograph developed during grinding of the sample after the curing process. The other smoother areas may also be an artefact of the grinding process.

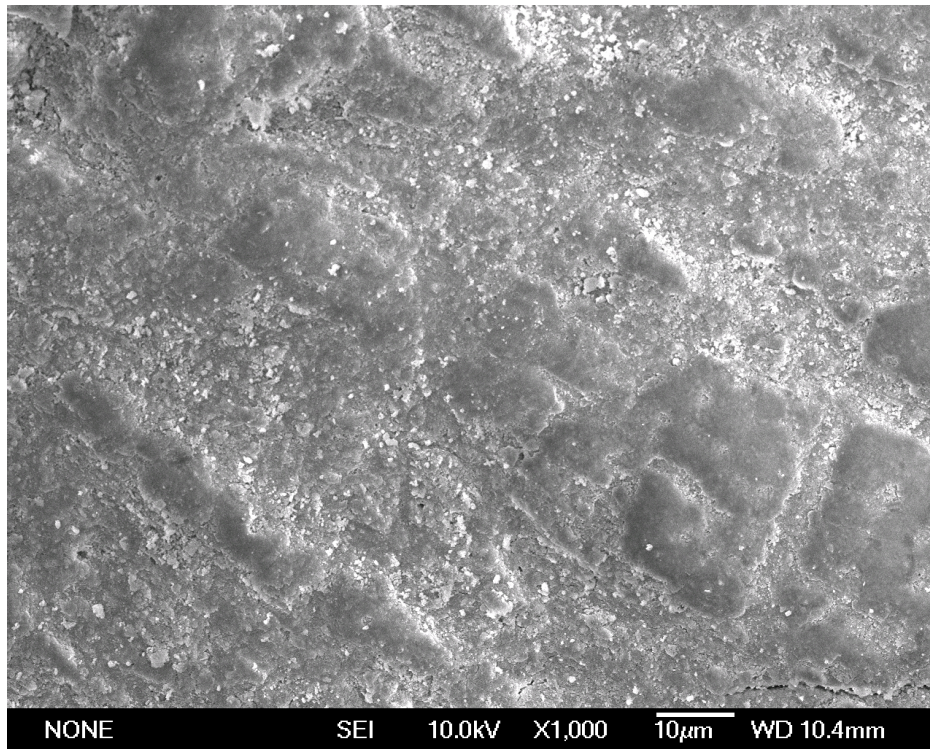


Figure 5.61: SEM micrograph of the calcium phosphate-containing geopolymer, heated to 600°C, $\times 1000$.

Micro cracks of about 50 - 60 nm and a ball-like texture become visible at higher magnification (Fig. 5.62). The particles are about 50 - 100 nm in size and form agglomerates ranging from approximately 200 - 500 nm in size. Some parts of the geopolymer seem to be more textured with higher porosity and larger pores, which are however smaller than the particles themselves. Charging problems are evidenced by the bright white appearance of the agglomerations.

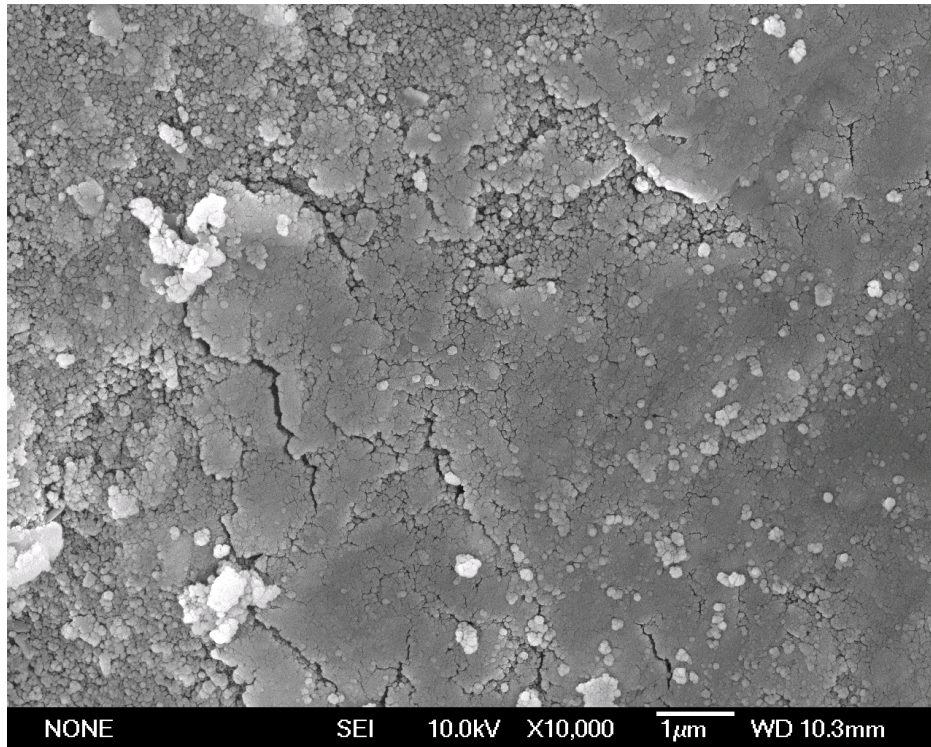


Figure 5.62: SEM micrograph of the calcium phosphate-containing geopolymer, heated to 600°C, x10k.

A higher magnification image of this sample is shown in Figure 5.63. This shows that the particles are agglomerates of even finer particles ranging in size from 30 - 140 nm. The visible micro cracks are less than 70 nm wide and are randomly distributed, possibly accounting for the porosity. However, the pore structure and pore size cannot be determined.

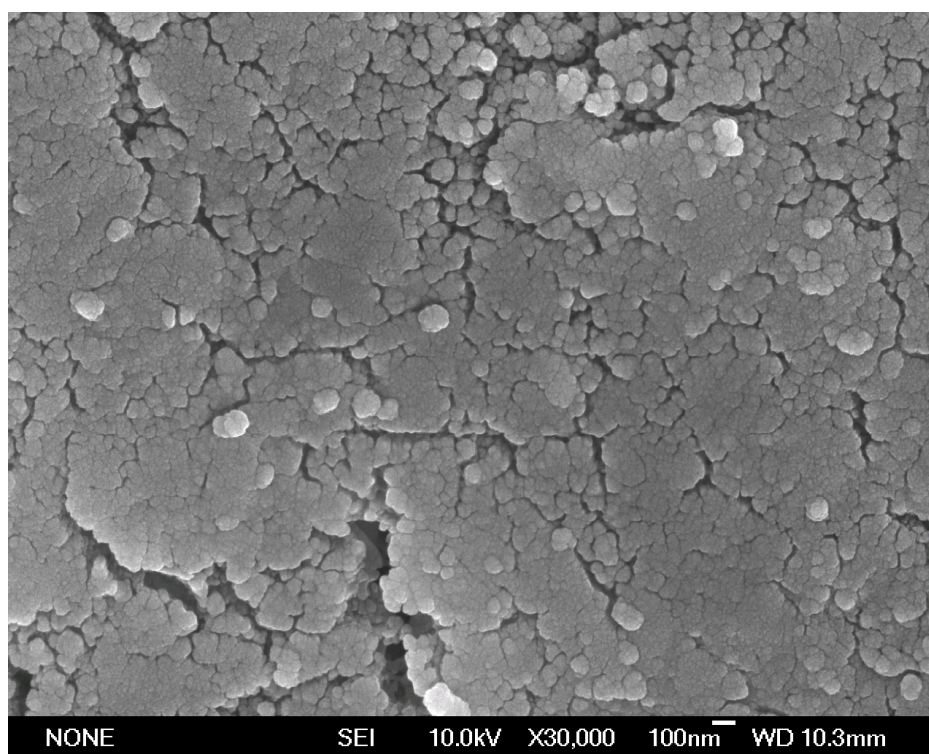


Figure 5.63: SEM micrograph of the calcium phosphate geopolymer, heated to 600°C, x30k.

Element mapping of the calcium phosphate geopolymer (Fig. 5.64) shows inhomogeneities in the of element distribution.

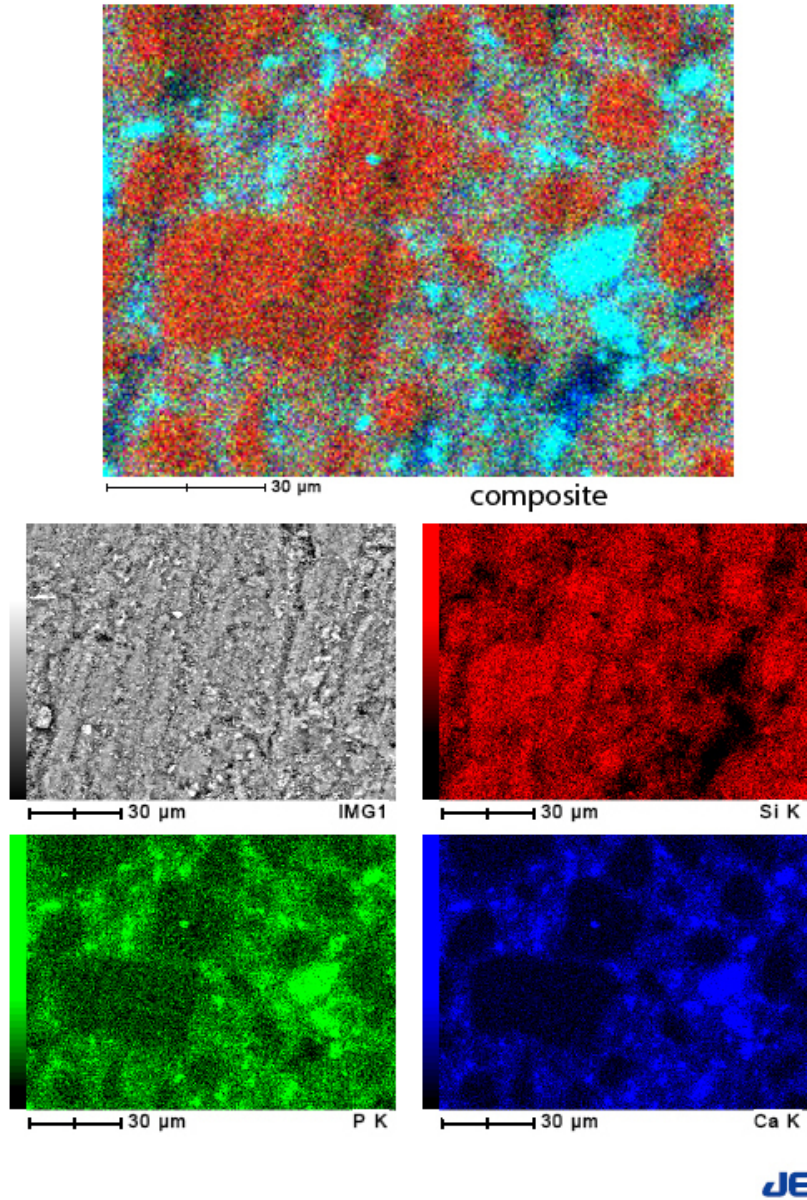


Figure 5.64: EDS element maps of the calcium phosphate-containing geopolymer, heated to 600°C, x1000.

The regions containing higher concentrations of calcium and phosphorus are shown as the blue areas in the composite map (top), the red regions in the composite map indicate the geopolymeric material itself containing mainly aluminium and silicon. EDS analysis shows that the sample is not a homogeneous mixture of geopolymer and calcium phosphate, possibly because the calcium phosphate may not have reacted with the alkaline geopolymer. Use of a finer calcium phosphate powder or more intensive mixing of the reagents may give better homogeneity.

5.6.4.2 After SBF exposure

The micro structure of the geopolymers containing calcium phosphate is slightly changed after exposure to simulated body fluid for seven weeks, shown in this section.

The scratches seen in Figure 5.65 are from the sample preparation, but agglomerates to up to about 5 μm in size are also visible.

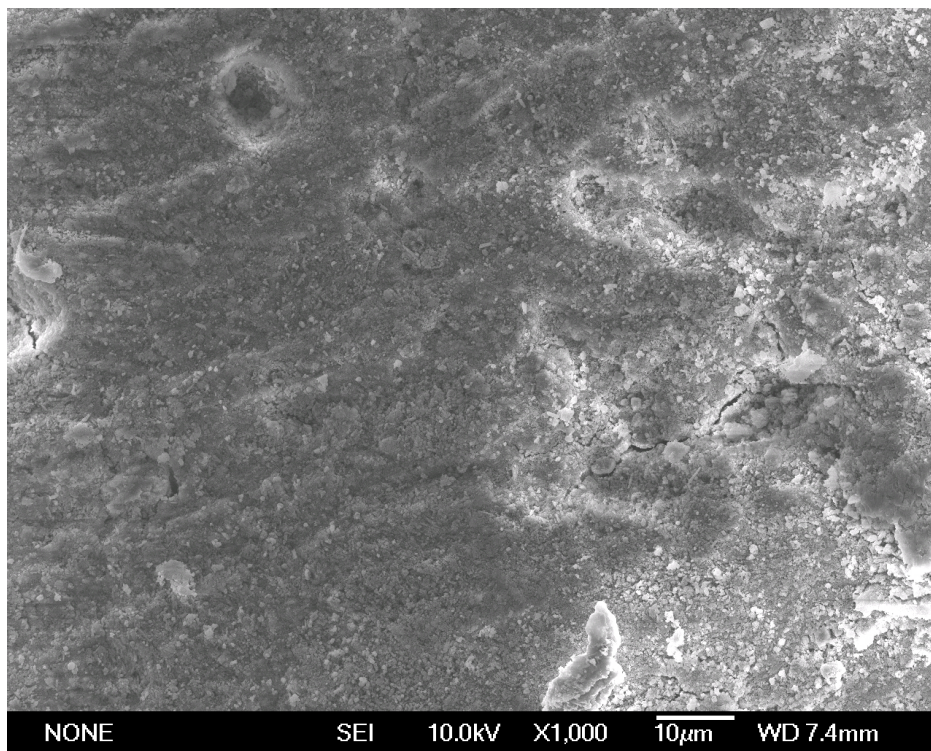


Figure 5.65: SEM micrograph of the calcium phosphate geopolymer, heated to 600°C, 7 weeks SBF exposure, x1000

The material appears relatively rough and the agglomerates rather less ball-shaped compared with the geopolymer before exposure to simulated body fluid. This geopolymer appears to be relatively porous, with the

porosity more or less evenly distributed throughout the sample.

At higher magnifications (Figs. 5.66 and 5.67), the changes resulting from exposure to simulated body fluid become more obvious. Although there are still agglomerates present, new morphologies such as needle-shaped crystals (marked 1 in Fig. 5.66) have developed. The agglomerates range in size between < 30 nm to > 2 μm , whereas the needle-shaped crystals range from 500 nm to 1.4 μm . Larger pores are present in the geopolymer, approximately 100 - 200 nm in size, together with a relatively large amount of nano porosity (pore sizes < 30 nm).



Figure 5.66: SEM micrograph of the calcium phosphate-containing geopolymer, heated to 600°C, 7 weeks SBF exposure, x10k

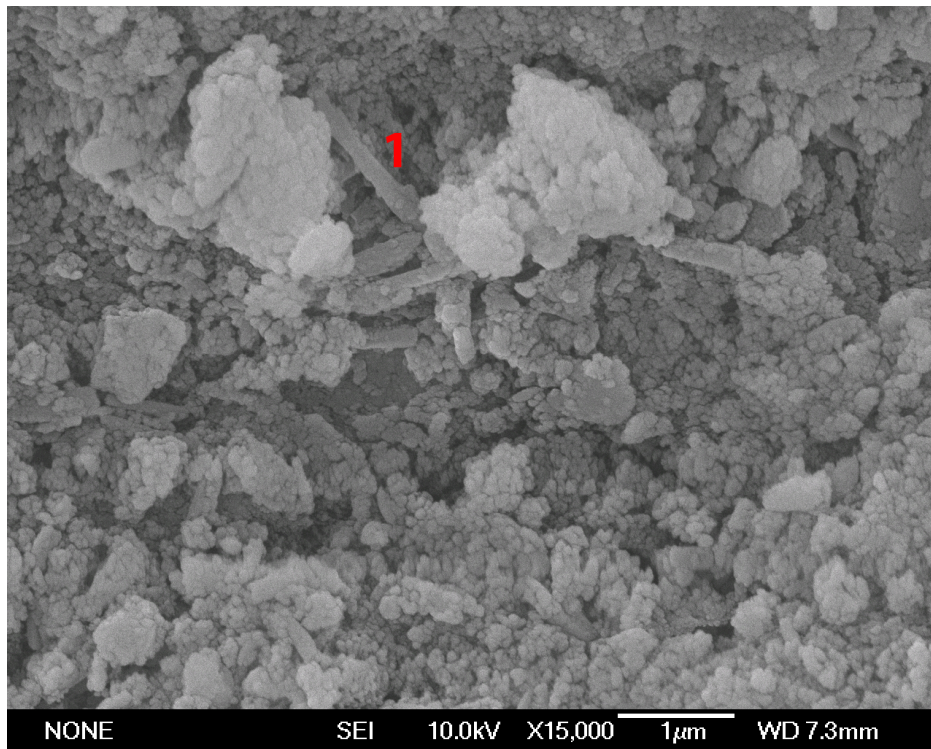


Figure 5.67: SEM micrograph of the calcium phosphate-containing geopolymer, heated to 600°C, 7 weeks SBF exposure, x15k

Element mapping (Fig. 5.68) shows that the element distribution is relatively homogeneous with respect to silicon, calcium and phosphorus.

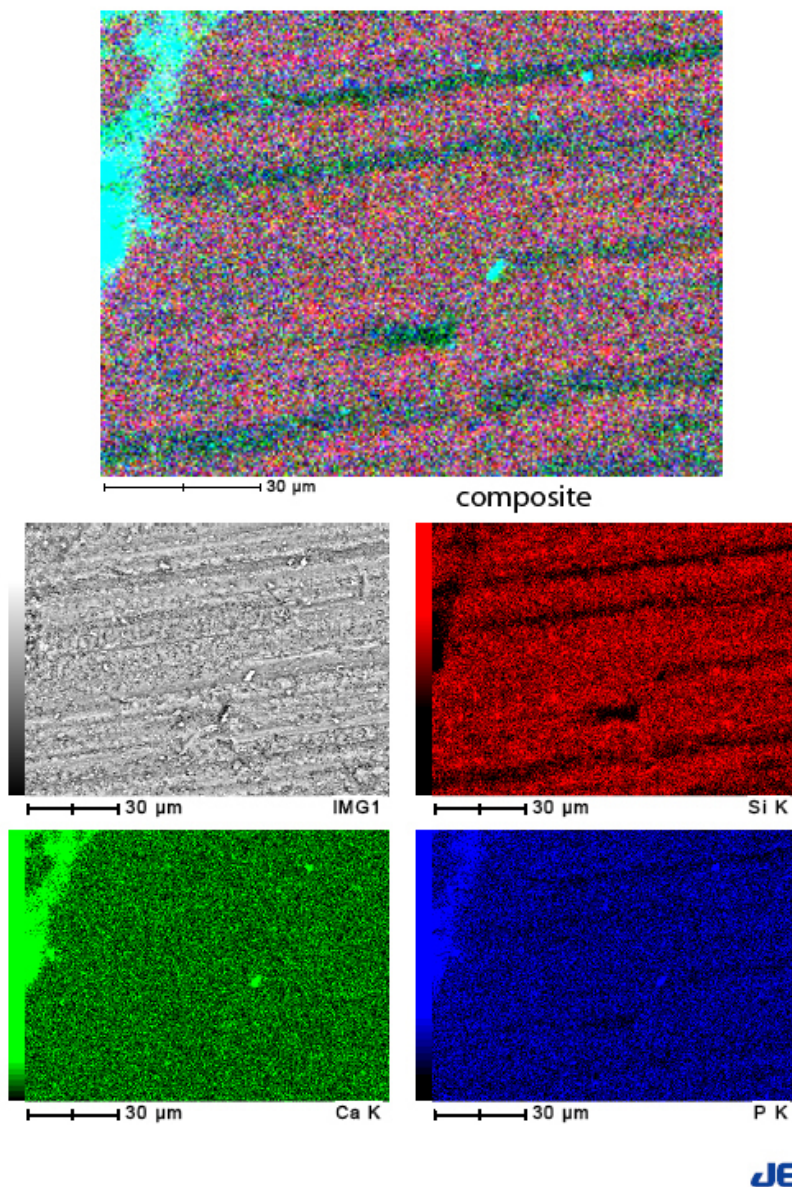


Figure 5.68: EDS element maps of the calcium phosphate-containing geopolymer, heated to 600°C, 7 weeks SBF exposure, x1000

Although these elements are evenly distributed, calcium and phosphorus appear to be concentrated in a scratch indicated by the greenish blue colour in the composite map (top). This may result from the presence of a softer area of calcium phosphate that was more readily damaged during grinding. Exposure of this geopolymer to SBF has eliminated the elemental inhomogeneity observed in the sample prior to SBF exposure. This is not an artefact, since a number of areas analysed by EDS all showed the same results.

A possible reason for the improved homogeneity is the exchange of elements with the compounds of the SBF with the formation of new x-ray amorphous phases. ICP analysis indicates an exchange of aluminium from the geopolymer to the SBF, and the absorption of calcium, silicon and phosphorus from the SBF by the geopolymer (section 5.5).

Chapter 6

Conclusions

The aim of this project was to produce aluminosilicate geopolymers with bioactive behaviour. Since such behaviour is observed in calcium-containing compounds, geopolymer composites using several inorganic calcium compounds were synthesised. Their mechanical properties and bioactivity were tested under laboratory conditions. Because geopolymers are highly alkaline, the pH of these composites needed to be reduced to non-hazardous levels. This was done by using the least possible alkali in the synthesis without compromising the mechanical properties, and by heating to 550°C - 600°C. Geopolymers contain aluminium, which must be fixed in the material's structure, to prevent leaching into the body.

The phases and structures formed in the geopolymers before and after exposure to SBF were determined by XRD, ^{27}Al , ^{29}Si and ^{43}Ca MAS NMR, and SEM/ EDS. The tensile strength of the materials before SBF exposure was determined by diametral compression testing. Alterations of the element concentrations in the SBF during the exposure experiments were determined by ICP analysis and changes of the pH were determined by direct measurements.

The most important properties in a geopolymer material for bioactive applications are:

- The ability to form bioactive compounds in contact with body fluid
- Near neutral pH
- Minimal release of aluminium
- Comparable strength to current materials

Table 6.1: Summary of the important properties of the geopolymers

Geopolymer	heating temp.	HA or HCA formation	pH	leached Al	Tensile strength
	(°C)			(ppm)	(MPa)
Reference	550	possible ¹	7.87	0.211	2.05
	600	possible ¹	7.78	0.135	1.22
Calcium hydroxide	550	present	9.00	6.350	0.64
	600	strongly present	8.96	2.680	1.46
Calcium silicate	550	absent	10.75	0.056	—
	600	present	9.30	0.027	1.38
Calcium phosphate	550	probable ¹	8.12	0.517	4.17
	600	probable ¹	8.03	0.442	1.73

¹: Not confirmed by XRD but suggested according to ICP, SEM and EDS results

From the results in Table 6.1 we conclude: The reference geopolymers both heated to 550°C and 600°C showed no confirmed evidence of bioactive phase formation after exposure to SBF. They produce the lowest pH values in the SBF and the tensile strength results are average. These samples released the second lowest amount of aluminium but the amount released dropped by 50% for the sample heated to 600°C.

After exposure to SBF, the calcium hydroxide geopolymers showed the formation of the bone-like phases HA and HCA. They released the highest amount of aluminium whereas it was significantly lower for the sample heated to 600°C but still excessive. The pH of the SBF produced by these

samples were not the highest but still do not meet the requirements for a bio-compatible material.

The presence of hydroxyl apatite phases after SBF exposure was confirmed for the calcium silicate sample heated to 600°C but this phase was absent for the sample heated to 550°C. These samples showed the lowest leaching of aluminium but produced the highest pH values.

Geopolymers containing calcium phosphate showed no confirmed formation of hydroxyl apatite or hydroxyl carbonate apatite after exposure to SBF. They produced pH values slightly above neutral and showed the highest tensile strength. However, these samples released the second highest amount of aluminium in critical levels.

The best properties in terms of bio-compatibility are shown by the reference and the calcium phosphate-containing geopolymer, with respect to their pH values and their tensile strength. Both compare favourably with the commercially available Bioglass/polysulfone composites and Bioglass®. The presence of bioactive phase formation could not be confirmed by XRD, however ICP, SEM and EDS results showed the absorption of calcium and phosphorus of the SBF and the formation of nano-scaled crystals rich in these elements. This probably indicates the formation of calcium phosphate phases, such as hydroxyl apatite, and therefore a degree of bioactivity. However, the release of aluminium is critical which makes them presently bio-incompatible.

The best bioactivity is shown by the geopolymers containing calcium hydroxide (550°C and 600°C) or calcium silicate (600°C). They show the formation of the bone-like phases HA and HCA which is confirmed by XRD. The release of aluminium is relatively low for the calcium silicate

containing samples (< 0.06 ppm) but critically high for the calcium hydroxide containing geopolymers (> 2.6 ppm). Both of the samples present tensile strength values comparable to Bioglass/polysulfone composites. The pH values of the calcium hydroxide and the calcium silicate geopolymers showing the trend to drop with increased heating temperature, but are still too high.

6.1 Future work

These are promising results but the synthesised geopolymers are not ready to use as biomaterials yet. Further improvement is required to lower the materials pH values and the release of aluminium. The strength of the geopolymers should be improved to make these materials available for a wider range of biomedical applications.

To get more information about the above-mentioned synthesised materials, additional examination is suggested. ^{31}P MAS NMR could be carried out to gain more information about the environment of the phosphorus in the calcium phosphate-containing geopolymer. This could deliver information whether the phosphorus forms part of the geopolymer network structure and whether heating induces phosphate-bonding. Analysis by ^{43}Ca MAS NMR was carried out on the calcium phosphate-containing geopolymers but should also be carried out on all the other geopolymers to determine the nature of the calcium sites in their structure. To augment the available reference spectra, ^{43}Ca MAS NMR spectra should be acquired for synthetic hydroxyl apatite and hydroxyl carbonate apatite.

Another method for producing bioactive geopolymer composites may

be to first synthesise a geopolymer without additives, then coat it with a thin layer of a calcium-containing compound, such as those used in the present work. This could be done in various ways.

By making a water-based solution containing the bioactive compound and applying it thinly to a conventional geopolymer monolith before curing, a bond to the sample surface may result. Alternatively, it may be possible to thinly sprinkle an uncured geopolymer slurry with a very finely powdered bioactive compound to achieve an attachment with the geopolymer.

These methods may reduce the amount of additive required, thereby lowering the amount of essential alkaline material. As shown in this work, a geopolymer without additives can be produced with much less alkaline reagents and therefore create a geopolymer with lower pH.

Bibliography

- [1] K.J.D. MacKenzie. *What are these things called Geopolymers? A Physico-Chemical Perspective*, volume 153 of *Ceramic Transactions*, pages 175–186. Am. Ceram. Soc., 2003.
- [2] J. Davidovits. Geopolymers: Inorganic polymeric new materials. *J. Thermal Analysis*, 37:1633–1656, 1991.
- [3] H. Oudadesse, A.C. Derrien, M. Mami, S. Martin, G. Cathlineau, and L. Yahia. Aluminosilicates and biphasic *HA-TCP* composites: studies of properties for bony filling. *Biomed. Mater.*, 2:59–64, 2007.
- [4] S. Martin, A.C. Derrien, H. Oudadesse, D. Chauvel-Lebret, and G. Cathelineau. Implantation of aluminosilicate/ calcium phosphate materials; influence on bone formation in rabbit tibias. *European Cells and Materials*, 9:71–72, 2005.
- [5] H. Yan, K. Zhang, C. Blanford, L. Francis, and A. Stein. In vitro hydroxycarbonate apatite mineralization of CaO-SiO_2 sol-gel glasses with a three-dimensionally ordered macroporous structure. *Chem. Mater.*, 13:1374–1382, 2001.
- [6] Online on Geopolymers Homepage, www.geopolymer.org.

BIBLIOGRAPHY

- [7] K.J.D. MacKenzie. Applications of solid state NMR spectroscopy to ceramic research. *British Ceramic Transactions*, 99:231–240, 2000.
- [8] W.M. Kriven, J.L. Bell, and M. Gordon. *Microstructure and Microchemistry of fully-reacted Geopolymers and Geopolymer Matrix Composites*, volume 153 of *Ceramic Transactions*, pages 227–250. Am. Ceram. Soc., 2003.
- [9] V.F.F. Barbosa, K.J.D. MacKenzie, and C. Thaumaturgo. Synthesis and characterisation of materials based on inorganic polymers of alumina and silica: sodium polysialate polymers. *Int. J. of Inorganic Mater*, 2:309–317, 2000.
- [10] J. Davidovits. 30 years of successes and failures in geopolymer applications. market trends and breakthroughs. Geopolymer Conference, Melbourne, 2002.
- [11] H. Oudadesse, A.C. Derrien, M. Lefloch, and J. Davidovits. MAS-NMR studies of geopolymers heat-treated for applications in biomaterials field. *J. Mater. Sci.*, 42:3092–3098, 2007.
- [12] D. Kim, H.-T. Lai, G.V. Chilingar, and T.F. Yen. Geopolymer formation and its unique properties. *Environ Geol*, 51:103–111, 2006.
- [13] M.G. Blackford, J.V. Hanna, K.J. Pike, E.R. Vance, and D.S. Perera. Transmission electron microscopy and nuclear magnetic resonance studies of geopolymers for radioactive waste immobilization. *J. Am. Ceram. Soc.*, 90:1193–1199, 2007.

BIBLIOGRAPHY

- [14] D.S. Perera, Z. Aly, E.R. Vance, and M. Mizumo. Immobilization of Pb in a geopolymer matrix. *J. Am. Ceram. Soc.*, 88(9):2586–2588, 2005.
- [15] J. Black, S.W. Shalaby, and M. LaBerge. Biomaterials education: An academic viewpoint. *Journal of Applied Biomaterials*, 3:231–236, 1992.
- [16] L.L. Hench. Bioceramics. *J. Am. Ceram. Soc.*, 81(7):1705–1728, 1998.
- [17] L.L. Hench. Bioceramics: From concept to clinic. *J. Am. Ceram. Soc.*, 74(7):1487–1510, 1991.
- [18] S.V. Dorozhkin. Calcium orthophosphate cements for biomedical application. *J. Mater. Sci.*, 43:3028–3057, 2008.
- [19] A.U.J. Yap, Y.S. Pek, R.A. Kumar, P. Cheang, and K.A. Khor. Experimental studies on a new bioactive material: HA/Ionomer cements. *Biomaterials*, 23:955–962, 2002.
- [20] G. Geyer, G. Baier, and J. Helms. Epidureal application of ionomeric cement implants. experimental and clinical results. *The Journal of Laryngology and Otology*, 112:344–350, 1998.
- [21] P. Hantson, P. Mathieu, M. Gersdorff, C.J.M. Sindic, and R. Lauwerys. Encephalopathy with seizures after use of aluminium-containing bone cement. *The Lancet*, 344:1647, 1994.
- [22] K.J.D. MacKenzie, S. Komphanchai, and R.A. Fletcher. *New Trends in the Chemistry of Inorganic Polymers for Advanced Applications*, volume 28 of *Ceramic Transactions*, pages 249–257. Ceramic Transactions, 2007.

BIBLIOGRAPHY

- [23] K.J.D. MacKenzie, D.R.M. Brew, R.A. Fletcher, C.L. Nicholson, R. Vagana, and M. Schmuecker. Towards an understanding of the synthesis mechanisms of geopolymeric materials. Proc. World Geopolymer Conference, St. Quentin, Paris, 2005.
- [24] K.J.D. MacKenzie, M.E. Smith, and A. Wong. A multinuclear MAS NMR study of calcium-containing aluminosilicate inorganic polymers. *J. Mater. Chem.*, 17:5090–5096, 2007.
- [25] K.J.D. MacKenzie, D.R.M. Brew, R.A. Fletcher, and R. Vagana. Formation of aluminosilicate geopolymers from 1 : 1 layer lattice minerals pre-treated by various methods: a comparative study. *J. Mater Sci*, 42:4667–4674, 2007.
- [26] A. Oyane, H.-M. Kim, T. Furuya, T. Kokubo, T. Miyazaki, and T. Nakamura. Preparation and assessment of revised simulated body fluids. *J. Biomed. Mater. Res.*, 65A:188–195, 2003.
- [27] C. Ohtsuki. How to prepare simulated body fluid (SBF) and its related solutions, proposed by Kokubo and his colleagues. <http://mswebs.naist.jp/english/index.html>.
- [28] H. Stanjek and W. Husler. Basics of x-ray diffraction. *Hyperfine Interactions*, 154:107–119, 2004.
- [29] Online, Bruker website, <http://www.bruker-axs.de>.
- [30] Basics of x-ray diffraction. online: University of New Mexico - Department of Earth and Planetary Science, <http://epswww.unm.edu/xrd/xrdbasics.pdf>, 1999.

BIBLIOGRAPHY

- [31] K.J.D. MacKenzie and M.E. Smith. *Multinuclear Solid-State NMR of Inorganic Materials*, volume 6 of *Pergamon Materials Series*, chapter 1, pages 3–18. Pergamon, 2002.
- [32] K.J.D. MacKenzie and M.E. Smith. *^{27}Al NMR*, volume 6 of *Pergamon Materials Series*, chapter 5, pages 271–330. Pergamon, 2002.
- [33] K.J.D. MacKenzie and M.E. Smith. *^{29}Si NMR*, volume 6 of *Pergamon Materials Series*, chapter 4, pages 201–268. Pergamon, 2002.
- [34] P.F. Schmidt. *Praxis der Rasterelektronenmikroskopie und Mikrobereichsanalyse*. Kontakt & Studium. 1994.
- [35] JEOL LTD. A guide to scanning microscope observation. JEOL Brochure.
- [36] C. Pittet and J. Lemaitre. Mechanical characterization of brushite cements: A mohr circles approach. *J. Biomed. Mater. Res.*, 53:769–780, 2000.
- [37] Y.-C. Chou and C.-S. Chen. Determining elastic constants of transversely isotropic rocks using brazilian test and iterative procedure. *Int. J. Numer. Anal. Meth. Geomech*, 32:219–234, 2008.
- [38] M.K. Kerber, A.A. Wereszczak, and M.G. Jenkins. *Fracture Strength*, chapter 4, pages 147–152. Marcel Dekker, INC, 1998.
- [39] T.J. Manning and W.R. Grow. Inductively coupled plasma - atomic emission spectroscopy. *The Chemical Educator*, 2, 1997.

BIBLIOGRAPHY

- [40] I. Odler. *Special Inorganic Cements*. E & FN Spon, London and New York, 2000.
- [41] R.B. Heimann. Materials science of crystalline bioceramics: A review of basic properties and applications. *CMU Journal*, 1:23–46, 2002.
- [42] I. D. Thompson and L.L. Hench. Mechanical properties of bioactive glasses, glass-ceramics and composites. *Proceedings of the Institution of Mechanical Engineers*, 212(Part H):127–136, 1998.
- [43] E. Bresciani, T. Barata, T.C. Fagundes, A. Adachi, M.M. Terrin, and M.F. Navarro. Compressive and diametral tensile strength of glass ionomer cements. *Journal of Applied Oral Science*, 4:344–348, 2004.
- [44] L. Yue, M. Shui, and Z. Xu. The decomposition kinetics of nanocrystalline calcite. *Thermochimica Acta*, 335:121–126, 1999.
- [45] L.L. Hench. Plenary Lecture, PACRIM Conference 8, Vancouver, 2009.
- [46] M. Schmuecker and K.J.D. MacKenzie. Microstructure of sodium polysialate siloxo geopolymer. *Ceramics International*, 31:433–437, 2005.